

Dynamics of a randomly kicked particle

Santanu Das, Anupam Kundu

International Center for Theoretical Sciences, TIFR, Bangalore 560089, India

Abstract. Lévy walk (LW) process has been used as a simple model for describing anomalous diffusion in which the mean squared displacement of the walker grows non-linearly with time in contrast to the diffusive motion described by simple random walks or Brownian motion. In this paper we study a simple extension of the LW model in one dimension by introducing correlation among the velocities of the walker in different (flight) steps. Such correlation is absent in the LW model. The correlations are introduced by making the velocity at a step dependent on the velocity at the previous step in addition to the usual random noise ('kick') that the particle gets at random time intervals from the surrounding medium as in the LW model. Consequently the dynamics of the position becomes non-Markovian. We study the statistical properties of velocity and position of the walker at time t , both analytically and numerically. We show how different choices of the distribution of the random time intervals and the degree of correlation, controlled by a parameter r , affect the late time behaviour of these quantities.

1 Introduction

Dynamics of a particle kicked at random by the surrounding medium is an exciting and widely investigated problem for studying wide varieties of stochastic processes in the field of physics, chemistry and biology [1–9]. There are numerous examples of such dynamics, which include the movement of a pollen grain in water or a dust particle in air [2,3], tracer particle dynamics in turbulent flows [4,5], grains in inelastic gases [6,7], charged particle in plasmas [8] and active particles in crowded environment [9] among many others. In the simplest setting, the dynamics of a randomly kicked particle can be modelled by random walk and Brownian motion and their different variants [10,11] which provide a suitable conceptual approach. Random walk is a simple process that can be used to study almost any stochastic dynamics at the basic level. The common feature of a particle performing random walk or a Brownian motion is that its mean squared displacement $\sigma_x^2(t)$ grows linearly with time and the late time distribution of the position of the particle is Gaussian. This behaviour is known as diffusion. On the contrary, in case of anomalous diffusion the mean square displacement is characterised by a non-linear growth with time $\sigma_x^2(t) \sim t^\nu$ with $\nu \neq 1$. The motion is called super-diffusive for $\nu > 1$ and sub-diffusive for $\nu < 1$. Super-diffusive regime is interesting and can be observed in different contexts such as energy transport phenomena in one-dimensional systems [12–15], Josephson junction [16,17], turbulent diffusion [18] and in

fluctuation of end-to-end distance of a polymer [19] to name a few. On the other hand sub-diffusive phenomena appears in the motion of atoms in optical lattice [20], tracer particle motion in turbulent flow [21], in food searching process by long-range hopping by animals [22, 23] among many others.

One of the simplest model that leads to anomalous diffusion is Lévy walk dynamics [15, 16, 24–27]. In one dimension the Lévy walk process can be described as follows [26]: a walker moves with a velocity v for some time duration τ chosen from some distribution $\rho(\tau)$. As a result, in this duration the walker makes a displacement $v\tau$ (which we call a ‘jump’) and at the end of this duration the walker chooses a new velocity v' from some distribution $p(v)$ and moves with that velocity for another random duration of time τ' again chosen (independently) from the distribution $\rho(\tau')$. This continues till the observation time t at which one is usually interested in the position $x(t)$ of the walker. Depending on the choices of the distributions $p(v)$ and $\rho(\tau)$ the mean square displacement $\sigma_x^2(t)$ of the walker can exhibit diffusive and super-diffusive growth with time. Although in most of the studies of Lévy walk in one dimension one considers velocity distribution with fixed speed v_0 and random direction [26], some of early studies consider random speed as well [14, 28–30]. In all these studies, the common feature is that the velocity at different ‘jumps’ are completely uncorrelated. In this paper we consider an extension of this model of Lévy walk in which the velocities at a jump is correlated to the velocities at previous ‘jumps’.

More elaborately, in this paper we study a simple model of random walk by considering correlation of velocity at different ‘jump’ steps which can describe a wide range of dynamics of a particle that is kicked at random by the surrounding medium. In our model, the walker/particle makes a ‘jump’ *i.e.* moves with a velocity for some random interval of time τ chosen from distribution $\rho(\tau)$. At the end of this time duration its velocity gets changed to a new one due to a ‘kick’ from the surrounding medium and another random time interval τ' is chosen independently (as in the Lévy walk model) for which it moves ballistically with the new velocity. Only difference is now that the velocity in the new ‘jump’ step also depends explicitly on the velocity in the previous ‘jump’ step. Let v_i and v_{i-1} are the velocities of the particle at the i^{th} and $(i-1)^{\text{th}}$ ‘jump’ steps (of different random durations) respectively. They are related via

$$v_i = -rv_{i-1} + \eta_i, \quad \text{for } i = 1, 2, \dots \quad \text{with } v_0 = \eta_0, \quad (1)$$

where η_i s are independent and identically distributed (i.i.d) random variables that represent the ‘kicks’ from the medium. These i.i.d. random variables are each chosen from a mean zero Gaussian distribution with variance σ^2

$$p(\eta) = \frac{e^{-\frac{\eta^2}{2\sigma^2}}}{\sqrt{2\pi\sigma^2}}. \quad (2)$$

Here r in Eq. (1) is a dimensionless parameter which takes values within $[-1 : 1]$. Note that for $r \neq 0$ the velocities of the particle at different ‘jump’ steps get correlated. The parameter r controls the degree of correlation in the problem similar to the Hurst exponent $H \in [0 : 1]$ in fractional Brownian motion [31, 32]. It is clear from the dynamics

that the correlations among velocities become extreme in the limits $r \rightarrow \pm 1$ while it is zero at $r = 0$. In particular, in the domain $-1 < r < 0$, the process becomes positively correlated like H in the range $1/2 < H \leq 1$. Similarly, the correlation is negative within $0 < r < 1$ as one observes in case of fractional Brownian motion for $0 < H < 1/2$. This correlated dynamics of the velocity, particularly in the extreme limits of $r = \pm 1$, is expected to yield many intriguing and non-trivial outcomes of any observable associated with the velocity. This motivates us to mainly focus on these two extreme limits and the $r = 0$ case.

The parameter r can also be interpreted as a restitution coefficient in a collision problem [33–35]. Imagine a granular particle is being driven and dissipating energy via inelastic collisions with a massive vibrating wall. The post collision velocities of this particle and the wall, v' and V' respectively, are related to the pre-collision velocities v and V through the relation $(v' - V') = -r(v - V)$ where r serves as the coefficient of restitution. Notably, this coefficient characterises the degree of inelasticity in the collision process. For example, for $r = 1$, collision is elastic while for $r = 0$ it is perfectly inelastic. Between these two limits ($0 < r < 1$) collisions are inelastic. Conservation of momentum of the particle and wall with masses m and M , respectively, implies that $mv' + MV' = mv + MV$. Solving the above two relations in the limit $M \gg m$ yields $V' = V$ and $v' = -rv + (1 + r)V$. In addition, if one assumes that the velocity of the vibrating wall is random, uncorrelated (in time) and independent of the motion of the particle then it allows to consider $V(1 + r) = \eta$, a random noise and to write $v' = -rv + \eta$ [35] which is same as Eq. (1). Only thing we added to this dynamics is that the collisions are occurring after random interval of times chosen independently from some distribution and this way we have introduced time in our model which allows us to study the displacement of the particle in addition to its velocity.

In this paper, we consider the following three choices for the distribution $\rho(\tau)$ of the ‘jump’ durations:

$$\rho(\tau) = \begin{cases} \delta(\tau - a); & a > 0, & \text{case I} \\ \beta e^{-\beta\tau}; & \beta > 0; \tau \in [0, \infty), & \text{case II} \\ \frac{\alpha}{\bar{\tau}} \left(\frac{\bar{\tau}}{\tau}\right)^{1+\alpha}; & \alpha > 0; \tau \in [\bar{\tau}, \infty), & \text{case III.} \end{cases} \quad (3)$$

The first choice is a simple case in which all the ‘jump’ durations are equal to a . In the 2nd case, we consider an exponential distribution characterised by the parameter $\beta > 0$. The third one is a power-law distribution characterized by the exponent $\alpha > 0$. For convenience, throughout this paper, we consider $\bar{\tau} = 1$. Note that the exponential distribution has all moments finite, while the power-law distribution has diverging moments which depends on exponent α .

In this paper, we study the velocity $v(t)$ and the position $x(t)$ of the particle at time t . Precisely, we study the distribution of these two quantities in the limit of large t . For a trajectory of duration t having m ‘jump’ steps of durations $\tau_0, \tau_1, \dots, \tau_{m-1}, \tau_m^*$

the velocity $v(t)$ at time t can be written from Eq. (1) as

$$v(t) = \sum_{i=0}^m \eta_{m-i} (-r)^i = \sum_{i=0}^m \eta_i (-r)^{m-i}, \quad (4)$$

such that

$$t = \sum_{j=0}^{m-1} \tau_j + \tau_m^*, \quad (5)$$

where τ_m^* is the duration of the last incomplete step. Note that $v(0) = v_0 = \eta_0$. The time τ_m^* is known as the backward recurrence time in the context of the renewal process [36]. In this context various extreme statistics of i.i.d time intervals $\tau_0, \tau_1, \dots, \tau_m^*$, also known as waiting times, has been studied in detail [36–38]. The position x_i of the particle after i^{th} ‘jump’ step satisfies the equation

$$x_i = x_{i-1} + v_i \tau_i, \quad \text{for } i = 0, 1, 2, \dots \text{ with } x_{-1} = \bar{x}, \quad (6)$$

where \bar{x} is the initial position. From this equation and Eqs. (1) and (5), the position at time t can be written as

$$x(t) = \sum_{j=0}^{m-1} v_j \tau_j + v_m \tau_m^* + \bar{x}, \quad (7)$$

Without any loss of generality, we choose $x(0) = \bar{x} = 0$ in this paper. Eqs. (1) and (6) along with Eq. (5) constitute the equations of motion for the particle. For specific choices of r and $\rho(\tau)$, these equations of motion lead to well known dynamics. For example, in case I and II it is easy to realise that the dynamics for $r = -1$ leads to the Random acceleration process (RAP) at large times. Similarly, in these two cases the evolution of the velocity for $r \rightarrow -1$ can be described by an Ornstein-Uhlenbeck process in limits of $a \rightarrow 0$ or $\beta \rightarrow \infty$. Also note that for general $r \neq 0$, the evolution for the position of the particle becomes non-markovian. In the following we study the variance and the distribution of the velocity and the position of the particle both theoretically and numerically for the three choices of the ‘jump’ time distribution $\rho(\tau)$ and different values of r .

The paper is organised as follows: In sec. 2, we study distribution of the velocity of the particle at time t where we obtain various scaling properties of this distribution for three choices of $\rho(\tau)$ in Eq. (3). In the next sec. 3 we study the variance of the position in detail again for these three choices of ‘jump’ time distributions. In this section we also study velocity-velocity correlation and discuss its relation with the variance of the position. This section is followed by the study of the distribution of the position $x(t)$ in sec. 4 where we again discuss the three choices of $\rho(\tau)$ and for each choices, we discuss the cases for $r = 0$ and $r = \pm 1$ separately. Finally, in sec. 5 we summarise our results with a brief discussion and conclusion. For clarity of the presentation, we provide some details of the analysis in the Appendix.

2 Distribution of the velocity

The distribution of velocity v at time t , denoted by $P(v, t)$ can be written as

$$P(v, t) = \sum_{m=0}^{\infty} \langle \delta(v - v_m) \rangle \left\langle \delta \left(t - \sum_{j=0}^{m-1} \tau_j - \tau_m^* \right) \right\rangle \quad (8)$$

where we have used the fact that v_m and τ_m are independent random variables. Performing Fourier-Laplace transform on both sides of the above equation and simplifying we get (see [Appendix A](#))

$$\begin{aligned} \widetilde{P}_v(k, s) &= \int_{v=-\infty}^{\infty} dv e^{ikv} \int_{t=0}^{\infty} dt e^{-st} P(v, t) \\ &= \sum_{m=0}^{\infty} \exp \left[-\frac{1}{2} k^2 \sigma^2 \frac{1 - r^{2+2m}}{1 - r^2} \right] \tilde{\psi}^m(s) \tilde{\Psi}(s), \end{aligned} \quad (9)$$

where $\tilde{\psi}(s)$ and $\tilde{\Psi}(s)$ are the Laplace transforms of $\rho(\tau)$ and $\Psi(\tau) = \int_{\tau}^{\infty} du \rho(u)$ respectively:

$$\tilde{\psi}(s) = \mathcal{L}(\rho(\tau)) = \int_0^{\infty} d\tau e^{-s\tau} \rho(\tau), \quad (10)$$

$$\tilde{\Psi}(s) = \mathcal{L} \left(\int_{\tau}^{\infty} du \rho(u) \right) = \int_0^{\infty} d\tau e^{-s\tau} \int_{\tau}^{\infty} du \rho(u) = \frac{1 - \tilde{\psi}(s)}{s}. \quad (11)$$

Using the last equation, one can simplify the expression of $\widetilde{P}_v(k, s)$ in Eq. (9) to get

$$\widetilde{P}_v(k, s) = \frac{1}{s} e^{-k^2 \sigma^2 / 2}, \quad \text{for, } r = 0, \quad (12)$$

$$= \frac{1 - \tilde{\psi}(s)}{s \left(e^{k^2 \sigma^2 / 2} - \tilde{\psi}(s) \right)}, \quad \text{for, } r = \pm 1, \quad (13)$$

from which one can get $P(v, t)$ by performing inverse Fourier-Laplace transform. One can see that the distribution $P(v, t)$ for $r = 0$, is same as that of η *i.e.*, mean zero Gaussian with variance σ^2 for any $\rho(\tau)$. This is expected and can be easily seen from Eq. (1). However for $r \neq 0$, the distribution $P(v, t)$ should depend on $\rho(\tau)$. In the following, we perform the inverse Fourier-Laplace transform of $\widetilde{P}_v(k, s)$ [given in Eq. (13)] for the three choices of $\rho(\tau)$ separately for $r = \pm 1$. In particular we are interested in the large t limit where $P(v, t)$ often satisfies a scaling form after rescaling the velocity v with respect to (some power of) time t . It is easy to see that for $r \neq 0$ the magnitude of typical velocity is large for large t and this suggests us to look at the behaviour of $P(v, t)$ for large v and t which can be obtained by looking at the $k \rightarrow 0$ and $s \rightarrow 0$ limit. For small k we approximate $e^{k^2 \sigma^2 / 2} \approx 1 + k^2 \sigma^2 / 2$ and for small s we approximate

$\tilde{\psi}(s)$ as

$$\tilde{\psi}(s) \simeq 1 - as + \mathcal{O}(s^2), \quad \text{Case I} \quad (14)$$

$$\tilde{\psi}(s) \simeq 1 - \frac{s}{\beta} + \mathcal{O}(s^2), \quad \text{Case II} \quad (15)$$

$$\tilde{\psi}(s) \simeq \begin{cases} 1 - \Gamma(1 - \alpha) s^\alpha + \mathcal{O}(s) & \text{for } 0 < \alpha < 1 \\ 1 - (1 - \gamma_e - \ln(s))s + \mathcal{O}(s^2) & \text{for } \alpha = 1 \\ 1 - \frac{\alpha s}{\alpha - 1} - \Gamma(1 - \alpha)s^\alpha + \mathcal{O}(s^2) & \text{for } 1 < \alpha < 2, \\ 1 - 2s + (\frac{3}{2} - \gamma_e - \ln(s))s^2 + \mathcal{O}(s^3) & \text{for } \alpha = 2 \\ 1 - \frac{\alpha s}{\alpha - 1} + \frac{\alpha s^2}{2(\alpha - 2)} - \Gamma(1 - \alpha)s^\alpha + \mathcal{O}(s^3) & \text{for } \alpha > 2, \end{cases} \quad \text{Case III} \quad (16)$$

where $\Gamma(x)$ is the Gamma function and γ_e denotes the Euler constant. In the following we use these approximations of $e^{k^2\sigma^2/2}$ and $\tilde{\psi}(s)$ to analyse the inverse Fourier-Laplace transform of $\tilde{P}(k, s)$ for the three choices of $\rho(\tau)$.

2.1 Case I: $\rho(\tau) = \delta(\tau - a)$.

For this case it is easy to see from Eq. (4) that $v(t) = \sum_{i=0}^{\lfloor \frac{t}{a} \rfloor} \eta_i (-r)^{\lfloor \frac{t}{a} \rfloor - i}$ where $\lfloor x \rfloor$ represents the largest integer but not larger than x . This expression of $v(t)$ represents a weighted sum of i.i.d. Gaussian random variables. Hence by central limit theorem, the distribution of $P(v, t)$ is also Gaussian with zero mean and variance

$$\sigma_v^2(t) = \langle v(t)^2 \rangle_c = \langle v(t)^2 \rangle - \langle v(t) \rangle^2 = \sigma^2 \sum_{i=0}^{\lfloor \frac{t}{a} \rfloor} (r^2)^{\lfloor \frac{t}{a} \rfloor - i} = \sigma^2 \frac{1 - (r^2)^{\lfloor \frac{t}{a} \rfloor + 1}}{1 - r^2}, \quad (17)$$

where subscript ‘c’ represents cumulant.

2.2 Case II : $\rho(\tau) = \beta e^{-\beta\tau}$.

Using $\tilde{\psi}(s) = \beta/(\beta + s) \simeq 1 - s/\beta$ for $s \rightarrow 0$ in Eq. (13) we write $\tilde{P}_v(k, s) \simeq (s + k^2\beta\sigma^2/2)^{-1}$, which after performing inverse Fourier-Laplace transform provides $P(v, t) \simeq \frac{1}{\sqrt{\beta\sigma^2 t}} \mathcal{F}\left(\frac{v}{\sqrt{\beta\sigma^2 t}}\right)$ for large t where $\mathcal{F}(u) = G(u)$ with

$$G(u) = \frac{1}{\sqrt{2\pi}} \exp\left(-\frac{u^2}{2}\right). \quad (18)$$

The fact that $P(v, t)$ for large t in this case is Gaussian can be understood very simply from the following: the average time duration between two successive velocity ‘jump’s is β^{-1} and the number of ‘jump’s till time t is typically of the order of $m \sim \beta t$ for large t . The velocity after these many ‘jump’s, each of duration β^{-1} can again be written as a weighted sum of Gaussian i.i.d. random variable η_s as in the previous case. Hence the distribution of the velocity at time t would be given by a mean zero Gaussian distribution with variance $\sigma^2\beta t$.

2.3 Case III: $\rho(\tau) \sim \tau^{-(1+\alpha)}$

Performing the inverse Fourier-Laplace transform of $\widetilde{P}_v(k, s)$ for this case is relatively harder. In this case one expects different results in different regimes of α . Below we discuss the following regimes $0 < \alpha < 1$, $\alpha = 1$, and $\alpha > 1$ separately.

2.3.1 For $0 < \alpha < 1$

For small s and k , using $\tilde{\psi}(s) \simeq 1 - \Gamma(1 - \alpha) s^\alpha$ and $e^{k^2\sigma^2/2} \simeq 1 - \frac{k^2\sigma^2}{2}$ in Eq. (13) we get

$$\widetilde{P}_v(k, s) \simeq \frac{1}{s} \frac{1}{1 + \frac{k^2\sigma^2}{2\Gamma(1-\alpha)s^\alpha}} \simeq \sum_{l=0}^{\infty} \frac{1}{s^{\alpha l+1}} \left(-\frac{k^2\sigma^2}{2\Gamma(1-\alpha)} \right)^l. \quad (19)$$

This expression suggests that the distribution $P(v, t)$ satisfies a scaling form

$$P(v, t) = \sqrt{\frac{2\Gamma(1-\alpha)}{\sigma^2 t^\alpha}} F_\alpha \left(\frac{\sqrt{2\Gamma(1-\alpha)} v}{\sqrt{\sigma^2 t^\alpha}} \right), \quad (20)$$

for large t . To see this we first perform inverse Laplace transform (with respect to s) of each term in the above series individually and then perform the infinite series sum to get,

$$\widetilde{P}_v(k, t) \simeq \sum_{l=0}^{\infty} \frac{1}{\Gamma(\alpha l + 1)} \left(-\frac{t^\alpha k^2 \sigma^2}{2\Gamma(1-\alpha)} \right)^l \simeq E_\alpha \left(-\frac{t^\alpha k^2 \sigma^2}{2\Gamma(1-\alpha)} \right), \quad (21)$$

with $E_\alpha(u)$ being the Mittag-Leffler function [39]. Next we perform the inverse Fourier transform with respect to k and get

$$\mathbb{F}_\alpha(u) = \frac{1}{2\pi} \int_{-\infty}^{\infty} d\tilde{k} e^{-i\tilde{k}u} E_\alpha(-\tilde{k}^2), \quad \text{where,} \quad u = \frac{\sqrt{2\Gamma(1-\alpha)} v}{\sqrt{\sigma^2 t^\alpha}}. \quad (22)$$

For $\alpha = 0$, using $E_0(-\tilde{k}^2) = 1/(1 + \tilde{k}^2)$ [39] in Eq. (22) it is possible to perform the inverse Fourier transform exactly to get $\mathbb{F}_0(u) = e^{-|u|}/2$. For any arbitrary $0 < \alpha < 1$ performing the integral in Eq. (22) analytically seems difficult though it can be performed numerically [red solid lines in figs. 1 (a), (b) and (c)]. However, the behaviour of $\mathbb{F}_\alpha(u)$ for large u can be obtained using saddle point approximation and we find that the tails of $\mathbb{F}_\alpha(u)$ are given by the following stretched exponential form (see Appendix B for details)

$$\mathbb{F}_\alpha(u) \simeq \frac{(\alpha|u|/2)^{-\frac{1-\alpha}{2-\alpha}}}{\sqrt{4\pi(2-\alpha)}} \exp \left[- (2/\alpha - 1) (\alpha|u|/2)^{2/(2-\alpha)} \right], \quad \text{for large } u. \quad (23)$$

This result is verified with our simulation data in figs. 1 (a), (b) and (c) for $\alpha = 0.3$, 0.5 and $\alpha = 0.7$, respectively, where we observe excellent agreement. The red solid lines in these plots are obtained by performing the integral in Eq. (22) numerically in Mathematica. Throughout this paper, we have considered $\sigma = 1$ for all our numerical computations.

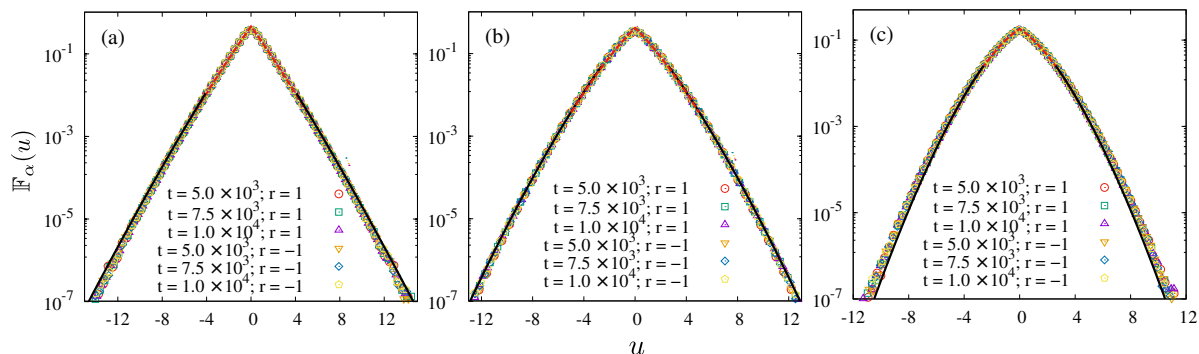


Figure 1. (Color online). Plot of the scaling distribution of the velocity as given in Eq. (20) at different times for $r = \pm 1$ with (a) $\alpha = 0.3$, (b) $\alpha = 0.5$ and (c) $\alpha = 0.7$. Discrete points in each plot are obtained from the numerical simulation whereas the (red) dashed lines correspond to the theoretical result obtained by performing the integral in Eq. (22) numerically. The (black) bold lines correspond to the approximate analytical expression of the scaling $\mathbb{F}_\alpha(u)$ valid for large $|u|$ as given in Eq. (23). We have taken $\sigma = 1$ for all the figures in this paper.

2.3.2 For $\alpha = 1$

In the $\alpha \rightarrow 1$ limit the stretched exponential form of the scaling distribution $F_\alpha(y)$ in Eq. (23) approaches a Gaussian distribution form with mean zero and variance growing linearly with time. However, the small s behaviour of $\tilde{\psi}(s)$ for $\alpha = 1$ given in Eq. (16) suggests us to expect a $\ln(t)$ dependence in the variance of v . To see this we use $\tilde{\psi}(s) \simeq 1 - (1 - \gamma_e - \ln(s))s$ for small s and $e^{k^2\sigma^2/2} \simeq 1 + k^2\sigma^2/2$ for small k in Eq. (13) and expanding we get

$$\tilde{P}_v(k, s) \simeq \sum_{l=0}^{\infty} \frac{1}{s^{l+1}} \left(\frac{1}{\ln(s)} \left(e^{k^2\sigma^2/2} - 1 \right) \right)^l. \quad (24)$$

We first perform the inverse Laplace transform with respect to s and to do that we employ the Tauberian theorem (see (C.5) in Appendix C). We finally get the following approximate result in the $t \rightarrow \infty$ limit

$$\tilde{P}_v(k, t) \simeq \sum_{l=0}^{\infty} \frac{1}{l!} \left(-\frac{t k^2 \sigma^2}{2 \ln(t)} \right)^l \simeq \exp \left[-\frac{t k^2 \sigma^2}{2 \ln(t)} \right]. \quad (25)$$

This suggests that for large t , the distribution $P(v, t)$ indeed has a mean zero Gaussian distribution but with variance growing with time as $\sigma^2 t / \ln(t)$. This means the scaling variable $u = v / \sqrt{\sigma^2 t / \ln(t)}$ has a scaling distribution $\mathbb{F}_1(u) = G(u)$ where $G(u)$ is given in Eq. (18). We attempt to illustrate this result numerically in fig. 2(a). In this figure, while we observe a nice data collapse in terms of the scaling variable u (with y-axis appropriately scaled), the scaling distribution $\mathbb{F}_1(u)$ does not match properly with the Gaussian form at the tails. We believe this happens because of the slow convergence arising due to the absence of a time scale for $\alpha = 1$. For both $\alpha < 1$ and $\alpha > 1$, there exist a time scale τ^* over which one expects the distribution $P(v, t)$ to approach an appropriate scaling distribution. As can be seen from Eq. (21) or Eq. (22),

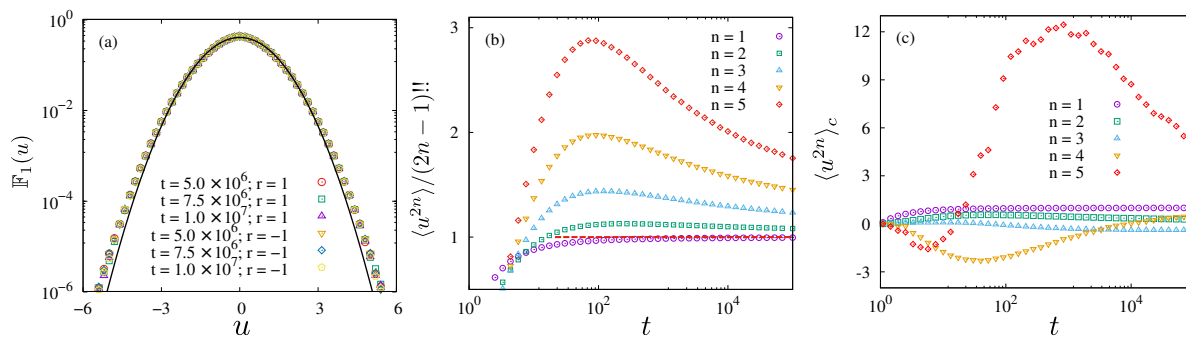


Figure 2. (Color online). (a) Probability distribution function of the scaled velocity $u = v/\sqrt{\sigma^2 t/\log(t)}$ is plotted at different times for $r = \pm 1$ for $\alpha = 1$. In (b) and (c): we plot the simulation result of the first five (non-zero) even-order moments $\langle u^{2n} \rangle$ and cumulants $\langle u^{2n} \rangle_c$ of the scaled variable u as function of time to demonstrate the slow convergence.

$\tau^* \sim \Gamma(1 - \alpha)^{1/\alpha}$ for $\alpha < 1$. On the other hand for $\alpha > 1$, as will be shown in the next section, $\tau^* \sim \alpha/(\alpha - 1)$. Observe from both these expressions of τ^* that it diverges as α approaches 1 either from below or above. To investigate further about the slow convergence and approach to the Gaussian scaling form, we compute the moments and cumulants of the scaling variable $u = v/\sqrt{\sigma^2 t/\ln(t)}$ as functions of t in numerical simulation and check if they converge to $\langle u^{2n} \rangle = (2n - 1)!!$ and $\langle u^{2n} \rangle_c = \delta_{n,1}$ at large t , where $\delta_{i,j}$ is the Kronecker delta. Note all odd order moments and cumulants are identically zero by symmetry. Here $(2n - 1)!!$ represents double factorial defined as $(2n - 1)!! = 1.3.5 \dots (2n - 1)$. In figs. 2(b) and 2(c) we plot the moments and cumulants till order 10 (*i.e.* $n = 5$) as functions of time. We observe that at large time the cumulants indeed approach zero. However, the convergence time become larger and larger as the order of the moments/cumulants increase as one expects.

2.3.3 For $\alpha > 1$

In this case we can see from Eq. (16) the function $\tilde{\psi}(s)$ in the $s \rightarrow 0$ has a linear order term *i.e.* $\tilde{\psi}(s) \simeq 1 - \alpha s/(\alpha - 1)$. As a consequence, following a similar procedure and arguments like case II in sec. 2.2, in this case also we find that the typical fluctuation around the mean is Gaussian with variance $\sigma^2 t(\alpha - 1)/\alpha$. This means that in this case also the scaling variable $u = v/\sqrt{\sigma^2 t(\alpha - 1)/\alpha}$ has a scaling distribution $\mathbb{F}_\alpha(u) = G(u)$ where $G(u)$ is given in Eq. (18). We demonstrate this result in fig. 3 in terms of the scaled variable u .

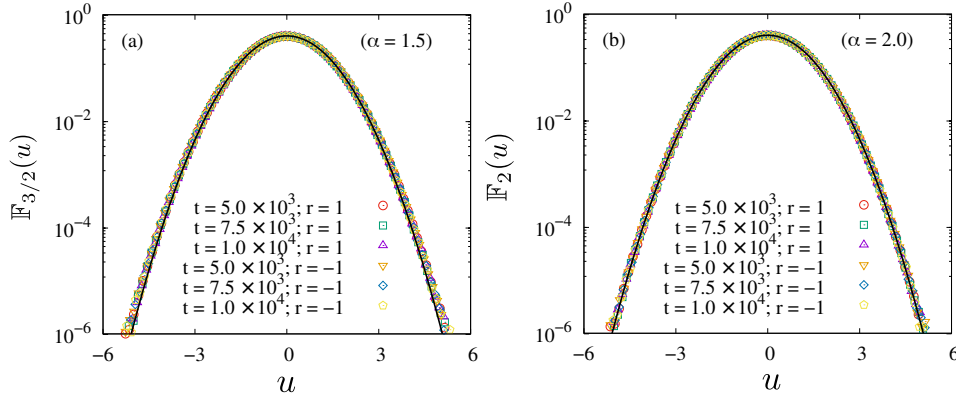


Figure 3. (Color online). Probability distribution function of the scaled variable $u = v/\sqrt{\sigma^2 t(\alpha - 1)/\alpha}$ is plotted at different times for $r = \pm 1$ with (a) $\alpha = 1.5$ and (b) $\alpha = 2.0$. Symbols in each plot correspond to numerical simulation results which show excellent agreement with the normal Gaussian distribution $\mathbb{F}_\alpha(u) = G(u)$ (solid black lines) predicted theoretically (see sec. 2.3.3).

3 Variance of the position

We now study the properties of the position $x(t)$ of the particle in time t when it starts at the origin *i.e.* $x(0) = 0$. The distribution $P(x, t)$ of the position can be written as

$$P(x, t) = \sum_{m=0}^{\infty} \left\langle \delta \left(x - \sum_{j=0}^{m-1} v_j \tau_j - v_m \tau_m^* \right) \delta \left(t - \sum_{j=0}^{m-1} \tau_j - \tau_m^* \right) \right\rangle, \quad (26)$$

where we have used Eqs. (7) and (5). Performing Fourier-Laplace transform of $P(x, t)$ we get

$$\begin{aligned} \widetilde{P}_x(k, s) &= \int_{x=-\infty}^{\infty} dx e^{ikx} \int_{t=0}^{\infty} dt e^{-st} P(x, t) \\ &= \sum_{m=0}^{\infty} \left\langle \exp \left[-\frac{1}{2} \sigma^2 k^2 \bar{\tau}_m^T \Sigma_m \bar{\tau}_m - s I_m^T \bar{\tau}_m \right] \right\rangle_{\{\tau_j\}} \end{aligned} \quad (27)$$

where $\bar{\tau}_m^T = (\tau_0 \ \tau_1 \ \tau_2 \ \dots \ \tau_m^*)_{1 \times (m+1)}$ and $I_m^T = (1 \ 1 \ 1 \ \dots \ 1)_{1 \times (m+1)}$ are two $(m+1)$ dimensional row vectors and Σ_m is a symmetric $(m+1) \times (m+1)$ dimensional matrix with elements given by

$$\begin{aligned} \Sigma_m(l, j) &= \underbrace{\delta_{l,j} \sum_{p=0}^{l-1} r^{2p}}_{\text{diagonal elements}} + \underbrace{(1 - \delta_{l,j}) \mathbb{I}(j > l) \sum_{p=0}^{l-1} (-r)^{j-l+2p}}_{\text{upper-half off-diagonal elements}} \\ &\quad + \underbrace{(1 - \delta_{l,j}) \mathbb{I}(l > j) \sum_{p=0}^{j-1} (-r)^{l-j+2p}}_{\text{lower-half off-diagonal elements}}, \end{aligned} \quad (28)$$

where $\mathbb{I}(\text{condition})$ is the indicator function and takes value 1 if the condition in the argument is true and 0 otherwise. The angular bracket in Eq. (27) represents average

over the time intervals $\{\tau_m\}$ which are chosen independently from distribution $\rho(\tau)$. We recall, in this paper we consider three choices of $\rho(\tau)$ as stated in Eq. (3). Since the τ s are positive random variables, performing the average over them in Eq. (27) for $r \neq 0$ is difficult. However, one can compute moments of different order by evaluating derivatives of $\tilde{P}_x(k, s)$ with respect to k in the $k \rightarrow 0$ limit. It is easy to observe from Eq. (27) that $P(x, t) = P(-x, t)$. Hence all odd order moments and the cumulants of the position are zero. The even order moments are non-zero. In this paper we discuss the variance $\sigma_x^2(t) = \langle x^2(t) \rangle_c = \langle x^2(t) \rangle$ in detail while making some comments on higher order moments/cumulants. The Laplace transform of the variance $\sigma_x^2(t)$ is given by [see Appendix D for details]

$$\tilde{\sigma}_x^2(s) = - \left[\frac{d^2}{dk^2} \tilde{P}_x(k, s) \right]_{k=0} = \frac{2\sigma^2}{s^3(1-r^2\tilde{\psi}(s))} \left(1 + \frac{s\tilde{\psi}'(s)}{1-\tilde{\psi}(s)} + \frac{rs\tilde{\psi}'(s)}{1+r\tilde{\psi}(s)} \right). \quad (29)$$

This is a general result valid for any $\rho(\tau)$ and $-1 \leq r \leq 1$. Next we discuss three choices of $\rho(\tau)$ separately.

3.1 Case I: $\rho(\tau) = \delta(\tau - a)$

The behaviour of the variance at large t can be easily found by using the small s asymptotic $\tilde{\psi}(s) = e^{-as} \simeq 1 - as + \mathcal{O}(s^2)$ in Eq. (29) and then performing the inverse Laplace transform. We get

$$\sigma_x^2(t) = \langle x^2(t) \rangle_c \simeq \begin{cases} a\sigma^2 t + \mathcal{O}(1) & \text{for } r = 0 \\ \frac{1}{3a}\sigma^2 t^3 + \mathcal{O}(t^2) & \text{for } r = -1 \\ \frac{1}{3}a\sigma^2 t + \mathcal{O}(1) & \text{for } r = 1. \end{cases} \quad (30)$$

As mentioned earlier, in this case one can actually perform the inverse Laplace transform exactly for arbitrary t and r . As shown in Appendix E, we get the following explicit expression of $\sigma_x^2(t) = \langle x^2(t) \rangle_c$

$$\begin{aligned} \sigma_x^2(t) = & \frac{\sigma^2(1-r)^{-1}}{(r+1)^3} \left[(r+1)^2 t^2 \left(1 - r^2 \lfloor \frac{t}{a} \rfloor^{+2} \right) - 2a(r+1)t \left\{ r + \left\lfloor \frac{t}{a} \right\rfloor (r+1) \right. \right. \\ & \left. \left. - r^2 \lfloor \frac{t}{a} \rfloor^{+2} \left(\left\lfloor \frac{t}{a} \right\rfloor (r+1) + 1 \right) - (-r) \lfloor \frac{t}{a} \rfloor (1-r^2) \right\} \right. \\ & \left. - a^2 \left\{ \left[\left(1 + \left\lfloor \frac{t}{a} \right\rfloor (r+1) \right) (-r)^{1+\lfloor \frac{t}{a} \rfloor} + r - 1 \right]^2 - (r+1)^2 \left\lfloor \frac{t}{a} \right\rfloor \left(\left\lfloor \frac{t}{a} \right\rfloor + 1 \right) - 1 \right\} \right]. \end{aligned} \quad (31)$$

From this expression it is easy to see that for $-1 < r < 1$

$$\sigma_x^2(t) \simeq \frac{a\sigma^2 t}{(1+r)^2} \quad \text{for large } t, \quad (32)$$

which for $r = 0$ correctly reproduces the result in Eq. (30). This result is easy to understand, because for $r = 0$ the position $x(t)$ at large t becomes a sum of many (of the order $\lfloor t/a \rfloor$) Gaussian random variables each of mean zero and variance $a^2\sigma^2$. Hence the variance of the position $x(t)$ should be $\sim a\sigma^2 t$ for large t . In particular for $|r| < 1$,

one can see that the motion of the particle at large t can be effectively described by a free particle with its velocity governed by a stochastic Ornstein-Uhlenbeck process characterised by dissipation strength $\gamma = (1+r)/a$ and noise strength $D = \sigma^2/a$. Such a particle is also known in the literature as active Ornstein-Uhlenbeck particle [40]. For such a particle it is easy to show that the variance of its position for large t is given by $\sigma_x^2(t) \simeq (D/\gamma^2) t$, which indeed is equal to $a\sigma^2 t/(1+r)^2$. This result is not valid for $r = \pm 1$ for which we have to analyse the large t behaviour of $\sigma_x^2(t)$ separately.

For $r = 1$, we see from Eq. (32) that $\sigma_x^2(t) \sim a\sigma^2 t/4$ for large t . On the other hand from the inverse Laplace transform calculation in Eq. (30) we get $\sigma_x^2(t) \sim a\sigma^2 t/3$ for large t . However, in numerical simulation we do not observe either of these two forms but we observe the variance to oscillate within an envelop which grows linearly with time (see fig. 4(b)). From the exact expression in Eq. (31) we find

$$\sigma_x^2(t) \simeq \frac{1}{2}\sigma^2 a^2 \left(1 + \left\lfloor \frac{t}{a} \right\rfloor\right) (2u^2 - 2u + 1). \quad (33)$$

at large t where $u = t/a - \lfloor t/a \rfloor$ with $u \in (0, 1)$. Clearly, the slope depends on the value of u at which one makes measurements in the simulation. For $u = 0$ *i.e.* at times integer multiples of a , one finds $\sigma_x^2(t) \simeq a\sigma^2 t/2$, whereas for $u = 1/2$ one finds $\sigma_x^2(t) \simeq a^2\sigma^2 \lfloor t/a \rfloor/4 \simeq a\sigma^2 t/4$ at large t . In fact, the slope of $\sigma_x^2(t) = \langle x^2(t) \rangle_c = \langle x^2(t) \rangle$ oscillates between $a\sigma^2/2$ and $a\sigma^2/4$. The result in Eq. (30) corresponds to the average value

$$\sigma_x^2(t) \simeq \frac{\sigma^2 a^2}{2} \left(1 + \left\lfloor \frac{t}{a} \right\rfloor\right) \int_0^1 du (1 - 2u + 2u^2) \simeq \left(1 + \left\lfloor \frac{t}{a} \right\rfloor\right) \frac{a^2 \sigma^2}{3} \simeq \frac{1}{3} a \sigma^2 t. \quad (34)$$

as stated in Eq. (33) and verified numerically in fig. 4(b).

Taking $r \rightarrow -1$ in Eq. (32) provides diverging result. One needs to take the $r \rightarrow -1$ limit first and then take the large t limit, following which we get $\sigma_x^2(t) \simeq \sigma^2 t^3/3a$. This result is verified numerically in fig. 4(a). In this figure we also observe that for r very close to -1 one finds that at moderately large t the variance $\sigma_x^2(t)$ grows as $\sim t^3$ as for $r = -1$ but at really large times the growth crosses over to linear growth. A careful analysis shows that for $r \rightarrow -1$, the time dependence of the variance crosses over from $\sigma_x^2(t) \simeq (1-r)\sigma^2 t^3/6a$ to $a\sigma^2 t/(1+r)^2$ as t increases and this crossover occurs at time scale $\tau_c \sim a/\sqrt{(1-r)(1+r)^2}$ which is indeed infinite at $r = -1$. This crossover behaviour is illustrated in fig. 4(a) for $r = -0.99$.

Before ending this section we make an additional remark about the $r = -1$ case. The late time growth $\sigma_x^2(t) \simeq \sigma^2 t^3/3a$ can be understood by realising the fact that at large time the motion of the particle can be effectively described by a random acceleration process [41, 42] with noise strength being $D = \sigma^2/a$. For such a motion the variance of the position grows at large time as $\sim Dt^3/3 = \sigma^2 t^3/3a$. A small discussion on the definition and properties of RAP is provided in Appendix F for completeness.

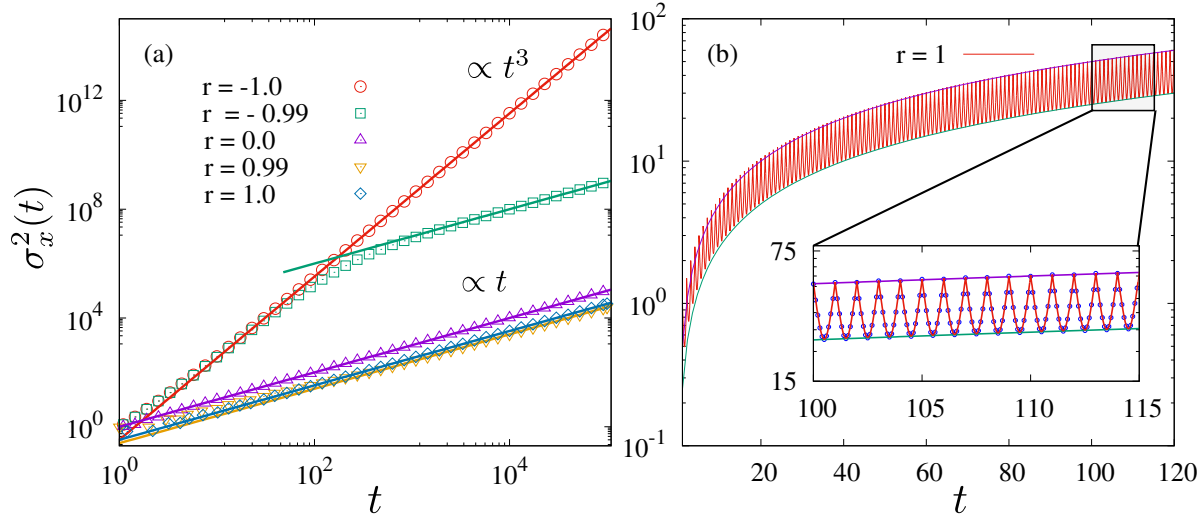


Figure 4. (Color online). Variance of the position is plotted as function of time for different r in case I with $a = 1$. Discrete symbols in each plot are simulation results which are showing excellent agreements with the analytical results as shown by lines.

3.2 Case II: $\rho(\tau) = \beta e^{-\beta\tau}$

In this case also one can perform the inverse Laplace transform in Eq. (29) exactly for $-1 \leq r \leq 1$ to get

$$\begin{aligned} \sigma_x^2(t) = \langle x^2(t) \rangle_c &= \frac{2\sigma^2 t}{\beta(1+r)(1-r^2)} - \frac{2\sigma^2(1-r+r^2)}{\beta^2(1+r)(1-r^2)^2} \\ &+ \frac{2\sigma^2}{\beta^2} \left(\frac{(1-r)^2 e^{-\beta t(1+r)} + r e^{-\beta t(1-r^2)}}{(1+r)(1-r^2)^2} \right). \end{aligned} \quad (35)$$

This result is verified numerically in fig. 5(a) for $r = \pm 0.9$. From this result we can see that there are two different time scales $\tau_v = (1-r^2)^{-1}/\beta$ and $\tau_c = (1+r)^{-1}/\beta$ involved in the process. These times scales arise, respectively, from the variance of the velocity $\sigma_v^2(t)$ and the velocity auto-correlation function $C_{vv}(t) = \langle v(t_1)v(t_2) \rangle - \langle v(t_1) \rangle \langle v(t_2) \rangle$. Taking second derivative of the Fourier-Laplace transform $\tilde{P}_v(k, s)$ in Eq. (9) with respect to k at $k \rightarrow 0$ and then performing inverse Laplace transform one can show that

$$\sigma_v^2(t) = \langle v^2(t) \rangle_c = \frac{\sigma^2}{1-r^2} \left(1 - r^2 e^{-\beta t(1-r^2)} \right). \quad (36)$$

It can be shown (see Appendix G) that the velocity auto correlation function $C_{vv}(t_1, t_2)$ is given by

$$C_{vv}(t_1, t_2) \simeq \langle v^2(\min\{t_1, t_2\}) \rangle_c e^{-\beta(1+r)|t_1-t_2|}. \quad (37)$$

for large t_1 and t_2 . From these expressions we observe that the variance approaches to a stationary value and the covariance decreases to zero as t increases but the time scales associated are given, respectively, by $\tau_v = (1-r^2)^{-1}/\beta$ and $\tau_c = (1+r)^{-1}/\beta$. From Eq. (35), it is easy to see that for $r = -1$ the variance behaves as $\sigma_x^2(t) \sim \beta\sigma^2 t^3/3$ at late times which is similar to the variance of a RAP driven by white noise of strength

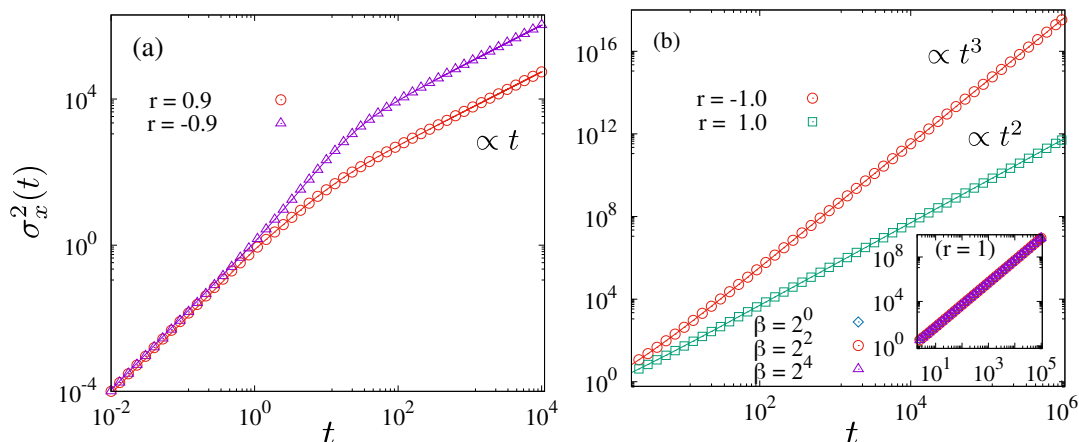


Figure 5. (Color online). The plots show $\sigma_x^2(t)$ vs. t in case II for (a) $r = 0.9$ and -0.9 and for (b) $r = \pm 1$ with $\beta = 1$. Symbols represent the simulation results and solid lines represent the analytical expression in Eq. (35). The inset of fig. (b) verifies the β independence of the variance for $r = 1$, where we plot $\sigma_x^2(t)$ for different values of β .

$D = \beta\sigma^2$. This cubic growth of $\sigma_x^2(t)$ is verified numerically in fig. 5(b). For $r = 1$ it is interesting to observe from Eq. (35) that $\sigma_x^2(t) \sim \sigma^2 t^2/2$ at large times. Following the discussion presented for $r \rightarrow 1$ in the last sec. 3.1, one may be tempted to assume that the motion of the particle can effectively be described by an active Ornstein-Uhlenbeck particle driven by white noise. But for such a particle the variance grows linearly instead of quadratically with time as we see in our case. Remarkably, we also observe that the variance is independent of β (see the inset of fig. 5(b)). It is easy to see that in this case the variance of the position after a large number of ‘jumps’, say m , is $\sim \sigma^2 m^2/2\beta^2$, whereas the typical number of ‘jump’ events in time t is $m \sim \beta t$ for large t . Hence the variance in the leading order for large t becomes β independent. This can also be easily seen from the small s behaviour of $\tilde{\sigma}_x^2(s) \simeq \sigma^2 s^{-3}$ [see Eq. (29)] which in the leading order is also β independent.

Above large time behaviours of the variance of the position for different values of r , can also be obtained from the large time behaviours of velocity-velocity correlation $C_{vv}(t_1, t_2)$. From $x(t) = \int_0^t dt_1 v(t_1)$, one can easily write

$$\sigma_x^2(t) = \langle x^2(t) \rangle_c = \left\langle \int_0^t dt_1 v(t_1) \int_0^t dt_2 v(t_2) \right\rangle_c = 2 \int_0^t dt_1 \int_{t_1}^t dt_2 C_{vv}(t_1, t_2). \quad (38)$$

For $r = 0$ it is easy to see from Eq. (12) that $\langle v^2(t) \rangle_c = \sigma^2$ using which in the above equation and performing the integral we get $\sigma_x^2(t) \simeq 2\sigma^2 t/\beta$ for large t .

For $r = -1$, one can obtain the variance of the velocity from $\tilde{P}_v(k, s)$ given in Eq. (13) as $\tilde{\sigma}_v^2(s) = - \left[\frac{d^2}{dk^2} \tilde{P}_v(k, s) \right]_{k=0} = \frac{\sigma^2}{s(1-\tilde{\psi}(s))}$ where for exponential distribution for the ‘jump’ durations one has $\tilde{\psi}(s) = \beta/(\beta + s)$. Furthermore, using this and performing the inverse Laplace transform one can easily show that $\sigma_v^2(t) \simeq \sigma^2 \beta t$ for large t . Using this result in Eq. (37) we get $C_{vv}(t_1, t_2) \simeq \sigma^2 \beta \min\{t_1, t_2\}$ putting which in Eq. (38) and performing the integrals we indeed get $\sigma_x^2(t) \simeq \beta\sigma^2 t^3/3$ for large t . Note that the

correlation function in this case comes out to be identical to the correlation function of the RAP [41, 42] with the strength of the noise correlator $D = \sigma^2\beta$. This similarity with RAP has been observed earlier in sec. 3.1.

Now, for $r = 1$, using $\sigma_v^2(t) \simeq \sigma^2\beta t$, same as the case of $r = -1$, we find the correlation function as $C_{vv}(t_1, t_2) = \langle v^2(\min\{t_1, t_2\}) \rangle_c e^{-2\beta|t_1-t_2|} \simeq \sigma^2\beta \min\{t_1, t_2\} e^{-2\beta|t_1-t_2|}$ for $0 \leq t_1, t_2 \leq t$. Using this expression in Eq. (38) we can easily see the dominant contribution of the integration $\int_0^{t-t_1} dz e^{-2\beta z} \propto 1/\beta$ which cancels out β in the numerator. It essentially makes $\sigma_x^2(t) = \langle x^2(t) \rangle_c \propto \sigma^2 \int_0^t dt_1 t_1 \propto \sigma^2 t^2$ to be independent of β .

3.3 Case III: $\rho(\tau) \sim \tau^{-(1+\alpha)}$

Unlike case I and II, in this case it is difficult to perform the inverse Laplace transform of $\tilde{\sigma}_x^2(s)$ in Eq. (29) exactly for arbitrary t . However, one can find the variance at large t at which we will mainly focus in the following. As mentioned earlier, we again note from Eqs. (4) and (7) that the position x_m of the particle after m ‘collisions’ or ‘jumps’ can be written as a sum of m terms: $x_m = \sum_{j=1}^m \xi_j$ with $\xi = v_{j-1}\tau_{j-1}$. The random variable ξ s are correlated and additionally can have fat tails in their (marginal) probability distributions for power law ‘jump’ time distributions. For $r = 0$, they become independent and the distribution of ξ has a power law tail of the form $\sim 1/|\xi|^{1+\alpha}$ (see sec. 4.1.3 for details). As a consequence, moments of order larger than $[\alpha]$ diverge. This suggests that the moments of x_m of order larger than $[\alpha]$ should also diverge. This is not true for $x(t)$. Since for a given t , the ‘jump’ duration (time between two successive ‘jumps’) variables τ -s can at maximum be t . Hence even for $\alpha < 1$ we find, as we will see, the variance of $x(t)$ is finite.

At large t , the dominant contribution to the variance of $x(t)$ comes from the small s properties of $\tilde{\sigma}_x^2(s)$ given in Eq. (29). In the following we present the computation of $\sigma_x^2(t)$ separately for $r = 0, -1$ and 1 .

3.3.1 For $r = 0$

We start with $r = 0$, for which we first obtain the small s behaviour of $\tilde{\sigma}_x^2(s)$ using the $s \rightarrow 0$ approximations of $\tilde{\psi}(s)$ given in Eq. (16). Then we perform the inverse Laplace transform using the Tauberian theorem (see Appendix C) to get $\sigma_x^2(t)$ for large

t . We get

$$\tilde{\sigma}_x^2(s) \underset{s \rightarrow 0}{\simeq} \begin{cases} \frac{2\sigma^2(1-\alpha)}{s^3} \\ \frac{2\sigma^2}{s^3} \frac{1}{1-\gamma_e - \ln(s)} \\ \frac{2\sigma^2(\alpha-1)\Gamma(2-\alpha)}{\alpha s^{4-\alpha}} \\ \frac{\sigma^2}{2s^2}(1 - 2\gamma_e - 2 \ln(s)) \\ \frac{\sigma^2(\alpha-1)}{(\alpha-2)s^2} \end{cases} \xrightarrow[t \rightarrow \infty]{\mathcal{L}_t^{-1}} \sigma_x^2(t) \simeq \begin{cases} (1-\alpha) \sigma^2 t^2 & \text{for } 0 < \alpha < 1 \\ \frac{\sigma^2 t^2}{\ln(t)} & \text{for } \alpha = 1 \\ \frac{2(\alpha-1)\Gamma(2-\alpha)}{\alpha\Gamma(4-\alpha)} \sigma^2 t^{3-\alpha} & \text{for } 1 < \alpha < 2 \\ \sigma^2 t \ln(t) & \text{for } \alpha = 2 \\ \frac{\alpha-1}{\alpha-2} \sigma^2 t & \text{for } \alpha > 2. \end{cases} \quad (39)$$

Here, remember, $\mathcal{L}_t^{-1}[\tilde{f}(s)]$ represents the inverse Laplace transform of a function $\tilde{f}(s)$ to get $f(t)$ in the time domain. We verify these results numerically in fig. 6(a) for different values of α in each of the five regimes displayed in Eq. (39). For each cases we observe excellent agreement. The time dependence of the variance are similar to that of one dimensional Lévy walk because, for $r = 0$ the process can be thought of as a Levy walk in one dimension in which the velocity after each ‘jump’ is chosen from a Gaussian distribution [16, 24–26].

In usual studies of Lévy walks in one dimension, the velocity distribution $p(v)$ is often taken of the form $p(v) = 1/2(\delta(v - v_0) + \delta(v + v_0))$ [25, 26] for some fixed magnitude v_0 of the velocity. Other velocity distributions with variable magnitude and direction have also been investigated in the literature but mostly with $v_0 \gg \sigma$ where σ is the variance of the velocity [26, 28]. For distributions $p(v)$ with $v_0 \gg \sigma$, one observes travelling peaks in the distribution of the position of the walker [14, 28]. In contrast we here are working in the opposite regime $v_0 < \sigma$ because $v_0 = \langle |v| \rangle = \sigma/\sqrt{2\pi}$ in our case and consequently we do not observe such travelling peaks (see sec. 4.1.3). We expect the time dependence of the variance of the position to remain same as in [26, 28], because for any symmetric velocity distribution $p(v)$ with zero mean and finite variance, the variance of the position exhibits a quite general form as $\tilde{\sigma}_x^2(s) = \langle v^2 \rangle_c \frac{\tilde{\psi}''(s) + s \tilde{\Psi}''(s)}{s(1-\tilde{\psi}(s))}$ (see Appendix H for details). The dependence of the velocity distribution $p(v)$ appears only through the time independent part of $\sigma_x^2(t)$ through σ_v^2 . For example, in our case, using $\tilde{\Psi}(s) = (1 - \tilde{\psi}(s))/s$ and $\langle v^2 \rangle_c = \sigma^2$, we can correctly recover the exact expression of $\tilde{\sigma}_x^2(s)$ for $r = 0$ given in Eq. (29) which at large time provides the behaviour in Eq. (39) for different values of α .

To understand these late time behaviours of the variance $\sigma_x^2(t)$, we recall that for $r = 0$, the position of the particle $x(t)$ at time t can be written as sum of displacements $v\tau \equiv \eta\tau$ after each ‘collision’ or ‘jump’. For $\alpha < 1$, both the first and second moments of the ‘jump’ time distribution $\rho(\tau)$ are divergent because the $\rho(\tau)$ has fat tail. In fact we have observed, as will be discussed in sec. 4.1.3.1, the position $x(t)$ for large t gets the most dominant contribution from the maximum jump duration $\tau_{\max}(t)$ which is typically of the order of t . So for large t we can approximate $x(t) \sim \eta\tau_{\max}$ which implies ballistic growth of the variance $\sigma_x^2(t) \sim \langle \eta^2 \tau_{\max}^2 \rangle_c \sim \sigma^2 t^2$ [see Eq. (57)]. In the $\alpha \rightarrow 1$ limit, the results in Eq. (39) both from below (1^-) and above (1^+), provides

$\sigma_x^2(t) \sim \sigma^2 t^2$. However, in our calculation we find an additional $\ln(t)$ modulation. Such a $\ln(t)$ correction appears through the distribution of $\tau_{\max}(t)$ [see [Appendix J](#)].

For $\alpha > 2$, all the terms in the sum of the individual jumps contribute to the final position $x(t)$ at time t at the same order. Hence, for this case $\sigma_x^2(t) \sim$ [variance of the position in a single ‘jump’] \times [number of ‘jump’s in time t]. For $\alpha > 2$ both, the first and the second moments of the ‘jump’ time distributions are finite and are given by $\alpha/(\alpha - 1)$ and $\alpha/(\alpha - 2)$, respectively. Consequently, the number of ‘jump’s in a large time interval is typically $m_t \sim t/\langle\tau\rangle = t(\alpha - 1)/\alpha$ using which one gets diffusive growth of the variance

$$\sigma_x^2(t) \sim \langle\eta^2\rangle\langle\tau^2\rangle \times \left[t \frac{(\alpha - 1)}{\alpha} \right] \sim \frac{(\alpha - 1)}{(\alpha - 2)} \sigma^2 t.$$

For α in the intermediate regime $1 < \alpha < 2$ the mean $\langle\tau\rangle = \alpha/(\alpha - 1)$ is finite but all higher order moments are divergent. These divergent higher order moments of the waiting time distribution give rise to the superdiffusive behaviour. For jump distributions with variance much smaller than the mean, it has been observed that the variance of the position gets the leading contributions from the last long ballistic jumps that has never changed till time t [[14, 28](#)]. In our case also we find that the leading contribution to the variance of the position $\sigma_x^2(t)$ comes from the tail of the distribution where trajectories with ‘jumps’ of duration $\sim \mathcal{O}(t)$ contribute. As shown in the [sec. 4.1.3.2](#) later, the behaviour of the distribution $P(x, t)$ has different scaling forms in the central part (Eq. [\(62\)](#)) and at the tails (Eq. [\(64\)](#)). Using these forms of the distribution, it is easy to show that the variance of the position for large t grows as $\sigma_x^2(t) \propto t^{3-\alpha}$.

Alternatively, this large t growth can be obtained from the two-point velocity correlation function as well. For $1 < \alpha \leq 2$, it is possible to show that the velocity-velocity correlation function decays slowly as a power-law

$$C_{vv}(t_1, t_2) \sim |t_1 - t_2|^{1-\alpha}, \quad (40)$$

(see [Appendix G.2.2](#) for details). Plugging this result into $\sigma_x^2(t) = \langle x^2(t) \rangle_c = 2 \int_0^t dt_1 \int_{t_1}^t dt_2 C_{vv}(t_1, t_2)$ and performing the integrations, we reproduce the behaviour of the variance $\propto t^{3-\alpha}$ for $1 < \alpha < 2$ and $\propto t \ln(t)$ for $\alpha = 2$ respectively.

3.3.2 For $r = -1$

For this case also we follow the same procedure as done for $r = 0$. We find the large t behaviour of $\sigma_x^2(t)$ from the small s behaviour of $\tilde{\sigma}_x^2(s)$. Performing inverse Laplace transform we get

$$\tilde{\sigma}_x^2(s) \underset{s \rightarrow 0}{\simeq} \begin{cases} \frac{2\sigma^2}{\Gamma(1-\alpha)} \frac{1}{s^{3+\alpha}} \\ \frac{2\sigma^2}{s^4} \frac{1}{1-\gamma e^{-\ln(s)}} \\ \frac{2\sigma^2}{s^4} \left(\frac{\alpha-1}{\alpha} \right) \end{cases} \xrightarrow{\mathcal{L}_t^{-1}} \sigma_x^2(t) \underset{t \rightarrow \infty}{\simeq} \begin{cases} \frac{2\sigma^2}{\Gamma(1-\alpha)\Gamma(3+\alpha)} t^{2+\alpha} & \text{for } \alpha < 1 \\ \frac{\sigma^2 t^3}{3 \ln(t)} & \text{for } \alpha = 1 \\ \frac{\sigma^2(\alpha-1)}{3\alpha} t^3 & \text{for } \alpha > 1. \end{cases} \quad (41)$$

In this case the variance of the position shows super-diffusive behaviour for all ranges of α . We observe that the exponent of super-diffusive growths depends on α for $0 < \alpha < 1$, whereas it becomes independent of it for $\alpha > 1$ with a logarithmic correction to $\propto t^3$ behaviour for $\alpha = 1$. These late time asymptotic behaviours of $\sigma_x^2(t)$ are verified numerically in fig. 6(b) for different values of α from the three regimes mentioned in Eq. (41) and we observe excellent agreement.

As can be observed from Eq. (1) that, for $r = -1$ the velocity after i^{th} ‘jump’ event is given by $v_i = \sum_{l=0}^i \eta_l$ and the velocity after $j^{\text{th}} (> i)$ ‘jump’ event is given by $v_j = v_i + \sum_{l=j+1}^i \eta_l$ for $j > i > 0$. Hence the two point velocity correlation $C_{vv}(t_1, t_2)$ is given by $C_{vv}(t_1, t_2) = \langle v_{n(\min(t_1, t_2))}^2 \rangle_c Q_{-1}(|t_1 - t_2|)$, where $n(\min(t_1, t_2))$ is the number of ‘jump’ events till time $\min(t_1, t_2)$. This can be seen from Eq. (G.11) of Appendix G where we note that $Q_{-1}(t) = 1$. From Eq. (38) it is easy to see that $\langle v_{n(\min(t_1, t_2))}^2 \rangle_c = \sigma^2 \langle n(\min(t_1, t_2)) \rangle$. The average number of events $\langle n(t) \rangle$ till time t can be computed from its Laplace transform $\widetilde{\langle n \rangle}(s) = \widetilde{\Psi}(s) \sum_{m=0}^{\infty} m \tilde{\psi}^m(s) = \frac{\tilde{\Psi}(s) \tilde{\psi}(s)}{(1 - \tilde{\psi}(s))^2}$ where $\tilde{\psi}(s)$ is the Laplace transform of the distribution $\rho(\tau)$ of the ‘jump’ duration and $\tilde{\Psi}(s) = \frac{1 - \tilde{\psi}(s)}{s}$. Hence $\widetilde{\langle n \rangle}(s) = \frac{\tilde{\psi}(s)}{s(1 - \tilde{\psi}(s))}$. Since we are interested in the large t behaviour of $\sigma_x^2(t)$, we require the large t behaviour of $\langle n(t) \rangle$ as well and for that we focus on the small s behaviour of $\tilde{\psi}(s)$ which are given in Eq. (16). Using these relations and performing the inverse Laplace transforms we get

$$\langle n(t) \rangle \simeq \begin{cases} \left(\frac{\text{Sin}(\pi\alpha)}{\pi\alpha} \right) t^\alpha & \text{for } \alpha < 1 \\ t \text{Log}^{-1}(t) & \text{for } \alpha = 1 \\ \left(\frac{\alpha-1}{\alpha} \right) t & \text{for } \alpha > 1 \end{cases} \quad \text{for large } t. \quad (42)$$

Thus we get explicit expressions of the two-point velocity correlation $C_{vv}(t_1, t_2) = \sigma^2 \langle n(\min(t_1, t_2)) \rangle$ for different values of α . We now use these expressions in the relation between $\sigma_x^2(t)$ and $C_{vv}(t_1, t_2)$ given in Eq. (38) and, performing the integrations we reproduce the superdiffusive growths of the variance of the position for different values of α as announced in Eq. (41). Note that for $\alpha > 1$ we once again observe agreement with RAP *i.e.* t^3 scaling for the variance of the position (see Appendix F for definition and properties of RAP).

3.3.3 For $r = 1$

Following a similar procedure like the previous two cases we, in this case, find the

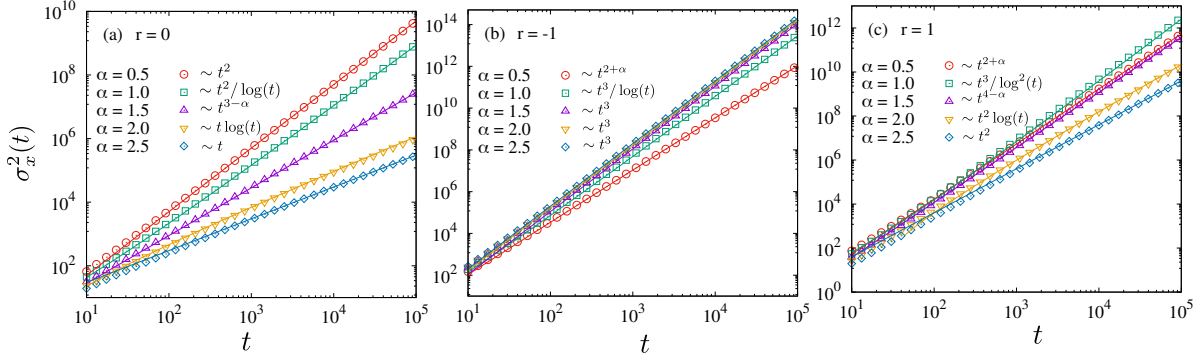


Figure 6. (Color online). Variance of position $\sigma_x^2(t)$ are plotted for different r and α . Symbols are from numerical simulation and the solid lines are the corresponding analytical results from Eqs. (39), (41) and (43) respectively.

following large t asymptotic behaviour of the variance $\sigma_x^2(t)$:

$$\tilde{\sigma}_x^2(s) \underset{s \rightarrow 0}{\simeq} \begin{cases} \frac{(1-\alpha)}{\Gamma(1-\alpha)} \frac{2\sigma^2}{s^{3+\alpha}} \\ \frac{2\sigma^2}{s^4(1-\gamma_e - \ln(s))^2} \\ \frac{(\alpha-1)^2 \Gamma(2-\alpha)}{\alpha^2} \frac{2\sigma^2}{s^{5-\alpha}} \\ -\frac{\sigma^2}{4s^3} (3 + 2\gamma_e + 2 \ln(s)) \\ \frac{\sigma^2}{\alpha(\alpha-2) s^3} \end{cases} \xrightarrow{\mathcal{L}_t^{-1}} \sigma_x^2(t) \underset{t \rightarrow \infty}{\simeq} \begin{cases} \frac{2\sigma^2(1-\alpha)}{\Gamma(1-\alpha)\Gamma(3+\alpha)} t^{2+\alpha} & \text{for } 0 < \alpha < 1 \\ \frac{\sigma^2 t^3}{3 \ln^2(t)} & \text{for } \alpha = 1 \\ \frac{2\sigma^2 \Gamma(2-\alpha)}{\Gamma(5-\alpha)} \left(\frac{\alpha-1}{\alpha}\right)^2 t^{4-\alpha} & \text{for } 1 < \alpha < 2 \\ \frac{1}{4} \sigma^2 t^2 (\ln(t) - 3) & \text{for } \alpha = 2 \\ \frac{\sigma^2 t^2}{2\alpha(\alpha-2)} & \text{for } \alpha > 2. \end{cases} \quad (43)$$

Once again these results are verified numerically in fig. 6(c) for α values lying in different regimes in Eq.(43).

Although the variance of the velocity $\sigma_v^2(t)$ is same for $r = \pm 1$, from Eqs. (41) and (43) we see the behaviour of $\sigma_x^2(t)$ are different for them. The growth of the variance $\sigma_x^2(t)$ increases with time with a α dependent exponent within the range $0 < \alpha < 1$. The exponent becomes maximum at $\alpha = 1$ with a logarithmic correction to $\sim t^3$ behaviour. Within the range $1 < \alpha < 2$ this exponent decreases as $\sim (4 - \alpha)$ and becomes α independent for $\alpha \geq 2$ with another logarithmic correction for $\alpha = 2$. In the following we try to understand the qualitative behaviour of the variance of the position in different regimes of α .

As done for $r = -1$ case in the previous sec. 3.3.2, in this case also starting from Eq. (1), one can easily see that the two point velocity correlation is given by $C_{vv}(t_1, t_2) \simeq \langle v_{n(\min(t_1, t_2))}^2 \rangle_c Q_1(|t_1 - t_2|)$ as derived in Eq. (G.10) of Appendix G for general r . Unlike the $r = -1$ case in this case $Q_1(t)$ is not equal to one in general. However, for $0 < \alpha < 1$ the dominant contribution to $Q_1(|t_1 - t_2|)$ comes from the event in which there are typically no ‘jump’ events in the time interval $|t_1 - t_2|$. This happens because for large t_1 and t_2 , the interval $|t_1 - t_2|$ typically falls in the last incomplete step which is usually the largest. Hence in this case also we approximate $Q_1(|t_1 - t_2|) \simeq 1$. Thus the velocity correlation function $C_{vv}(t_1, t_2) \simeq \sigma^2 \langle n(\min(t_1, t_2)) \rangle \simeq \sigma^2 \min(t_1, t_2)^\alpha$

as found in the previous sec. 3.3.2 [see after Eq. (42)]. An alternative derivation of this result for $C_{vv}(t_1, t_2)$ is given in Appendix G.2.3. Using this expression in Eq. (38) and, performing the integrations we reproduce the superdiffusive behaviour $\sim t^{2+\alpha}$ as announced in Eq. (43) which obviously is same as for $r = -1$ in the $0 < \alpha < 1$ range.

A little more rigorous argument can be presented for the superdiffusive behaviour $\sim t^{2+\alpha}$ of $\sigma_x^2(t)$ for $r = 1$ in the regime $0 < \alpha < 1$. As has been encountered, in this case the dominant contribution to the position comes from the largest jump duration τ_{\max} within time t . Evidence of this fact will be provided in sec. 4.2.3.1 [see fig. 13 bottom panel] where we study the distribution $P(x, t)$ of the position. So writing $x(t) \simeq v_l \tau_{\max}$ where τ_{\max} is the duration of the largest jump and v_l is the velocity of the particle during this jump event. If in a particular trajectory, the particle makes m jumps then this longest jump could happen at any of the steps or at the last incomplete step. Using this information one can compute the variance $\sigma_x^2(t)$. The Laplace transform of this variance is given by

$$\begin{aligned} \tilde{\sigma}_x^2(s) &\simeq \sum_{m=0}^{\infty} \left[\left\langle \left(\mathbb{I}(m \geq 1) \sum_{l=0}^{m-1} \langle v_l^2 \rangle \tau_l^2 + \langle v_l^2 \rangle \tau_m^{*2} \right) e^{-s(\tau_0 + \tau_1 + \dots + \tau_{m-1} + \tau_m^*)} \right\rangle \right] \\ &= \frac{\sigma^2}{s(1 - \tilde{\psi}(s))^2} \left(\tilde{\psi}''(s) + s \tilde{\Psi}''(s) \right), \end{aligned} \quad (44)$$

where we have used $\langle v_l^2 \rangle = \sigma^2(l+1)$ for $r = 1$. Given that there are m number of jump events within time t , the first term inside the first parenthesis corresponds to the case when the particle makes the longest jump at the l th step and the second term corresponds to the case when longest jump occurs at the last incomplete step.

Recalling $\tilde{\Psi}(s) = (1 - \tilde{\psi}(s))/s$ and using $\tilde{\psi}(s) \simeq 1 - \Gamma(1 - \alpha)s^\alpha$ in Eq. (44) we get $\tilde{\sigma}_x^2(s) \simeq \frac{2\sigma^2(1-\alpha)}{\Gamma(1-\alpha)s^{3+\alpha}}$ (for small s) which after performing inverse Laplace transform would provide $\sigma_x^2(t) \simeq \frac{2\sigma^2(1-\alpha)}{\Gamma(1-\alpha)\Gamma(3+\alpha)}t^{2+\alpha}$ for large t .

We now focus for $1 < \alpha \leq 2$, in which regime it is clear that one can not approximate $Q_1(|t_1 - t_2|) \simeq 1$. In fact it is possible to show that the two-point velocity correlation function behaves for large t_1, t_2 as

$$C_{vv}(t_1, t_2) \sim \min\{t_1, t_2\} |t_1 - t_2|^{1-\alpha} \quad (45)$$

(see Eq. (G.21) in Appendix G.2.3). Using this result in Eq. (38) and performing the integrals, one can easily recover large t behaviours $\sigma_x^2(t) \propto t^{4-\alpha}$ for $1 < \alpha < 2$ and $\propto t^2 \ln(t)$ and for $\alpha = 2$.

On the other hand, for $\alpha > 2$, the behaviour of $\sigma_x^2(t) \propto t^2$ dominates over the $\sigma_x^2(t) \propto t^{4-\alpha}$, *i.e.*, the variance shows ballistic growth with time as in case II. The explanation of this behaviour is similar to that of the exponential case discussed in sec. 3.2.

4 PDF of the position

We now study the distribution of the position. Like earlier two sections, here also we discuss three different cases of $\rho(\tau)$ separately for three limiting values of $r = 0, -1$ and

1. We start with $r = 0$ case.

4.1 For $r = 0$

This case is relatively simpler than $r = \pm 1$ because for the later case the velocity of the particle at different time gets correlated as we have seen earlier. From Eq. (1), it is possible to see that the position after m th jump event can be described by a simple random walk of independent steps *i.e* $x_m = \sum_{j=0}^{m-1} \xi_j$ where $\xi_j = \eta_j \tau_j$. Clearly, ξ is a random variable which is a multiplication of two independent random variables τ and η . The distribution of $\xi = \eta\tau$ can be easily computed as

$$\varrho(\xi) = \int_0^\infty d\tau \rho(\tau) \int_{-\infty}^\infty d\eta p(\eta) \delta(\xi - \eta\tau), \quad (46)$$

where recall $p(\eta)$ is Gaussian given in Eq. (2) and $\rho(\tau)$ for the three cases are given in Eq. (3). Since τ is a positive random variable and the distribution of η is symmetric about zero, the distribution of ξ is also symmetric about zero. The characteristic function $\lambda(k)$ of $\varrho(\xi)$ is defined as

$$\lambda(k) = \langle e^{ik\xi} \rangle_{\varrho(\xi)} = \int_{-\infty}^\infty d\xi e^{ik\xi} \varrho(\xi), \quad (47)$$

which will be used later.

4.1.1 Case I: $\rho(\tau) = \delta(\tau - a)$

In this case the number of complete steps in time t is $[t/a]$ where $[z]$ represents the largest integer but not larger than z . It is easy to see from Eq. (46) that the position in each step is a Gaussian random variable (RV) with the variance $a^2\sigma^2$. The position made by the particle in the last incomplete step is also a Gaussian RV with variance $u^2\sigma^2$ where $u = t - a[t/a]$. Hence, the distribution of the position at time t is a Gaussian distribution with variance $([t/a]a^2 + u^2)\sigma^2 \simeq a\sigma^2 t$ for large t which describes typical fluctuations. The tails of the distribution should be described by an appropriate Large deviation function

4.1.2 Case II: $\rho(\tau) = \beta e^{-\beta\tau}$

We recall that in this case $\rho(\tau) = \beta e^{-\beta\tau}$, inserting which in Eq. (46) one finds that the distribution of ξ is given by

$$\begin{aligned} \varrho_1(u) &= \int_0^\infty d\tau \rho(\tau) \int_{-\infty}^\infty d\eta p(\eta) \delta(\xi - \eta\tau) \\ &= \frac{\beta}{\sqrt{2\pi\sigma^2}} \int_0^\infty \frac{d\tau}{\tau} \exp\left[-\beta\tau - \frac{\xi^2}{2\sigma^2\tau^2}\right] \end{aligned} \quad (48)$$

which is a symmetric distribution and decays for large $|\xi|$ as $\varrho(\xi) \propto |\xi|^{-1/3} \exp[-3/2 (|\xi|\beta/\sigma)^{2/3}]$. Hence, by virtue of central limit theorem, the fluctuation

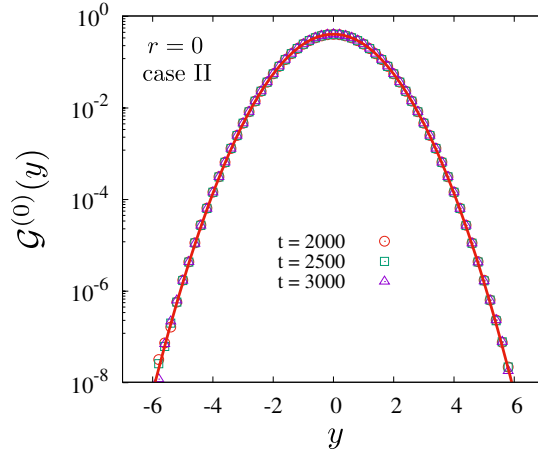


Figure 7. (Color online). Probability distribution function of scaled position $y = x/\sqrt{2\sigma^2 t/\beta}$ are plotted for $r = 0$ with exponential waiting time distribution. Symbols are from numerical simulation which show good agreement with the analytical prediction (red solid line) given in Eq. (49).

of the position x_m after m ‘jump’ events is Gaussian with variance $\langle x_m^2 \rangle = 2m(\sigma/\beta)^2$ and mean zero. On the other hand, since each τ is chosen from exponential distribution, the average time duration between two successive steps is β^{-1} and the number of steps taken by the particle till time t is typically of the order of $m \sim \beta t$ for large t . As a result for large t , the distribution of the position $x(t)$ made by the particle till time t is a Gaussian distribution with zero mean and variance $\simeq \langle x_{[\beta t]}^2 \rangle_c \simeq 2\sigma^2 t/\beta$ *i.e.*

$$P(x, t) \simeq \sqrt{\frac{\beta}{2t\sigma^2}} \mathcal{G}^{(0)}\left(\frac{x}{\sqrt{2\sigma^2 t/\beta}}\right), \text{ where, } \mathcal{G}^{(0)}(y) = \frac{1}{\sqrt{2\pi}} \exp\left[-\frac{y^2}{2}\right]. \quad (49)$$

This result is verified numerically in fig. 7. For a more detailed calculation of $P(x, t)$ in this case, see Appendix I. It is known that for x really large, the distribution $P(x, t)$ can not be described by the above Gaussian form but in terms of a Large deviation function $\Phi_{II}(x/t)$ such that $P(x, t) \asymp e^{-t\Phi_{II}(x/t)}$ with $\Phi_{II}(v) = \min_k [ikv - \beta \ln \lambda(k)]$ [43].

4.1.3 Case III: $\rho(\tau) = \alpha\tau^{-(1+\alpha)}$

In this case the distribution of jump time durations is given by $\rho(\tau) = \alpha\tau^{-(1+\alpha)}$ (see Eq. (3)). Inserting this distribution in Eq. (46) we get

$$\varrho(\xi) = \frac{\alpha}{\sqrt{2\pi\sigma^2}} \int_1^\infty \frac{d\tau}{\tau^{1+\alpha}} \int_{-\infty}^\infty dv e^{-v^2/2\sigma^2} \delta(\xi - v\tau) \quad (50)$$

$$= \frac{\alpha}{2\sqrt{2\pi\sigma^2}} \left(\frac{2\sigma^2}{\xi^2}\right)^{\frac{1+\alpha}{2}} \gamma\left(\frac{1+\alpha}{2}, \frac{\xi^2}{2\sigma^2}\right) \quad (51)$$

where $\gamma(s, z)$ is the incomplete gamma function defined by $\gamma(s, z) = \int_0^z dw e^{-w} w^{s-1}$. The distribution $\varrho(\xi)$ at the tails $|\xi|$ decays as

$$\varrho(\xi \rightarrow \pm\infty) \simeq \frac{\alpha}{2\sqrt{2\pi\sigma^2}} \Gamma\left(\frac{\alpha+1}{2}\right) \left(\frac{2\sigma^2}{\xi^2}\right)^{\frac{\alpha+1}{2}}. \quad (52)$$

As realised earlier, in this case the position can be described by a Lévy walk with velocity chosen from a Gaussian distribution of variance σ^2 [16, 24–26]. As also mentioned earlier, in our case the velocity distribution has zero mean and non-zero variance σ^2 . The characteristic function of the distribution $\varrho(\xi)$ in Eq. (51) is given by

$$\begin{aligned} \lambda(k) &= \int_{-\infty}^{\infty} d\xi e^{ik\xi} \varrho(\xi) = \frac{\alpha}{2} \left(\frac{k^2\sigma^2}{2}\right)^{\frac{\alpha}{2}} \Gamma\left(-\frac{\alpha}{2}, \frac{k^2\sigma^2}{2}\right) \\ &\underset{k \rightarrow 0}{\simeq} \begin{cases} 1 - \frac{1}{2}\mathcal{D}_\alpha \sigma^\alpha |k|^\alpha + \mathcal{O}(k^2) & \text{for } \alpha < 2 \\ 1 + \frac{1}{2}\sigma^2 k^2 \ln(|k|^2) + \mathcal{O}(k^2) & \text{for } \alpha = 2, \\ 1 - \frac{1}{2}\mathcal{D}_\alpha \sigma^2 k^2 + \mathcal{O}(|k|^\alpha) & \text{for } \alpha > 2 \end{cases} \quad \text{with} \quad (53) \\ \mathcal{D}_\alpha &= \begin{cases} \left|\frac{\alpha}{2^{\alpha/2}} \Gamma\left(-\frac{\alpha}{2}\right)\right|, & \text{for } 1 < \alpha < 2 \\ \frac{\alpha}{\alpha-2}, & \text{for } \alpha > 2. \end{cases} \end{aligned}$$

Here, $\Gamma(s, z)$ represents the upper incomplete gamma function $\Gamma(s, z) = \Gamma(s) - \gamma(s, z)$.

4.1.3.1 For $0 < \alpha < 1$:

In this domain of α , all the moments of the waiting time distribution diverge. We expect that in this case, for a given large but finite t , the number of jump events are not proportional to t (see Eq. (42)). The final position $x(t)$ of the walker gets the most dominant contribution from the displacement made in the largest jump duration $\tau_{\max}(< t)$. Consequently, we expect the distribution of the position $P(x, t)$ of the walker would be given by the distribution of the position $\Delta_{\max} = \eta\tau_{\max}$ made in the largest jump duration in the interval $[0, t]$. Since for large t , τ_{\max} is typically of the order of t , it is expected to have a ballistic scaling for the position distribution $P(x, t)$ *i.e.*

$$P(x, t) \simeq \frac{1}{t} \mathbb{G}_{\alpha < 1}^{(0)}\left(\frac{x}{t}\right). \quad (54)$$

Such ballistic scaling have been discussed in previous studies of Lévy walks [26, 27]. In fact for arbitrary velocity distribution $p(\eta)$, a general exact but implicit expression for the scaling distribution $\mathbb{G}_{\alpha < 1}^{(0)}$ has been obtained as [29]

$$\mathbb{G}_{\alpha < 1}^{(0)}(y = x/t) = -\frac{1}{\pi} \lim_{\epsilon \rightarrow 0} \text{Im} \frac{\int_{-\infty}^{\infty} d\eta p(\eta) (y + i\epsilon - \eta)^{\alpha-1}}{\int_{-\infty}^{\infty} d\eta p(\eta) (y + i\epsilon - \eta)^\alpha}. \quad (55)$$

Recall in this paper we consider $p(\eta)$ to be a zero mean Gaussian with variance σ^2 . From this expression one can in principle compute the scaling distribution but it is difficult

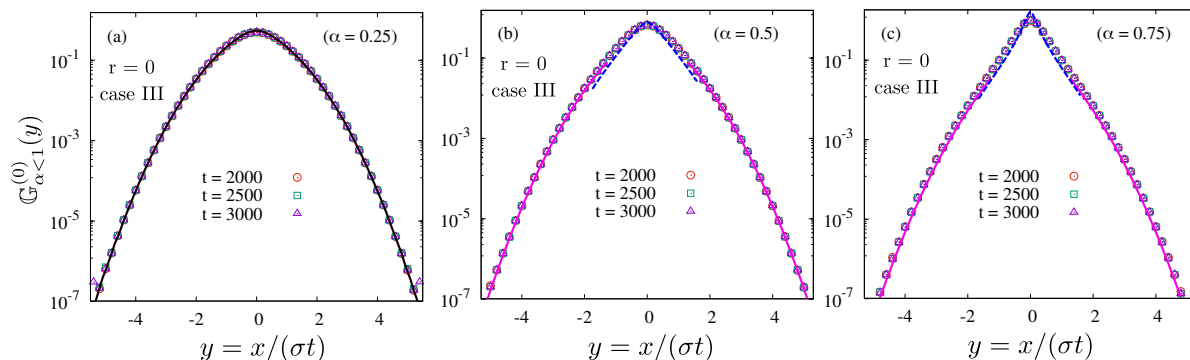


Figure 8. (Color online). PDF of the scaled position $y = x/(\sigma t)$ are plotted for $r = 0$ and for (a) $\alpha = 0.25$, (b) $\alpha = 0.5$ and (c) $\alpha = 0.75$. In panel (a), we compare the distribution of $x(t)$ (symbols) and the distribution $\Delta_{\max}(t)$ (black solid line). The excellent agreement justifies the dominant contribution of the displacement Δ_{\max} made in the longest jump duration to the final position $x(t)$ for large t . In panels (b) and (c), we verify our theoretical expressions of the distribution $P(x, t)$ in Eq. (60) with numerical simulation. In both plots symbols correspond to simulation data whereas the blue dashed line around the central part and the magenta solid lines at the tails of the distribution, respectively, correspond to analytical expressions given in Eq. (60) along with Eq. (60).

to find an explicit form. However, from the distribution of Δ_{\max} it is possible to obtain an approximate but more explicit expression of the distribution $P(x, t)$.

A numerical verification of the fact that the distribution of $\Delta_{\max} = \eta\tau_{\max}(t)$ describes the distribution of the final position $x(t)$ well, is presented in fig. 8(a) where for $\alpha = 0.25$ the scaling distribution of the position is compared with the scaling distribution of $\Delta_{\max}(t)$. The symbols are obtained from the direct numerical simulation of the dynamics in Eqs. (4-7) and corresponds to the (scaled) distribution of the position $x(t)$ whereas the solid (red) lines correspond to the (scaled) distribution of $\Delta_{\max} = \eta\tau_{\max}(t)$ also obtained numerically. We observe excellent match between the two which justifies the arguments given in the previous paragraph.

For given realisation of the trajectory of length t , the duration τ_{\max} depends on t as can be clearly seen from the definition $\tau_{\max}(t) = \max[\tau_0, \tau_1, \dots, \tau_{m(t)-1}, \tau_{m(t)}^*]$ where $m(t)$ is the number of jumps occurred within time t in that particular trajectory and $\tau_{m(t)}^*$ is the duration of the last incomplete jump. If $\mathcal{P}(\tau_{\max}|t)$ denotes the distribution of τ_{\max} then, using the above arguments we write

$$\begin{aligned}
 P(x, t) &\simeq \int_{-\infty}^{\infty} d\eta p(\eta) \int_1^t d\tau_{\max} \mathcal{P}(\tau_{\max}|t) \delta(x - \eta\tau_{\max}) \\
 &\simeq \int_1^t \frac{d\tau_{\max}}{\tau_{\max}} \mathcal{P}(\tau_{\max}|t) p\left(\frac{x}{\tau_{\max}}\right).
 \end{aligned} \tag{56}$$

What is the distribution $\mathcal{P}(\tau_{\max}|t)$ of τ_{\max} for given t ? This quantity has recently been studied in detail in Ref: [36] where it has been shown that for large t this distribution

satisfy the following scaling form

$$\mathcal{P}(\tau_{\max}|t) = \frac{1}{t} f_{\alpha} \left(\frac{\tau_{\max}}{t} \right), \quad (57)$$

with $f_{\alpha}(w)$ having the following asymptotic forms [36]

$$f_{\alpha}(w) \simeq \begin{cases} \frac{c_{\alpha}}{\alpha w^2} e^{-c_{\alpha}/w}, & \text{for } w \rightarrow 0^+ \\ \frac{\text{Sin}(\pi\alpha)}{\pi} (1-w)^{\alpha-1} \Theta(1-w), & \text{for } w \rightarrow 1^- \end{cases} \quad (58)$$

Here $\Theta(x)$ is Heaviside theta function and c_{α} is a constant obtained from the solution of ${}_1F_1(1; 1-\alpha; -c_{\alpha}) = 0$. Here ${}_1F_1(a; b; x)$ is hypergeometric function. Inserting the expression of $\mathcal{P}(\tau_{\max}|t)$ from Eq. (56) along with Eq. (58) and using the explicit form of $p(\eta)$ from Eq. (2), we get

$$P(x, t) \simeq \frac{1}{t} \mathbb{G}_{\alpha < 1}^{(0)} \left(\frac{x}{t} \right) \quad \text{where} \\ \mathbb{G}_{\alpha < 1}^{(0)}(y) \simeq \frac{1}{\sqrt{2\pi\sigma^2}} \int_0^1 \frac{dw}{w} f_{\alpha}(w) \exp \left[-\frac{y^2}{2\sigma^2 w^2} \right]. \quad (59)$$

for large t . Using the asymptotic forms of $f_{\alpha}(w)$ from Eq. (58) in the above equation we get the approximate forms of the scaling function $\mathbb{G}_{\alpha < 1}^{(0)}(y)$ in different asymptotic regimes. The $w \rightarrow 0$ asymptotic of $f_{\alpha}(w)$ provide us the central part of the scaling distribution $\mathbb{G}_{\alpha < 1}^{(0)}(y)$ valid for small $|y|$ whereas the asymptotic form of $f_{\alpha}(w)$ for $w \rightarrow 1$ provides $\mathbb{G}_{\alpha < 1}^{(0)}(y)$ for large $|y|$. We get,

$$\mathbb{G}_{\alpha < 1}^{(0)}(y) \simeq \begin{cases} \frac{c_{\alpha}}{\alpha\sqrt{2\pi\sigma^2}} \int_0^1 \frac{dw}{w^3} \exp \left[-\frac{c_{\alpha}}{w} - \frac{y^2}{2\sigma^2 w^2} \right], & \text{for } |y| \text{ small} \\ \frac{\Gamma(\alpha)}{\sqrt{2\pi\sigma^2}} \left(\frac{\text{Sin}(\pi\alpha)}{\pi} \right) \frac{\sigma^{2\alpha} \exp \left(-\frac{y^2}{2\sigma^2} \right)}{|y|^{2\alpha}}, & \text{for } |y| \text{ large.} \end{cases} \quad (60)$$

For $\alpha \rightarrow 0$, employing $\Gamma(\alpha) \text{Sin}(\pi\alpha) \rightarrow \pi$ in the above equation, one can easily show $\mathbb{G}_0^{(0)}(y) \underset{y \rightarrow \pm\infty}{\simeq} e^{-\frac{y^2}{2\sigma^2}} / \sqrt{2\pi\sigma^2} \simeq p(y)$ (see Eq. (18)). This behaviour is intuitively expected because for ($\alpha \rightarrow 0$) the first stem remains incomplete up to time t in almost all realizations which effectively makes $\mathcal{P}(\tau_{\max}|t) \simeq \delta(\tau_{\max} - t)$ for large t which can also be easily proved [36]. Using this result in Eq. (56) immediately implies $\mathbb{G}_{\alpha < 1}^{(0)}(y) \simeq p(y)$ for $\alpha \rightarrow 0$. The theoretical expression of $P(x, t)$ in Eq. (59) along with Eq. (60) is verified in fig 8(b) and fig. 8(c) where the magenta solid lines describe the tail behaviour and the blue dashed lines describe the central part. We observe nice agreement between theory and simulation. Note that the central regime becomes narrower as α decreases and the tail behaviour in Eq. (60) describes the distribution $P(x, t)$ over almost the entire region of y . As mentioned earlier, most of the earlier works of finding $P(x, t)$ for $0 < \alpha < 1$ have considered velocity distribution of the form $p(v) = 1/2(\delta(v - v_0) + \delta(v + v_0))$ [25, 26] with constant magnitude for which the distribution $P(x, t)$ is supported over finite range $-v_0 t \leq x \leq v_0 t$ and has a minimum at the center (U-shape) with integrable singularities (called ‘‘chubchiks’’) at the edges of the interval [26, 27]. This is in sharp contrast with

what we obtain for Gaussian velocity distribution $p(v) = e^{-v^2/2\sigma^2}/\sqrt{2\pi\sigma^2}$. We get $P(x, t)$ defined over $-\infty \leq x \leq \infty$ with a peak at the center $x = 0$ and decaying as power law for $|x| \rightarrow \infty$ as shown in fig. 8.

4.1.3.2 For $\alpha > 1$

We first note that for $\alpha > 1$, the waiting time distribution $\rho(\tau)$ has finite mean $\langle \tau \rangle = \alpha/(\alpha - 1)$. This implies that within a large time t the number of jump events on an average is $t/\langle \tau \rangle$. Following a similar procedure as done for case II with $r = 0$ (see sec. 4.1.2), it is possible to write the following approximate equation for the distribution $P(x, t)$ for large t

$$P(x, t) \simeq \frac{1}{2\pi} \int_{-\infty}^{\infty} dk \exp \left[-ikx + \frac{t}{\langle \tau \rangle} \ln \lambda(k) \right]. \quad (61)$$

where $\lambda(k)$ is given in Eq. (53). Note that small k behaviour of $\lambda(k)$ is different for $\alpha < 2$ and $\alpha > 2$. So we need to perform the above integral separately for these cases. Executing this integral we find that for $\alpha > 1$, the position distribution $P(x, t)$ satisfies the following scaling form [14, 26–28]

$$P(x, t) \simeq \left(\frac{\langle \tau \rangle}{\mathcal{D}_\alpha \sigma^{\alpha_0} t} \right)^{\frac{1}{\alpha_0}} H_{\alpha_0} \left[x \left(\frac{\langle \tau \rangle}{\mathcal{D}_\alpha \sigma^{\alpha_0} t} \right)^{\frac{1}{\alpha_0}} \right], \quad \text{where} \\ H_{\alpha_0}(y) = \frac{1}{2\pi} \int_{-\infty}^{\infty} dk e^{-iky - \frac{|k|^{\alpha_0}}{2}}, \quad \text{and } \alpha_0 = \min(\alpha, 2), \quad (62)$$

with \mathcal{D}_α is given in Eq. (53). This scaling form is valid for $\alpha > 1$ except for $\alpha = 2$ where we expect some $\ln(t)$ dependence in the distribution (see remarks later). Also this scaling function should describe the central part of the distribution $P(x, t)$ well *i.e.* for $|x| \lesssim \mathcal{O}(t^{1/\min(\alpha, 2)})$. Note that for $\alpha < 2$ the scaling function $H_\alpha(y)$ is Lévy stable Law which has a power law tail $H_\alpha(y) \sim 1/|y|^{1+\alpha}$ [11, 44] which, as will see, smoothly connects to the tail of $P(x, t)$. On the other hand for $\alpha > 2$ it is a Gaussian of mean zero and unit variance *i.e.* $H_2(y) = G(y)$ as in Eq. (18). The above scaling behaviour of $P(x, t)$ in the central part is verified numerically in fig. 9(a) for $\alpha = 1.5$ where we observe excellent agreement.

The behavior of $P(x, t)$ for Lévy walks with constant speed has widely been studied for $1 < \alpha < 2$ [14–16, 24–28]. Cases with velocity distributions different from the ones with constant magnitude of speed have also been investigated in detail in Refs. [14, 28]. It has been observed that the central part of the PDF $P(x, t)$ is universal across velocity distributions (with finite mean). However the behavior of the ballistic region at the tail depends strongly on the choice of the velocity distribution [14, 28]. As mentioned earlier, most of the investigations are made in the limit $v_0 \gg \sigma$ where v_0 and σ are the mean speed and standard deviation of velocity [28]. In such cases, one observes bumps corresponding to those trajectories which have never changed velocity since the start. These bumps move ballistically with speed v_0 on both sides of the origin. Remember, in our case we consider Gaussian velocity distribution corresponding to the opposite limit

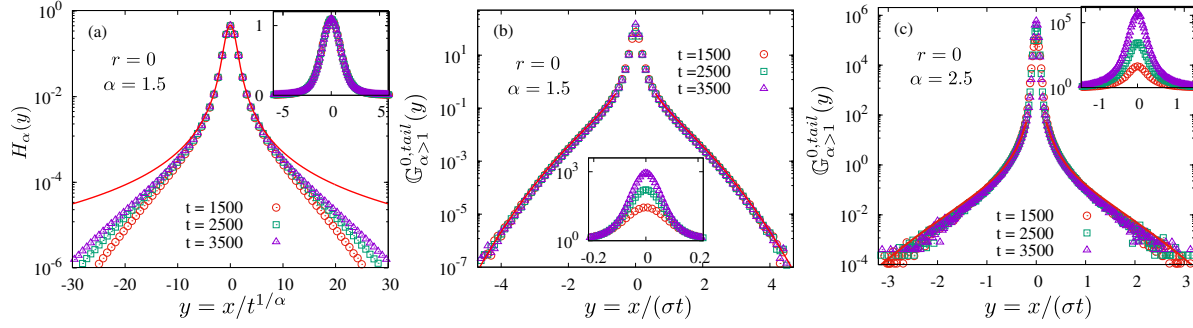


Figure 9. (Color online). In panel (a), PDF of scaled displacement $y \propto xt^{-1/\alpha}$, obtained from simulation (symbols), is compared with theoretical expression in Eq. (62) (red solid line) for $r = 0$ and $\alpha = 1.5$. The excellent agreement (shown in the inset) verifies the scaling behaviour described by Lévy stable function $H_\alpha(y)$ in the central part. Discrete symbols in this plot are the simulation result and the solid (red) line is the numerical result of the Lévy stable function $H_\alpha(y)$ defined in Eq. (62). In panels (b) and (c), we numerically verify the theoretical expressions for the tail behaviour of $P(x, t)$ given in Eq. (64) (solid red lines) for $\alpha = 1.5$ and $\alpha = 2.5$ with $r = 0$. Once again symbols in these plots are obtained from numerical simulation. In the inset of all the plots we have zoomed the distribution near the peak (in normal scale).

$v_0 < \sigma$. Hence, we expect different behaviours at the tail which we explore in the next.

Tail behaviour: Similar to $\alpha < 1$ case, in this regime ($\alpha > 1$) also we find that the dominant contributions to the tail of $P(x, t)$ come from the largest jump duration τ_{\max} for large t . Numerical evidence of this fact is provided in fig. 9(b) and fig. 9(c) for $\alpha = 1.5$ and $\alpha = 2.5$ respectively. The distribution $\mathcal{P}_\tau(\tau_{\max}|t)$ of largest time interval $\tau_{\max}(t)$ within time t for $\alpha > 1$ is given by [36]

$$\mathcal{P}_\tau(\tau_{\max}|t) \simeq \frac{t}{\langle \tau \rangle} \frac{\alpha}{\tau_{\max}^{\alpha+1}} \exp \left[-\frac{t}{\langle \tau \rangle} \tau_{\max}^{-\alpha} \right]. \quad (63)$$

Using this result in Eq. (56) along with $\langle \tau \rangle = \alpha/(\alpha-1)$ and the explicit form of Gaussian velocity distribution we get following scaling form valid for $|x| \gtrsim \sigma t$

$$P(x, t) \simeq \frac{1}{\sigma t^\alpha} \mathbb{G}_{\alpha>1}^{(0),tail} \left(\frac{x}{\sigma t} \right) \quad \text{where} \\ \mathbb{G}_{\alpha>1}^{(0),tail}(y) \simeq \frac{(\alpha-1)}{2\sqrt{2\pi}} \left(\frac{2}{y^2} \right)^{\frac{1+\alpha}{2}} \Gamma \left(\frac{1+\alpha}{2}, \frac{y^2}{2} \right). \quad (64)$$

This result is verified numerically for $\alpha = 1.5$ and $\alpha = 2.5$ in figs. 9(b) and (c) respectively, where red solid lines correspond to the above analytical expression and the symbols are obtained from numerical simulation. It is interesting to observe that for $1 < \alpha < 2$ the form of the distribution $P(x, t)$ at the tails smoothly connects to the form of the distribution in the central part. This can be seen by comparing the $y \rightarrow \infty$ asymptotic of the central part in Eq. (62) with the $y \rightarrow 0$ asymptotic of the tail part in Eq. (64). To do so, we define $y_c = (\langle \tau \rangle / \mathcal{D}_\alpha)^{1/\alpha} \times x / (\sigma t^{1/\alpha})$ to denote the scaling variable in the central part and $y_t = x / (\sigma t)$ for the tail part. Note that these

two variables are related via $y_c = y_t \times t^{1-1/\alpha} (\langle \tau \rangle / \mathcal{D}_\alpha)^{1/\alpha}$. Now, using the asymptotic form of Lévy stable function [44]

$$H_\alpha(y_c) \underset{y_c \rightarrow \pm\infty}{\sim} \frac{\Gamma(1+\alpha) \text{Sin}(\pi\alpha/2)}{\pi |y_c|^{1+\alpha}}, \quad (65)$$

in Eq. (62) we express it in terms of y_t as

$$P(y_t) \underset{y_t \rightarrow \pm\infty}{\sim} \frac{(\alpha-1)}{2\sqrt{\pi}} \Gamma\left(\frac{1+\alpha}{2}\right) 2^{\alpha/2} \frac{t^{1-\alpha}}{|y_t|^{1+\alpha}}. \quad (66)$$

On the other hand from Eq. (64) we find

$$P(y_t) \underset{y_t \rightarrow 0}{\simeq} \frac{(\alpha-1)}{2\sqrt{\pi}} \Gamma\left(\frac{1+\alpha}{2}\right) 2^{\alpha/2} \frac{t^{1-\alpha}}{|y_t|^{1+\alpha}}, \quad (67)$$

which is exactly same as Eq. (66). Hence the central behaviour of $P(x, t)$ smoothly connects to the behaviour at the tails. Such matching does not happen for $\alpha > 2$, possibly indicating the existence of an intermediate regime which seems difficult to find exactly.

4.1.3.3 For $\alpha = 1$

For $\alpha = 1$ the mean and all the higher order moments of the waiting time distribution diverges. Like $\alpha < 1$, here also we numerically observe in fig. 10(a) that the dominant contribution of the total position $x(t)$ within time t is coming from the displacement associated with the largest jump time interval $\tau_{\max}(t)$ within time t (solid lines). The distribution of $\tau_{\max}(t)$ for $\alpha = 1$ can be written as

$$\mathcal{P}(\tau_{\max} = \tau|t) \simeq \frac{t(\ln(\tau) + 1)}{\tau^2(\ln \tau)^2} \text{Exp} \left[-\frac{t}{\tau \ln(\tau)} \right] \quad (68)$$

for large t (see Appendix J for details).

Although it seems difficult to find a scaling behavior of $\mathcal{P}(\tau_{\max}|t)$ as we got for $\alpha < 1$. However, it is possible to show from Eq. (68) that the distribution $P(x, t)$ at the tails (large $|x|$) poses a scaling form:

$$P(x, t) \simeq \frac{1}{\sigma t \ln(t)} \mathbb{G}_1^{(0), \text{tail}} \left(\frac{x}{\sigma t} \right) \quad \text{where} \\ \mathbb{G}_1^{(0), \text{tail}}(y) = \frac{1}{\sqrt{2\pi}} \int_0^1 \frac{dw}{w^3} \text{Exp} \left[-\frac{y^2}{2w^2} \right] = \frac{e^{-y^2/2}}{\sqrt{2\pi} y^2} \quad (69)$$

for large t at large y . This scaling result at the tails is plotted in fig. 10(b) where we once again observe good agreement.

4.1.3.4 For $\alpha = 2$

For $\alpha = 2$ one can compute the distribution $P(x, t)$ from Eq. (61) where $\lambda(k)$ is given in Eq. (53). From this equation we expect a $\ln(t)$ dependence in the variance $\sigma_x^2(t)$ as also observed in Eq. (39). In this case it turns out difficult to find any scaling form of

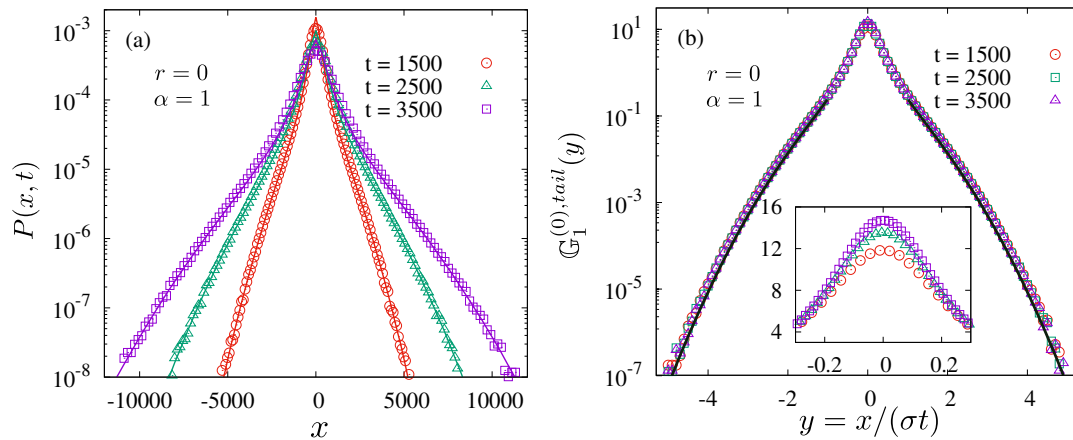


Figure 10. (Color online). **Panel (a):** Distributions of the position $x(t)$ (symbols) and the displacement $\Delta_{\max}(t)$ in the longest jump (solid lines) are plotted at different times for $\alpha = 1$ with $r = 0$. The good agreement verifies the approximation $x(t) \simeq \Delta_{\max}(t)$ for typical trajectories. **Panel (b):** The scaling behaviour distribution $P(x, t)$ at the tail described by $\mathbb{G}_1^{0, \text{tail}}(y)$ in Eq. (69), is verified numerically. Symbols are from numerical simulation and the solid black line represents analytical result. Inset shows zoomed version of the central part (in normal scale), exhibiting $x(t)$ does not scale ballistically there.

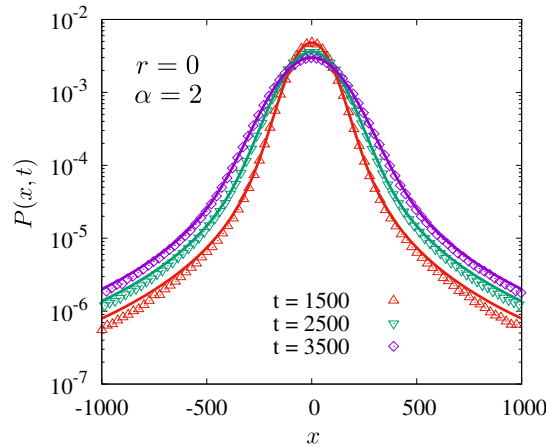


Figure 11. (Color online). PDF of the position $x(t)$ are plotted at different times for $r = 0$ with $\alpha = 2$. Symbols correspond to simulation results, whereas the solid lines are obtained performing the inverse Fourier transform in Eq. (61) numerically with $\alpha = 2$.

the distribution evidently. However, one can compute the distribution by evaluating the integral in Eq. (61) numerically which is plotted in fig. 11 where we observe excellent agreement with the distribution obtained from simulation (symbols).

4.2 For $r = \pm 1$

We now study the distribution $P(x, t)$ of the position for $r = \pm 1$. We discuss the three cases of jump time distribution separately.

4.2.1 Case I: $\rho(\tau) = \delta(\tau - a)$

First, in case of $\rho(\tau) = \delta(\tau - a)$ we can recall that the number of complete steps up to time t is $\lfloor t/a \rfloor$. It allows us to express $x(t)$ for an arbitrary r as

$$x(t) = \sum_{j=0}^{\lfloor t/a \rfloor - 1} \tau_j v_j + \underbrace{\left(t - a \left\lfloor \frac{t}{a} \right\rfloor \right)}_{\tau_{\lfloor t/a \rfloor}^*} v_{\lfloor t/a \rfloor}. \quad (70)$$

Note that the second term on the right hand side of Eq. (70) is denoting the contribution of the last incomplete step. Using $v_j = \sum_{l=0}^j (\pm 1)^{j-l} \eta_l$ for $r = \mp 1$ from Eq. (4) we can further simplify and express $x(t)$ in Eq. (70) as

$$x(t) = \sum_{j=0}^{\lfloor t/a \rfloor} \eta_i \chi_j(\mp 1, a, t) \quad \text{with} \\ \chi_j(\mp 1, a, t) = a \left(\frac{1 - (\pm 1)^{\lfloor t/a \rfloor - j}}{1 - (\pm 1)} \right) + \left(t - a \left\lfloor \frac{t}{a} \right\rfloor \right) (\pm 1)^{\lfloor t/a \rfloor - j}. \quad (71)$$

This $x(t)$ Eq. (71) represents a weighted sum of i.i.d. Gaussian random variables. Hence, by employing the central limit theorem we find the distribution of $x(t)$ is also a Gaussian distribution with the variance $\propto t$. A detailed discussion and explicit expression of the variance are provided in sec. 3.1.

4.2.2 Case II: $\rho(\tau) = \beta e^{-\beta\tau}$

First we discuss the $r = -1$ case. We have observed earlier that in this case, for large time t , the dynamics of the particle can be effectively described by a random acceleration process with noise strength $D = \sigma^2\beta$. Hence we expect the distribution $P(x, t)$ is a Gaussian with zero mean and variance $Dt^3/3 \simeq \beta\sigma^2t^3/3$ for $t \gg \beta^{-1}$ *i.e.*

$$P(x, t) \simeq \frac{\sqrt{3}}{\sqrt{\beta\sigma^2t^3}} \mathcal{G}^{(-1)} \left(\frac{\sqrt{3}x}{\sqrt{\beta\sigma^2t^3}} \right), \quad \text{with } \mathcal{G}^{(-1)}(y) = \frac{1}{\sqrt{2\pi}} \exp \left(-\frac{y^2}{2} \right). \quad (72)$$

We verify this result using numerical simulation in fig. 12(a).

Computing the distribution $P(x, t)$ for $r = 1$ turns out to be difficult. To compute the distribution $P(x, t)$ one can in principle perform the inverse Fourier-Laplace transform in Eq. (27). Since in this case the jump time distribution is exponentially distributed, all the jump durations in a trajectory of length t are typically of same order *i.e.* $\mathcal{O}(\beta^{-1})$. Consequently, all jump durations contribute to same order in $x(t)$ and they are strongly correlated which makes it difficult to compute $P(x, t)$. From the microscopic dynamics in Eqs. (1) and (4) with $r = 1$, it is easy to see that the motion of the particle should have a ballistic scaling *i.e.* $x \sim t$. In fig. 12(b) we plot the distribution of the scaled variable $y = \sqrt{2}x/(\sigma t)$ obtained in numerical simulation at times $t = 800, 900$ and $t = 1000$ and observe excellent data collapse. Since computing

this scaling distribution exactly seems difficult we, instead, perform an approximate calculation below which proposes a stretched exponential form for the distribution.

As has been observed earlier, the second moment $\langle x_m^2 \rangle$ of the position after m^{th} jump grows quadratically as

$$\langle x_m^2 \rangle \simeq \frac{\sigma^2 m^2}{2\beta^2}, \quad (73)$$

for $r = 1$. Similarly, after a lengthy and tedious computation one can show that $\langle x_m^4 \rangle \simeq 7(m\sigma/\beta)^4/4$ in the limit of large m (see Eq. (K.8) in Appendix K). Since for large t , typical number of jump events is $m \sim \beta t$, we get $\langle x^2(t) \rangle \simeq \sigma^2 t^2/2$ and $\langle x^4(t) \rangle \simeq 7(\sigma t)^4/4$. In terms of the scaled variable $y = \sqrt{2}x/(\sigma t)$ we get $\langle y^2 \rangle \simeq 1$ and $\langle y^4 \rangle \simeq 7$. Similarly, one can compute higher order moments but the computation quickly becomes too involved. However from the first two moments and the plots in fig. 12(b) we make a guess for $P(x, t)$. We assume a stretched-exponential of the form

$$P(x, t) \simeq \frac{\sqrt{2}}{\sigma t} \mathcal{G}^{(1)}\left(\frac{\sqrt{2}x}{\sigma t}\right), \quad \text{with}$$

$$\mathcal{G}^{(1)}(y) = \frac{1}{2\Gamma(1+\lambda)} \left(\frac{\Gamma(3\lambda)}{\Gamma(\lambda)}\right)^{1/2} \exp\left[-\left(\frac{\Gamma(3\lambda)}{\Gamma(\lambda)}y^2\right)^{1/2\lambda}\right]. \quad (74)$$

For an arbitrary $\lambda \in (0 : \infty)$ this distribution is normalised and has $\langle y^2 \rangle = 1$ and $\langle y^4 \rangle = \frac{\Gamma(\lambda)\Gamma(5\lambda)}{(\Gamma(3\lambda))^2}$. Note that for $\lambda = 1/2$, $\mathcal{G}^{(1)}(y)$ is Gaussian distribution with $\langle y^2 \rangle = 1$ and $\langle y^4 \rangle = 3$. For $\lambda = 1$, the distribution in Eq. (74) is a double-sided exponential distribution with $\langle y^2 \rangle = 1$ and $\langle y^4 \rangle = 6$. This means in our case we should expect $\lambda > 1$. To find the value of λ we numerically solve $\langle y^4 \rangle = \frac{\Gamma(\lambda)\Gamma(5\lambda)}{(\Gamma(3\lambda))^2} \simeq 7$ and get $\lambda \simeq 1.109$. Using this value for λ in Eq. (74) we find that $\mathcal{G}^{(1)}(y)$ matches remarkably well with the numerical simulation result as displayed in fig. 12(b). In the inset of this figure we show that, not only the variance (see fig. 5(c)) but the full scaling distribution is also independent of β .

4.2.3 Case III: $\rho(\tau) \sim \tau^{-(1+\alpha)}$

Like $r = 0$ case discussed in sec. 4.1.3, here also we discuss different regimes of α separately.

4.2.3.1 For $0 < \alpha < 1$

Let us first consider the $r = -1$ case. Computing the distribution $P(x, t)$ for power law ‘jump’ time distribution with $r \neq 0$ is even harder than previous cases because the velocity of the particle at different times are strongly correlated in addition to the fact that all the moments of the jump time distribution diverge. Instead of computing an analytical expression for the distribution, we focus on the scaling behaviour of $P(x, t)$ if there exists any. Since $r \neq 0$, we expect the velocity to appear as a function of time t is a smoother function (upto first derivative) over a long time duration than the velocity

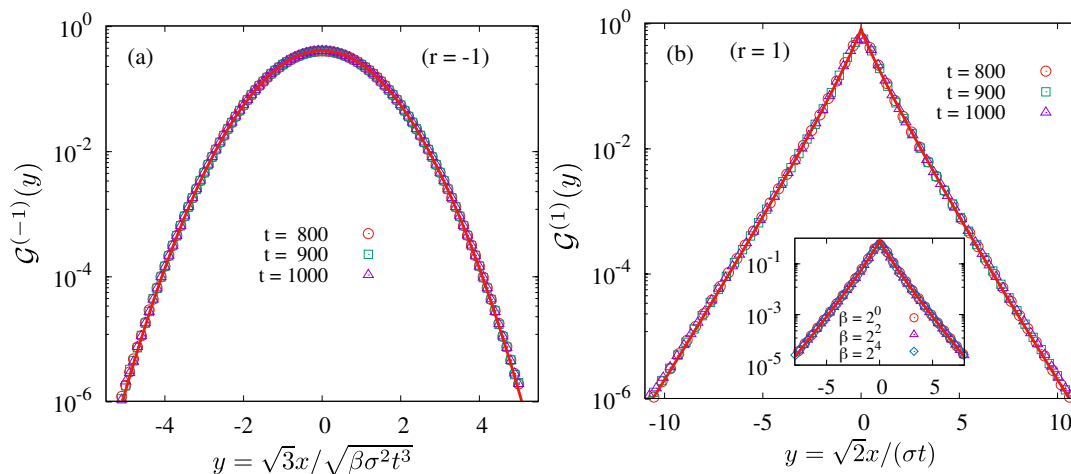


Figure 12. (Color online). **Panel (a):** PDF of the scaled position $y = \sqrt{3}x/\sqrt{\beta\sigma^2t^3}$ are plotted at different times for $r = -1$ and $\beta = 1$ in case II and compared with theoretical expression in Eq. (72). **Panel (b):** PDF of the scaled position $y = \sqrt{2}x/(\sigma t)$ are plotted at different times for $r = -1$ and $\beta = 1$ and compared with approximate theoretical result in Eq. (74) with $\lambda = 1.109$. In both plots symbols correspond to simulation results and solid red lined correspond to the respective theoretical results. In the inset of (b) numerically verify the β independence of the distribution of $x(t)$ at $t = 900$.

in $r = 0$ case. Hence, we write the position as $x(t) = \int_0^t dw (t-w) \frac{dv}{dw}$ (recall, $x(0) = 0$) where $v(w)$ is the velocity at time t . It is easy to see from Eq. (20) that for large t , $v(w) \sim w^{\alpha/2}$, using which in the above equation we find that typically $x(t) \sim t^{1+\alpha/2}$. This suggests the following scaling form for the distribution

$$P(x, t) \simeq \frac{1}{t^{1+\alpha/2}} \mathbb{G}_{\alpha < 1}^{(1)} \left(\frac{x}{t^{1+\alpha/2}} \right). \quad (75)$$

where $\mathbb{G}_{\alpha < 1}^{(1)}(y)$ is the scaling distribution of scaled variable $y = x/t^{1+\alpha/2}$. In fig. 13 (top row) we numerically verify this scaling form where we plot the distribution of the scaled variable y obtained in simulation at three times $t = 2000$, 2500 and $t = 3000$ and for three values of α . In all cases we observe excellent data collapse.

The above argument should also work for $r = 1$ and hence the scaling form in Eq. (75) should also hold as can be seen in the bottom row of fig. 13 where we plot the scaling distribution obtained in numerical simulation (symbols). In this case, we however note that for large t the dominant contribution to the position comes from the jumps with longest duration τ_{\max} . This fact is verified in fig. 13 (bottom row) where solid lines correspond to the distribution of $\Delta_{\max}(t) = v_l \tau_{\max}$ with v_l being the velocity in the longest jump duration. We observe that for large t the distributions of $\Delta_{\max}(t)$ and $x(t)$ match very well. Using the fact $x(t) \simeq \Delta_{\max}(t)$ it is possible to argue that $x(t) \sim t^{1+\alpha/2}$ in an alternative way. This idea has been used in Eq. (44) where we show that $\tilde{\sigma}_x^2(s) \simeq s^{-(3+\alpha)}$ yielding $\sigma_x^2(t) = \langle x^2(t) \rangle \sim t^{2+\alpha}$. Following a similar calculation, one can show that $\langle x^{2n}(t) \rangle \sim t^{2n+\alpha}$ for $n = 1, 2, 3, \dots$ (see Appendix Appendix L). This behaviour is consistent with the scaling form in Eq. (75). We end this section by making

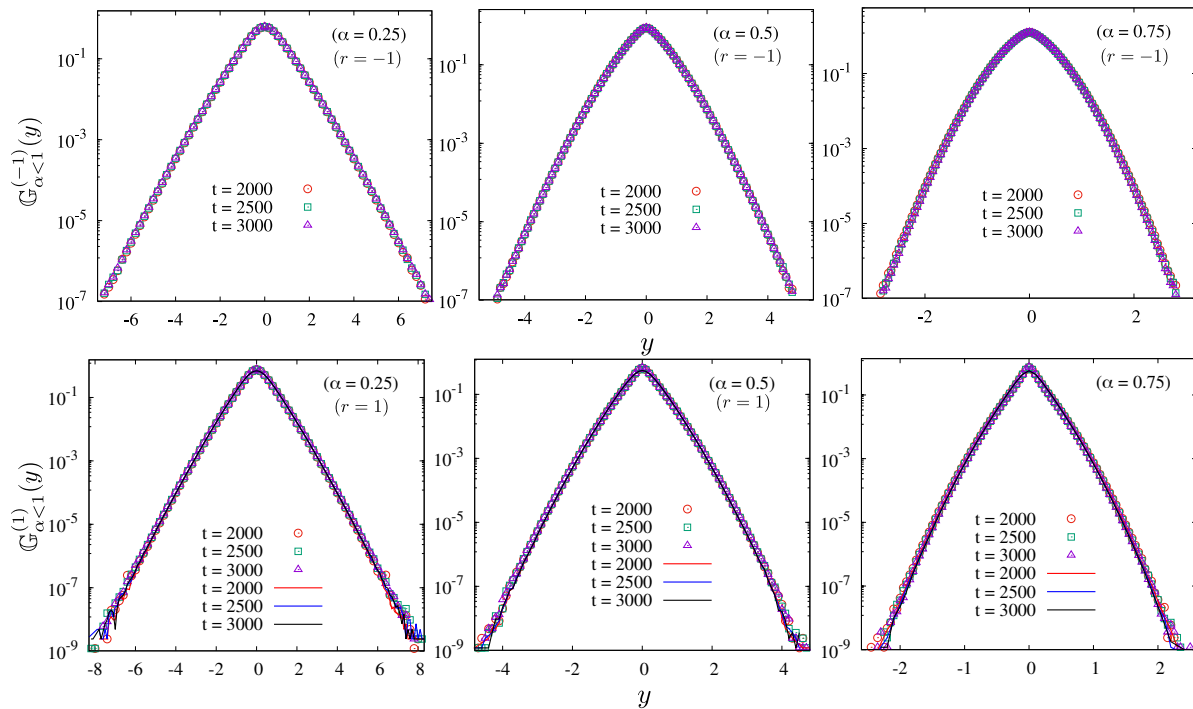


Figure 13. (Color online). Probability distribution function of the scaled position $y = x(t)/t^{1+\alpha/2}$ are plotted at different times for $r = -1$ (first row) and $r = 1$ (second row) with different values of α . Solid lines in each plot in the second row (for $r = 1$) represent the (scaled) distribution of displacement $\Delta_{\max}(t)$ made in the longest jump duration τ_{\max} . These distributions are obtained numerically and plotted in terms of the scaling variable $y = \Delta_{\max}/t^{1+\alpha/2}$. We observe excellent agreement between the (scaled) distributions of $x(t)$ and $\Delta_{\max}(t)$ for all values of α .

a remark that even though the scaling behaviour of $P(x, t)$ is same for both $r = 1$ and $r = -1$ in this range of α , the argument based on dominant contribution from longest jump duration does not work for $r = -1$ at least over the range of position x accessible in numerical simulation.

4.2.3.2 For $1 < \alpha < 2$

Recall that for α in this range, the mean jump duration is finite $\langle \tau \rangle = \frac{\alpha}{\alpha-1}$. As in the exponential case studied previously in sec. 4.2.2, in this case also for $r = -1$ we expect the distribution of the position $x(t)$ after a long time t is given by Gaussian with the variance $Dt^3/3 \simeq (\alpha-1)\sigma^2 t^3/(3\alpha)$ as in a random acceleration process driven by a zero mean white noise having strength $D = \sigma^2(\alpha-1)/\alpha$. Although in this section we are focusing in the range $1 < \alpha < 2$, this Gaussian scaling form is also valid for $\alpha > 2$. Hence it is more appropriate to denote the distribution of the scaling variable $y = x(t)\sqrt{3\alpha/((\alpha-1)\sigma^2 t^3)}$ by $\mathbb{G}_{\alpha>1}^{(-1)}(y)$ which is essentially $\mathbb{G}_{\alpha>1}^{(-1)}(y) = G(y)$ where $G(y)$ is given in Eq. (18). This distribution is verified numerically for $\alpha = 1.5, 2.0$ and 2.5 in fig. 14, where the red solid lines represent theoretical result and the symbols are from numerical simulation.

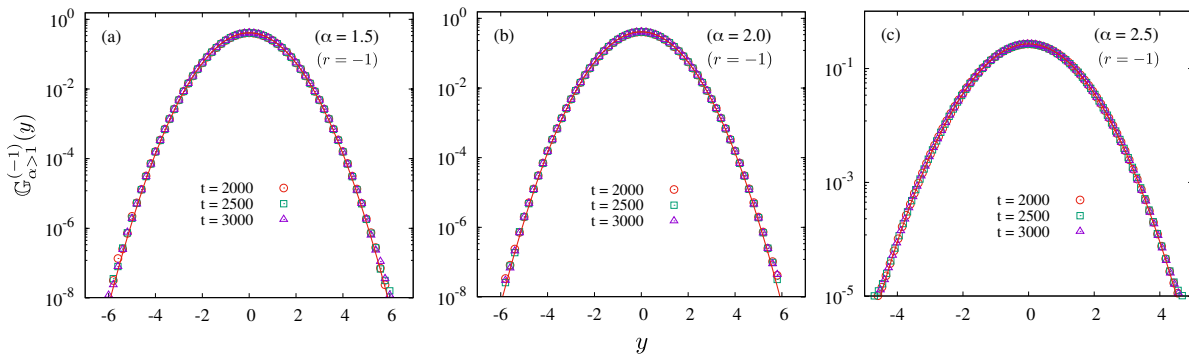


Figure 14. (Color online). Probability distribution functions of the scaled position $y = x(t)\sqrt{3\alpha}/((\alpha-1)\sigma^2 t^3)$ are plotted for $r = -1$ and different values α . Symbols are obtained from simulation results which show good agreement with the analytical distribution $\mathbb{G}_{\alpha>1}^{(-1)}(y)$ (red solid lines) discussed in sec. 4.2.3.2.

We now discuss the behaviour of $P(x, t)$ for $r = 1$ with $1 < \alpha < 2$. As shown in Eq. (L.9) of Appendix L, in this case the variance grows as $\sigma_x^2(t) = \langle x^2(t) \rangle_c \sim t^{4-\alpha}$. This may naively suggest a scaling form once $x(t)$ is scaled by $\sigma_x(t)$ *i.e.*

$$P(x, t) \approx \frac{1}{t^{2-\alpha/2}} \mathbb{G}_{1<\alpha<2}^{(1),cen} \left(\frac{|x|}{t^{2-\alpha/2}} \right). \quad (76)$$

In figs. 15(a) and 15(c) we try to numerically verify this for $\alpha = 1.5$ and 1.75 where we plot data of $P(x, t)$ obtained from simulation in this scaling form. We observe excellent data collapse but only over the central part ($|x| \lesssim \sigma_x(t)$) of the distribution implying that such a scaling form is not valid outside this region *i.e.* at the tails of the distribution. This can also be seen from the large t growth of the higher order moments: $\langle x^{2n}(t) \rangle \sim t^{3n+1-\alpha}$ (see Appendix L) which, one will not be able to obtain from the scaling form in Eq. (76). This suggests a different scaling form at the tails of the distribution $P(x, t)$ as in the $r = 0$ case discussed in sec. 4.1.3.2.

The late time behaviour of the higher moments suggests us to guess the following scaling form for the distribution at the tail ($|x| \gg \sigma_x(t)$ possibly $|x| \gtrsim t^{3/2}$)

$$P(x, t) \approx \frac{1}{t^{\alpha+1/2}} \mathbb{G}_{1<\alpha<2}^{(1),tail} \left(\frac{|x|}{t^{3/2}} \right), \quad (77)$$

which is verified numerically in figs. 15(b) and 15(d) for $\alpha = 1.5$ and 1.75 , respectively. The symbols are from simulation. Note in these figures that the data collapse is excellent at the tails but do not collapse at the central part as shown in the insets. The fact that the distribution at the tail has a different scaling form stems from the fact that here also for large t , the dominant contribution at the tails comes the displacement $\Delta_{\max}(t)$ in the longest jump duration τ_{\max} which indeed leads to $\langle x^{2n}(t) \rangle \sim t^{3n+1-\alpha}$ (see Appendix L).

Like $\alpha < 1$ case (discussed in the previous section), in this range of α also, the fact of dominant contribution from Δ_{\max} is also true as verified in figs. 15(b) and 15(d) where we observe excellent match between the distributions of $x(t)$ (symbols) and $\Delta_{\max}(t)$

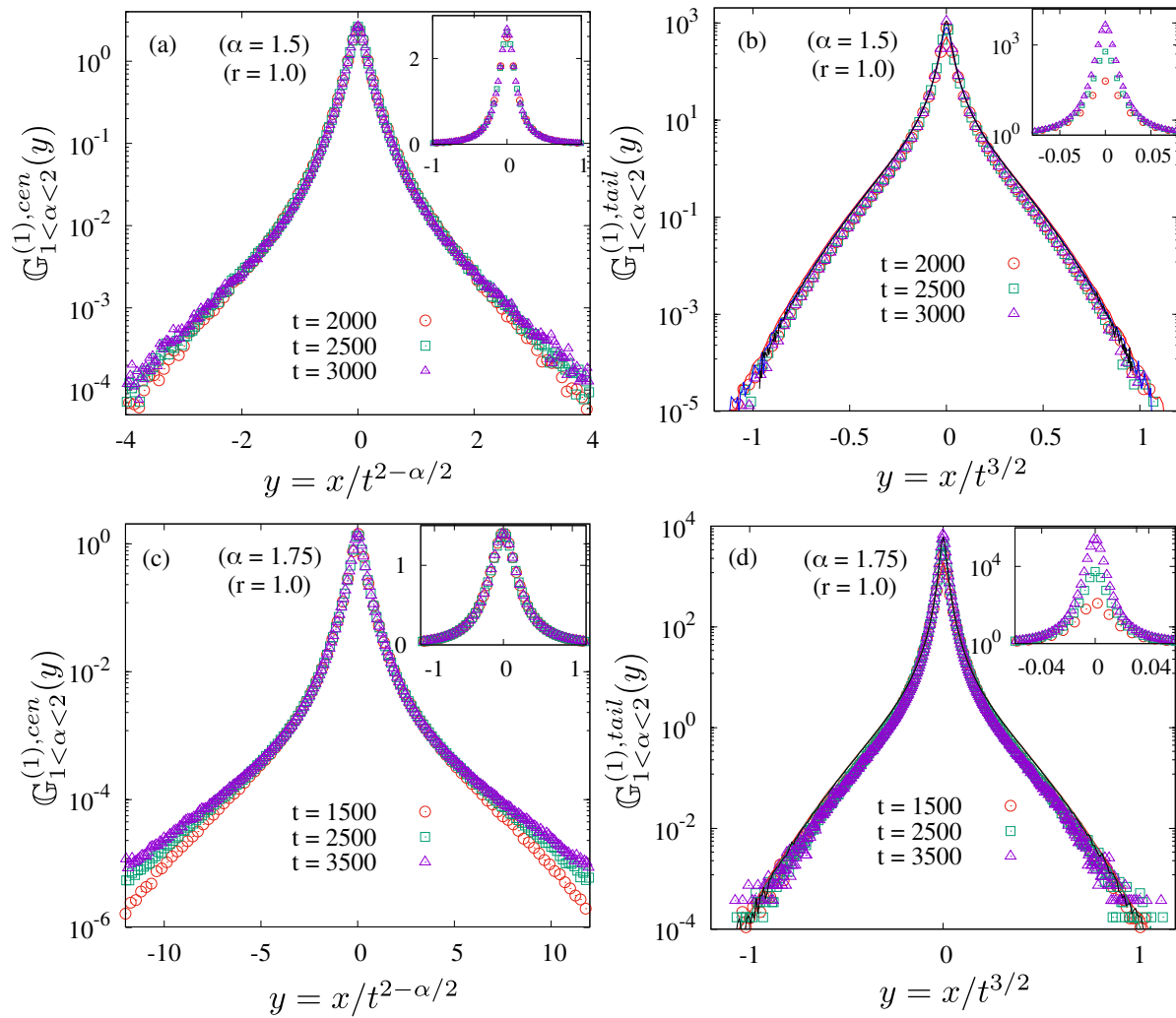


Figure 15. (Color online). Distributions $\mathbb{G}_{1 < \alpha < 2}^{1, cen}(y)$ and $\mathbb{G}_{1 < \alpha < 2}^{1, tail}(y)$ of the scaled positions $y = x/t^{2-\alpha/2}$ and $y = x/t^{3/2}$ are plotted, respectively, in the left (a,c) and right (b,d) columns for $r = 1$ [see Eqs. (76) and (77)]. The top row corresponds plots for $\alpha = 1.5$ and the bottom row corresponds plots for $\alpha = 1.75$. Solid lines in figures (b) and (d) plot the numerical data for the distribution of scaled variable $\Delta_{\max}/t^{3/2}$ associated to the displacement $\Delta_{\max}(t)$ made in the longest jump duration for $\alpha = 1.5$ and $\alpha = 1.75$ respectively. In the inset of figures (b) and (d) we highlight that $t^{3/2}$ scaling of the position $x(t)$ does not work in the central part as can be seen from the data collapse failure whereas scaling with $t^{2-\alpha/2}$ works very well in the central part. Note that the distributions in the insets of all the plotted in normal scale.

(solid lines) both obtained numerically. Note these distributions are plotted in terms of the scaling variables $y = x/t^{3/2}$ and $y = \Delta_{\max}/t^{3/2}$.

We close this section by mentioning that unlike the $r = 0$ case, for $r = \pm 1$ it seems difficult to find analytical expressions of the scaling functions mainly because the velocity at different steps are highly correlated which makes it harder to compute the joint probability of the velocity at l^{th} jump and this jump being the longest one.

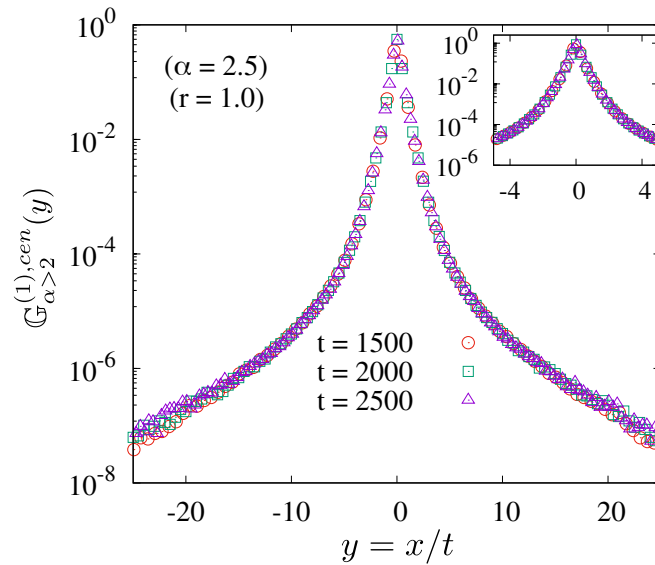


Figure 16. (Color online). Distribution $\mathbb{G}_{\alpha > 2}^{(1), cen}(y)$ of the scaled variable position $y = x/t$ is plotted for $\alpha = 2.5$ and $r = 1$ at different times. The excellent data collapse validates the scaling form in Eq. (78). Inset shows a zoomed version of the distribution near the peak. The inset in figure (b) shows the distribution in normal scale.

4.2.3.3 For $\alpha > 2$

For this range of α , since both mean and variance of the jump time distribution are finite, all jump steps contribute more or less equally to the total position. Unlike the $0 < \alpha < 1$ case, the single jump of longest duration does not dominate in this case. Hence for large t the distribution can not be described by the position made in the longest jump. However, such events in fact should provide dominant contribution at the tail for large t . The central part of the distribution would be described by a scaling distribution when $x(t)$ is scaled by the standard deviation $\sigma_x(t)$ which in this case is given by $\sigma_x^2(t) \simeq \frac{\sigma^2 t^2}{2\alpha(\alpha-2)}$ (see Eq. (43)). Hence the scaling form for the distribution $P(x, t)$ seems to be

$$P(x, t) \approx \frac{1}{t} \mathbb{G}_{\alpha > 2}^{(1), cen} \left(\frac{|x|}{t} \right), \quad (78)$$

which is verified numerically in fig. 16 for $\alpha = 2.5$.

4.2.3.4 For $\alpha = 1$ and $\alpha = 2$

Finally we make some remarks about $\alpha = 1$ and $\alpha = 2$ cases. These cases represent marginal cases in which one expects to have some $\ln(t)$ dependences in the moments (see Appendix L) as well as in the distributions. It turns out that for these two cases also the position $x(t)$ can be well approximated the displacement $\Delta_{\max}(t)$ in the longest jump duration $\tau_{\max}(t)$ within a large time interval t . This fact is numerically verified in fig. 17 where we compare the distributions of $x(t)$ and $\Delta_{\max}(t)$ for both $\alpha = 1$ and $\alpha = 2$. The good agreement indeed justifies the approximation $x(t) \simeq \Delta_{\max}(t)$ for large t .

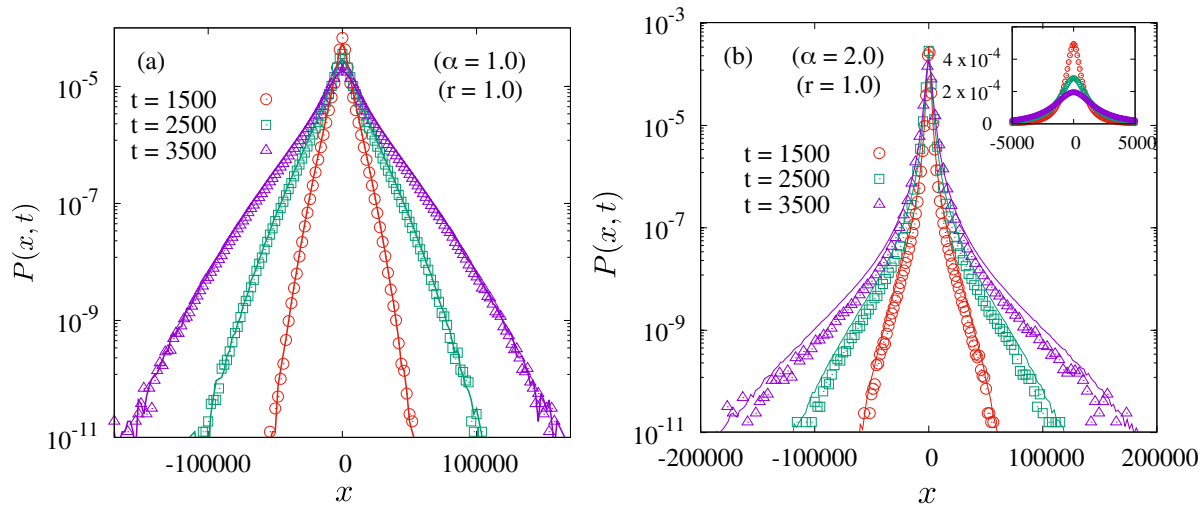


Figure 17. (Color online). Distributions of the position $x(t)$ (symbols) and the displacement $\Delta_{\max}(t)$ made in the longest ‘jump’ duration τ_{\max} are plotted for $\alpha = 1.0$ (a) and 2.0 (b), respectively, at different times. Both distributions are obtained numerically and we observe they match quite well.

5 Summary and conclusion

In this paper we have studied a simple extension of the LW walk model by introducing correlation among the velocities of the walker at different steps. This correlation has been introduced by relating the velocities of two successive ‘jump’ steps such that the velocity at any step retains some part of the velocity in the previous step plus a random noise coming from the surrounding medium as written in Eq. (1). The parameter r controls the degree of correlation which becomes largest in the limit $r \rightarrow \pm 1$ and zero for $r = 0$. Also the process discussed in this paper can describe the dynamics of a granular particle being driven and dissipating energies from the collision with a heavy wall at thermal equilibrium. The parameter r in this context serves as a coefficient of restitution.

The particle in a ‘jump’ step moves with a fixed velocity for a random interval of time drawn from a distribution $\rho(\tau)$. For different choices of $\rho(\tau)$ and values of r (with more focus on $r = \pm 1$ and 0) we have studied the statistical properties of the velocity $v(t)$ and position $x(t)$ of the particle at time t . We have shown that for different values of r with these choices of $\rho(\tau)$ one finds interesting ballistic, super-diffusive, diffusive and sub-diffusive scaling of these quantities. In particular, we find that in case of power law ‘jump’ time distribution (case III) with $\alpha \leq 2$ the distribution of the position $x(t)$ is dominated by the displacement $\Delta_{\max}(t)$ made in the longest ‘jump’ interval at the leading order for large t . This allowed us to find explicit asymptotic form for the distribution $P(x, t)$ at the tails for $r = 0$ and enabled us to make guess on the scaling behaviour, again at the tails of the distributions for $r = \pm 1$.

We believe that our study provides another simple yet nontrivial model of non-Markovian process for which many things can be computed analytically and understood

theoretically. Several important future questions can be asked as well as extensions can be made. While the observation that the $\Delta_{\max}(t)$ provides dominating contribution to $x(t)$ for large t allows us to guess the scaling behaviour for position distribution $P(x, t)$ at the tails, it does not immediately tell us the form at the tails. It would be interesting to explore in this direction by studying the joint distribution of the velocity at a step and that step being the longest one. Another direction to explore would be to look at survival problem of the walker in our model and ask how does the persistent properties depend on r and $\rho(\tau)$. Also studying, extreme statistics and path functionals would lead to interesting directions.

6 Acknowledgement

We would like to thank Urna Basu, Sanjib Sabhapandit and Abhishek Dhar for their comments and suggestions. We thank Prashant Singh for a careful reading of the manuscript and interesting suggestions. SD and AK would like to thank financial support from DST, Government of India grant under project No. ECR/2017/000634. SD would also like to acknowledge the hospitality of the International Centre for Theoretical Sciences, Bangalore. AK would like to acknowledge support of the Department of Atomic Energy, Government of India, under project no.12-R&D-TFR-5.10-1100.

Appendix

Appendix A Calculation of $\tilde{P}_v(k, s)$ in Eq. (9)

We can write and simplify the Fourier-Laplace transform of Eq. (8) as

$$\begin{aligned} \tilde{P}_v(k, s) &= \sum_{m=0}^{\infty} \int_{v=-\infty}^{\infty} dv e^{ikv} \int_{t=0}^{\infty} dt e^{-st} \langle \delta(v - v_m) \rangle \left\langle \delta \left(t - \sum_{j=0}^{m-1} \tau_j - \tau_m^* \right) \right\rangle \\ &= \sum_{m=0}^{\infty} \langle e^{ikv_m} \rangle \langle e^{-s \sum_{j=0}^{m-1} \tau_j - s\tau_m^*} \rangle. \end{aligned} \quad (\text{A.1})$$

Since the time intervals are independent of each others we, using Eqs. (10) and (11) we can simplify Eq. (A.1) as

$$\tilde{P}_v(k, s) = \sum_{m=0}^{\infty} \left\langle e^{ik \sum_{j=0}^m \eta_{m-j} (-r)^j} \right\rangle \tilde{\psi}^m(s) \tilde{\Psi}(s). \quad (\text{A.2})$$

where we have used $v_m = \sum_{j=0}^m \eta_{m-j} (-r)^j$ from Eq. (4). Also since, all the η 's are independent Gaussian noise with mean zero and variance σ^2 , we can further simplify

Eq. (A.2) as

$$\begin{aligned}\widetilde{P}_v(k, s) &= \sum_{m=0}^{\infty} \exp \left[-\frac{1}{2} k^2 \sigma^2 \sum_{j=0}^m (-r)^{2j} \right] \widetilde{\psi}^m(s) \widetilde{\Psi}(s) \\ &= \sum_{m=0}^{\infty} \exp \left[-\frac{1}{2} k^2 \sigma^2 \frac{1 - r^{2m+2}}{1 - r^2} \right] \widetilde{\psi}^m(s) \widetilde{\Psi}(s),\end{aligned}\quad (\text{A.3})$$

which is what we have written in Eq. (9) in the main text.

Appendix B Saddle point integration of Eq. (22) for $0 < \alpha < 1$

For $0 < \alpha < 1$, the asymptotic form of the Mittag-Leffler function $E_\alpha(u)$ is $E_\alpha(u) \simeq \exp[u^{1/\alpha}]/\alpha$ for $|u| \rightarrow \infty$ [39]. It allows us to write

$$E_\alpha(-\tilde{k}^2) \simeq \frac{1}{\alpha} \exp \left[(-\tilde{k}^2)^{1/\alpha} \right], \quad (\text{B.1})$$

for large $|\tilde{k}|$, inserting which in Eq. (22) and using the $\tilde{k} \rightarrow -\tilde{k}$ symmetry we get

$$\mathbb{F}_\alpha(y) \simeq \frac{1}{2\pi\alpha} \int_{-\infty}^{\infty} d\tilde{k} e^{iy\varphi(\tilde{k}, y)}, \quad \text{where, } \varphi(\tilde{k}, y) = (i\tilde{k})^{2/\alpha}/|y| - i\tilde{k}. \quad (\text{B.2})$$

We now evaluate this integral using saddle point method. It is easy to see that the saddle point is $\tilde{k}^* = (\frac{\alpha|y|}{2})^{\frac{\alpha}{2-\alpha}} e^{-i\frac{\pi}{2}}$, at which

$$\varphi(\tilde{k}^*) = -\left(\frac{2}{\alpha} - 1\right) \left(\frac{\alpha|y|}{2}\right)^{\frac{2}{2-\alpha}}, \quad \text{and} \quad \varphi''(\tilde{k}^*) = -\frac{1}{|y|} \frac{2}{\alpha} \left(\frac{2}{\alpha} - 1\right) \left(\frac{\alpha|y|}{2}\right)^{\frac{2(1-\alpha)}{2-\alpha}} \quad (\text{B.3})$$

Performing the saddle point integration and using the above expressions we finally get

$$\mathbb{F}_\alpha(y) \simeq \frac{e^{y\varphi(\tilde{k}^*)}}{\alpha \sqrt{2\pi y |\varphi''(\tilde{k}^*)|}} \simeq \frac{1}{\sqrt{4\pi(2-\alpha)}} \left(\frac{\alpha y}{2}\right)^{-\frac{1-\alpha}{2-\alpha}} \exp \left[-\left(\frac{2}{\alpha} - 1\right) \left(\frac{\alpha y}{2}\right)^{\frac{2}{2-\alpha}} \right] \quad (\text{B.4})$$

Note that $\mathbb{F}_\alpha(y)$ has the symmetry $\mathbb{F}_\alpha(y) = \mathbb{F}_\alpha(-y)$.

Appendix C Inverse Laplace transform: Bromwich integral and Tauberian theorems

In this section we discuss few inverse Laplace transform results which we have used in the main text. The well known methods to compute inverse Laplace transform is to evaluate the Bromwich integral (BI) [45]. Using the formalism of Bromwich integral we first find out the inverse Laplace transform of $\ln(s)/s^n$ for any $n \geq 1$ [45] as

$$\mathcal{L}_t^{-1} \left(\frac{\ln(s)}{s^n} \right) = \left(1 + \frac{1}{2} + \dots + \frac{1}{n-1} - \gamma - \ln(t) \right) \frac{t^{n-1}}{(n-1)!}. \quad (\text{C.1})$$

Often we are interested in the large t asymptotic for which one can use the Tauberian theorem [46] instead of performing the BI. This theorem states that if $L(t)$ is a slowly varying function at infinity and $0 \leq \nu < \infty$, then each of the relation

$$f(t) \simeq \frac{t^\nu L(t)}{\Gamma(\nu+1)} \quad \text{for } t \rightarrow \infty \quad (\text{C.2})$$

$$\tilde{f}(s) = \mathcal{L}[f(t)] \simeq s^{-(\nu+1)} L(1/s) \quad \text{for } s \rightarrow 0 \quad (\text{C.3})$$

implies the others [46]. For an arbitrary constant c the slowly varying function L implies $L(cu)/L(u) \rightarrow 1$ in the limit of $u \rightarrow \infty$. For example, if $L(u) = \ln(u)$, then it satisfy the limiting condition. Hence, by using this theorem we can find out an approximate result

$$\mathcal{L}_t^{-1} \left(\frac{\ln(s)}{s^n} \right) \simeq -\frac{t^{n-1}}{(n-1)!} \ln(t) \quad (\text{C.4})$$

for any integer $n \geq 1$ in the limit $t \rightarrow \infty$. Clearly, this result agrees with the large t asymptotic of the result in Eq. (C.1).

Similarly, we can consider $L(u) = \ln^{-1}(u)$ which also satisfies the above condition of a slowly varying function. It enable us to find an approximate, asymptotic result of the inverse Laplace transform of $s^{-n} \ln^{-m}(s)$ as

$$\mathcal{L}_t^{-1} \left(\frac{1}{s^n \ln^m(s)} \right) \simeq (-1)^m \frac{t^{n-1}}{(n-1)!} \ln^{-m}(t) \quad (\text{C.5})$$

for any integer $n, m \geq 1$ in the limit $t \rightarrow \infty$.

Appendix D Calculation of $\tilde{\sigma}_x^2(s)$ for $-1 \leq r \leq 1$

Here we show the details of calculation of $\tilde{\sigma}_x^2(s)$ in Eq. (29).

$$\begin{aligned} \tilde{\sigma}_x^2(s) &= \langle \widetilde{x^2} \rangle(s) = - \left[\frac{d^2}{dk^2} \widetilde{P}_x(k, s) \right]_{k=0} = \sigma^2 \sum_{m=0}^{\infty} \left\langle \left(\bar{\tau}_m^T \Sigma_m \bar{\tau}_m \right) e^{-s I_m^T \bar{\tau}_m} \right\rangle_{\{\tau_j\}} \\ &= \sigma^2 \sum_{m=0}^{\infty} \left\langle \left(\mathbb{I}(m \geq 1) \sum_{l=0}^{m-1} \tau_l^2 \sum_{j=0}^l r^{2j} + \tau_m^{*2} \sum_{l=0}^m r^{2l} + 2 \mathbb{I}(m \geq 2) \sum_{l=0}^{m-1} \tau_l \right. \right. \\ &\quad \left. \left. \times \sum_{j=l+1}^{m-1} \tau_j (-r)^{j-l} \sum_{p=0}^l r^{2p} + 2 \mathbb{I}(m \geq 1) \tau_m^* \sum_{l=0}^{m-1} \tau_l (-r)^{m-l} \sum_{p=0}^l r^{2p} \right) e^{-s(\tau_0 + \tau_1 + \dots + \tau_m^*)} \right\rangle_{\{\tau_j\}} \\ &= \sigma^2 \sum_{m=0}^{\infty} \left(\frac{m(1-r^2) - r^2(1-r^{2m})}{(1-r^2)^2} \tilde{\Psi}(s) \tilde{\psi}^{m-1}(s) \tilde{\psi}''(s) + \frac{1 - (r^2)^{1+m}}{1-r^2} \tilde{\psi}^m(s) \tilde{\Psi}''(s) \right. \\ &\quad \left. + 2 \frac{(1-r)^2 (-r)^{m+1} - r^{2+2m} + r(1-m-r+r^2+mr^2)}{(1-r)^2(1+r)^3} \tilde{\Psi}(s) \tilde{\psi}^{m-2}(s) \tilde{\psi}'^2(s) \right. \\ &\quad \left. - 2 \frac{(-r)^{1+m}(1-r) + r - r^{2(1+m)}}{(1-r)(1+r)^2} \tilde{\psi}^{m-1}(s) \tilde{\psi}'(s) \tilde{\Psi}'(s) \right) \quad (\text{D.1}) \end{aligned}$$

Executing all the summation over m and using $\tilde{\psi}(s) = \langle e^{-s\tau} \rangle$, $\tilde{\psi}'(s) = -\langle \tau e^{-s\tau} \rangle$, $\tilde{\psi}''(s) = \langle \tau^2 e^{-s\tau} \rangle$, $\tilde{\Psi}(s) = \langle e^{-s\tau^*} \rangle$, $\tilde{\Psi}'(s) = -\langle \tau^* e^{-s\tau^*} \rangle$, $\tilde{\Psi}''(s) = \langle \tau^{*2} e^{-s\tau^*} \rangle$ (here the averages are over $\rho(\tau)$) we find

$$\begin{aligned} \tilde{\sigma}_x^2(s) &= \sigma^2 \left(\underbrace{\frac{\tilde{\Psi}(s) \tilde{\psi}''(s)}{(1-\tilde{\psi}(s))^2 (1-r^2 \tilde{\psi}(s))}}_{\text{I}} + \underbrace{\frac{\tilde{\Psi}''(s)}{(1-\tilde{\psi}(s)) (1-r^2 \tilde{\psi}(s))}}_{\text{II}} \right. \\ &\quad \left. - \underbrace{\frac{2r \tilde{\Psi}(s) \tilde{\psi}'^2(s)}{(1-\tilde{\psi}(s))^2 (1+r \tilde{\psi}(s)) (1-r^2 \tilde{\psi}(s))}}_{\text{III}} - \underbrace{\frac{2r \tilde{\Psi}'(s) \tilde{\psi}'(s)}{(1-\tilde{\psi}(s)) (1+r \tilde{\psi}(s)) (1-r^2 \tilde{\psi}(s))}}_{\text{IV}} \right) \quad (\text{D.2}) \end{aligned}$$

Simplifying this equation further by using $\tilde{\Psi}(s) = (1 - \tilde{\psi}(s))/s$ we get Eq. (29).

Appendix E Exact result of $\sigma_x^2(t)$ in case I *i.e.* for $\rho(\tau) = \delta(\tau - a)$

In case of $\rho(\tau) = \delta(\tau - a)$, using $\tilde{\psi}(s) = e^{-as}$ in Eq. (29) we can write

$$\tilde{\sigma}_x^2(s) = \frac{2\sigma^2}{s^3(1 - r^2e^{-as})} \left(1 - \frac{as e^{-as}}{1 - e^{-as}} - \frac{ras e^{-as}}{1 + r e^{-as}} \right). \quad (\text{E.1})$$

Let us first consider $r = -1$ case, for which the above equation simplifies to

$$\tilde{\sigma}_x^2(s) = \frac{2\sigma^2}{s^3(1 - e^{-as})} = 2\sigma^2 s^{-3} \sum_{n=0}^{\infty} e^{-nas}. \quad (\text{E.2})$$

Performing inverse Laplace transform yields

$$\begin{aligned} \sigma_x^2(t) &= \sigma^2 \sum_{n=0}^{\lfloor t/a \rfloor} (t - an)^2 = \frac{\sigma^2}{6} \left((a^2 - 6at + 6t^2) \left\lfloor \frac{t}{a} \right\rfloor \right. \\ &\quad \left. + (3a^2 - 6at) \left\lfloor \frac{t}{a} \right\rfloor^2 + 2a^2 \left\lfloor \frac{t}{a} \right\rfloor^3 + 6t^2 \right) \simeq \frac{\sigma^2 t^3}{3a} + \mathcal{O}(t^2) \end{aligned} \quad (\text{E.3})$$

in the limit of large time assuming $\lfloor t/a \rfloor \simeq t/a$. Following a similar procedure we can find out the exact result for $-1 < r < 1$ as

$$\begin{aligned} \sigma_x^2(t) &= \frac{\sigma^2(r-1)^{-1}}{(r+1)^3} \left(a^2 \left(r^{2\lfloor \frac{t}{a} \rfloor + 2} \left(\left\lfloor \frac{t}{a} \right\rfloor (r+1) + 1 \right)^2 - 2(r-1)r \left(\left\lfloor \frac{t}{a} \right\rfloor (r+1) + 1 \right) \right. \right. \\ &\quad \left. \left. \times (-r)^{\lfloor \frac{t}{a} \rfloor} - (r+1)^2 \left\lfloor \frac{t}{a} \right\rfloor^2 - (r+1)^2 \left\lfloor \frac{t}{a} \right\rfloor + (r-2)r \right) + (r+1)^2 t^2 \left(r^{2\lfloor \frac{t}{a} \rfloor + 2} - 1 \right) \right. \\ &\quad \left. + 2a(r+1)t \left(-r^{2\lfloor \frac{t}{a} \rfloor + 2} \left(\left\lfloor \frac{t}{a} \right\rfloor (r+1) + 1 \right) + (-r)^{\lfloor \frac{t}{a} \rfloor + 1} \right. \right. \\ &\quad \left. \left. + (-r)^{\lfloor \frac{t}{a} \rfloor + 2} + \left\lfloor \frac{t}{a} \right\rfloor (r+1) + r \right) \right) \simeq \frac{a\sigma^2}{(1+r)^2} t \end{aligned} \quad (\text{E.4})$$

in the limit of large time t . Similarly, for $r = 1$, we calculate

$$\begin{aligned} \sigma_x^2(t) &= \frac{\sigma^2}{2} \left((a^2 - 2at + 2t^2) + (3a^2 - 6at + 2t^2) \left\lfloor \frac{t}{a} \right\rfloor \right. \\ &\quad \left. + 4a(a-t) \left\lfloor \frac{t}{a} \right\rfloor^2 + 2a^2 \left\lfloor \frac{t}{a} \right\rfloor^3 \right). \end{aligned} \quad (\text{E.5})$$

For any real t/a we can write $t/a = \lfloor t/a \rfloor + u$ with $u \in (0 : a)$. Using this in the above expression we get

$$\sigma_x^2(t) = \frac{1}{2} \sigma^2 a^2 \left(1 + \left\lfloor \frac{t}{a} \right\rfloor \right) (2u^2 - 2u + 1), \quad (\text{E.6})$$

as announced in Eq. (33).

Appendix F Variance and the distribution of the position in random acceleration process (RAP)

Random acceleration process is a simple non-Markovian stochastic process that yields several non-trivial results [41, 42]. In RAP, a point particle moving in one dimension is accelerated by white noise as

$$\ddot{x}(t) = \zeta(t) \quad (\text{F.1})$$

where $\zeta(t)$ is a Gaussian white noise with the zero mean and delta correlation of the strength D , *i.e.*,

$$\langle \zeta(t) \rangle = 0, \quad \text{and} \quad \langle \zeta(t)\zeta(t') \rangle = D\delta(t - t'). \quad (\text{F.2})$$

Notably, the velocity $v(t) = \dot{x}(t)$ in this process executes a Brownian motion and the position $x(t)$ is the area under the Brownian motion trajectory. Using Eq. (F.2) we can calculate the velocity-velocity correlation function

$$C_{vv}(t', t'') = \langle v(t')v(t'') \rangle_c = \int_0^{t'} d\tau_1 \int_0^{t''} d\tau_2 \langle \zeta(\tau_1)\zeta(\tau_2) \rangle = D \min(t', t''). \quad (\text{F.3})$$

where we have used $\langle v(t) \rangle = 0$. Writing the position $x(t)$ up to time t by the integral $x(t) = \int_0^t dt' v(t')$. Clearly, it provides $\langle x(t) \rangle = 0$. Hence the variance can be written in terms of the correlation as

$$\begin{aligned} \sigma_x^2(t) &= \langle x^2(t) \rangle_c = \langle x^2(t) \rangle = \int_0^t dt' \int_0^t dt'' C_{vv}(t', t'') \\ &= \underbrace{\int_0^t dt' \int_0^{t'} dt'' C_{vv}(t', t'')}_{t' > t''} + \underbrace{\int_0^t dt' \int_{t'}^t dt'' C_{vv}(t', t'')}_{t' < t''} = \frac{1}{3}Dt^3. \end{aligned} \quad (\text{F.4})$$

The joint probability distribution of position and velocity (x, v) for a random accelerated particle at time t starting initially from x_0 and v_0 reads [47, 48]

$$\mathcal{P}(x, v, t | x_0, v_0) = \frac{\sqrt{3}}{\pi Dt^2} \exp \left[-\frac{6}{Dt^3} \left((x - x_0 - v_0 t)(x - x_0 - vt) + \frac{1}{3}(v - v_0)^2 t^2 \right) \right] \quad (\text{F.5})$$

Integrating out v_0 and v with the zero mean gaussian distribution with variance D , one gets

$$P(x - x_0, t) \simeq \sqrt{\frac{3}{2\pi Dt^3}} \exp \left[-\frac{3(x - x_0)^2}{2Dt^3} \right] \quad (\text{F.6})$$

in the limit of large t .

Appendix G Velocity-velocity correlation function

Consider our walker starts at $x(0) = 0$ and is moving with a velocity $v(t)$ at time t . We can define the velocity-velocity correlation function in this case as $C_{vv}(t_1, t_2) = \langle v(t_1)v(t_2) \rangle - \langle v(t_1) \rangle \langle v(t_2) \rangle$. Since the noise in our case has symmetric distribution (see

from Eq. (1)) it makes $\langle v(t) \rangle = 0$, and hence $C_{vv}(t_1, t_2) = \langle v(t_1)v(t_2) \rangle$. Assumin $t_2 > t_1$ we write

$$C_{vv}(t_1, t_2)_{t_2 > t_1} = \langle v(t_1)v(t_2) \rangle = \sum_{m=0}^{\infty} \sum_{n=0}^{\infty} \mathcal{P}(m, n; t_1, t_2 - t_1) \langle v_m v_{m+n} \rangle_c \quad (\text{G.1})$$

where $\mathcal{P}(m, n; t_1, t_2 - t_1)$ is the joint probability of m and n ‘jump’ events to occur within time intervals t_1 and $(t_2 - t_1)$ respectively. From the dynamical rule of the velocity in Eq. (1) it is easy to write $v_{m+n} = (-r)^n v_m + \sum_{j=1}^n (-r)^{n-j} \eta_{m+j}$ for any $n \geq 0$. This suggests $\langle v_m v_{m+n} \rangle_c = (-r)^n \langle v_m^2 \rangle_c$. Hence, from Eq. (G.1) we write,

$$C_{vv}(t_1, t_2)_{t_2 > t_1} = \sum_{m=0}^{\infty} \langle v_m^2 \rangle_c \sum_{n=0}^{\infty} (-r)^n \mathbb{P}(n, t_2 - t_1 | m, t_1) \mathcal{P}(m, t_1) \quad (\text{G.2})$$

where we have written

$$\mathcal{P}(m, n; t_1, t_2 - t_1) = \mathbb{P}(n, t_2 - t_1 | m, t_1) \mathcal{P}(m, t_1). \quad (\text{G.3})$$

Here $\mathcal{P}(m, t_1)$ is the probability of having m number of ‘jump’ events within time t_1 and $\mathbb{P}(n, t_2 - t_1 | m, t_1)$ is the conditional probability to have n ‘jump’ events in duration $t_2 - t_1$ given that there were m ‘jump’ events till time $t_1 < t_2$. The correlation in Eq. (G.2) can now be written as

$$C_{vv}(t_1, t_2)_{t_2 > t_1} = \sum_{m=0}^{\infty} \mathcal{P}(m, t_1) \langle v_m^2 \rangle_c \sum_{n=0}^{\infty} (-r)^n \mathbb{P}(n, t_2 - t_1 | m, t_1). \quad (\text{G.4})$$

To compute $\mathbb{P}(n, t_2 - t_1 | m, t_1)$ one needs to be careful because the m^{th} jump event may not occur exactly at time t_1 . It can occur before time t_1 and the $(m+1)^{\text{th}}$ jump event occurs after time t_1 . In this case the problem of computing $\mathbb{P}(n, t_2 - t_1 | m, t_1)$ is equivalent to finding the probability $\bar{\mathcal{P}}(n, t; t_0)$ of having n renewal events in a renewal process within a observation time interval $[t_0, t + t_0]$ where t_0 is not the starting time of the process. Like in the random incidence problem [46, 49], the incident time t_0 can fall at a random moment between two consecutive renewal events (in our problem the ‘kick’ events), one before t_0 and one after t_0 . Following [49], let the time interval between these two events is denoted by w and the probability distribution of the length w of the interval between two successive renewal events in which the incidence time t_0 falls, is denoted by $f_w(w)$. Assuming that the probability that a random incidence occurs in an interval (gap) of length between w to $w + dw$ is proportional to the gap length itself, we write $f_w(w) \propto w\rho(w)$ implying

$$f_w(w) = \frac{w\rho(w)}{\langle w \rangle}. \quad (\text{G.5})$$

Now assume that, starting from t_0 the 1st event (equivalently $(m+1)^{\text{th}}$ event in our problem) occurs after duration r *i.e.* at time $t_0 + r$. The duration r is called the residual time in the context of renewal process. The joint probability distribution of the residual time r and the length w of the gap in which the random incidence time t_0 falls, is given by $f_{rw}(r, w) = f_{r|w}(r|w)f_w(w)$ where $f_{r|w}(r|w)$ is the conditional probability

distribution of the residual time given that gap length is w . Since, the random incidence time t_0 falls uniformly within the gap, we should have $f_{r|w}(r|w) = \frac{1}{w}$ which implies $f_{rw}(r, w) = f_{r|w}(r|w)f_w(w) = \frac{\rho(w)}{\langle w \rangle}$. Integrating this joint probability distribution over w we get the distribution of the residual time τ (denoted by $f_r(r)$) as

$$f_r(r) = \frac{1}{\langle w \rangle} \int_r^\infty dw \rho(w). \quad (\text{G.6})$$

We can now write the probability $\bar{\mathcal{P}}(n, t; t_0)$ of having n renewal events within the interval $[t_0, t_0 + t]$. Let the first event occurs at time $t_1 = t_0 + r_1$, the second at $t_2 = t_0 + r_1 + r_2$ and so on and the last (n^{th}) event occurs at time $t_n = t_0 + r_1 + r_2 + \dots + r_n$. The joint probability distribution of having n events with the following time interval configuration $(r_1, r_2, \dots, r_n, r_l)$ is given by

$$\begin{aligned} \bar{\mathcal{P}}(n, t; t_0) &= \int \int \dots \int dr_1 dr_2 \dots dr_n dr_l f_r(r_1) \rho(r_2) \dots \rho(r_n) \\ &\times \Psi(r_l) \delta(t - r_1 - r_2 - \dots - r_n - r_l), \quad \text{for } n > 0, \end{aligned} \quad (\text{G.7})$$

where $r_l = t - t_n$ is the last incomplete interval and recall, $\Psi(t) = \int_t^\infty d\tau \rho(\tau)$. Similarly for $n = 0$ we have

$$\bar{\mathcal{P}}(n = 0, t; t_0) = g_r(t), \quad \text{where } g_r(t) = \int_t^\infty dr f_r(r). \quad (\text{G.8})$$

Since the events after t_0 are independent of events or the number of events before t_0 , we should have

$$\begin{aligned} \mathbb{P}(n, t_2 - t_1 = t \mid m, t_1) &= \delta_{n,0} g_r(t) + (1 - \delta_{n,0}) \int \int \dots \int dr_1 dr_2 \dots dr_n dr_l \\ &\times f_r(r_1) \rho(r_2) \dots \rho(r_n) \Psi(r_l) \delta\left(t - \sum_{i=1}^n r_i - r_l\right). \end{aligned} \quad (\text{G.9})$$

Note that $\mathbb{P}(n, t_2 - t_1 = t \mid m, t_1)$ does not depend explicitly on t_1 and m . Hence we can omit their explicit appearance in this distribution and denote it by just $\mathbb{P}(n, t_2 - t_1 = t)$.

The velocity correlation can now be written as

$$C_{vv}(t_1, t_2) = \underbrace{\sum_{m=0}^{\infty} \mathcal{P}(m, t_1) \langle v_m^2 \rangle}_{\langle v^2(t_1) \rangle} \times \underbrace{\sum_{n=0}^{\infty} (-r)^n \mathbb{P}(n, t_2 - t_1)}_{Q_r(t_2 - t_1)} \simeq \langle v^2(t_1) \rangle_c Q_r(t_2 - t_1). \quad (\text{G.10})$$

Hence for large t_1 and t_2 we get

$$C_{vv}(t_1, t_2) = \langle v^2(\min\{t_1, t_2\}) \rangle_c Q_r(|t_2 - t_1|), \quad \text{with, } Q_r(t) = \sum_{n=0}^{\infty} (-r)^n \mathbb{P}(n, t). \quad (\text{G.11})$$

Taking Laplace transform of $Q_r(t)$ with respect to time we get

$$\tilde{Q}_r(s) = \sum_{n=0}^{\infty} (-r)^n \tilde{\mathbb{P}}(n, s), \quad (\text{G.12})$$

where from Eq. (G.9) (after taking Laplace transform with respect to t on both sides) we get,

$$\tilde{\mathbb{P}}(n, s) = \tilde{g}_r(s) \delta_{n,0} + \tilde{f}_r(s) \tilde{\psi}^{n-1}(s) \tilde{\Psi}(s) (1 - \delta_{n,0}), \quad (\text{G.13})$$

where $\tilde{f}_r(s)$ and $\tilde{g}_r(s)$ are Laplace transforms of $f_r(r)$ and $g_r(r)$ respectively and, $\tilde{\psi}(s)$ and $\tilde{\Psi}(s)$ are defined in Eqs. (10-11). Using this expression of $\tilde{\mathbb{P}}(n, s)$ in Eq. (G.12) we get

$$\tilde{Q}_r(s) = \tilde{g}_r(s) - \frac{r \tilde{\Psi}(s) \tilde{f}_r(s)}{1 + r \tilde{\psi}(s)}. \quad (\text{G.14})$$

Appendix G.1 Velocity-velocity correlation function in case II

In case II, *i.e.*, for exponential waiting time distribution $\rho(\tau) = \beta e^{-\beta\tau}$, we have $f_r(\tau) = \beta \int_{\tau}^{\infty} dz \rho(z) = \beta e^{-\beta\tau} = \rho(\tau)$. Hence, in this case $\tilde{f}_r(s) = \tilde{\psi}(s)$ and $\tilde{g}_r(s) = \tilde{\Psi}(s)$, using which in Eq. (G.14) we get

$$\tilde{Q}_r(s) = \frac{\tilde{\Psi}(s)}{1 + r \tilde{\psi}(s)}. \quad (\text{G.15})$$

Remember for exponential waiting time distribution $\tilde{\psi}(s) = \beta/(\beta + s)$ and $\tilde{\Psi}(s) = 1/(\beta + s)$. Using these expressions in the above equation we get $\tilde{Q}_r(s) = (s + (1+r)\beta)^{-1}$. Performing inverse Laplace transform provides $Q_r(|t_2 - t_1|) = e^{-\beta(1+r)|t_1 - t_2|}$, using which in Eq. (G.11) yields

$$C_{vv}(t_1, t_2) \simeq \langle v^2(\min\{t_1, t_2\}) \rangle_c e^{-\beta(1+r)|t_1 - t_2|}. \quad (\text{G.16})$$

Note for $r = 0$, the variance of the velocity $\langle v^2(\min\{t_1, t_2\}) \rangle_c = \sigma^2$.

Appendix G.2 Velocity-velocity correlation function in case III with $\alpha > 1$

Appendix G.2.1 For $r = -1$

Computing $C_{vv}(t_1, t_2)$ in this case is simpler because for $r = -1$, it is easy to see that $Q_{-1}(u) = \sum_{m=0}^{\infty} \mathbb{P}(m, u) = 1$ due to the normalization of $\mathbb{P}(m, u)$. Hence, in this case we simply get

$$C_{vv}(t_1, t_2) \simeq \langle v^2(\min\{t_1, t_2\}) \rangle_c. \quad (\text{G.17})$$

Appendix G.2.2 For $r = 0$

For $r = 0$, we see from Eq. (G.14) that $\tilde{Q}_0(s) = \tilde{g}_r(s)$. Performing inverse Laplace transform we get

$$Q_0(u) = g_r(u) = \int_u^{\infty} dw f_r(w) = \frac{1}{\langle \tau \rangle} \int_u^{\infty} dw \int_w^{\infty} dz \rho(z) = \frac{1}{\alpha} u^{-\alpha+1}, \quad (\text{G.18})$$

$$\text{which finally provides } C_{vv}(t_1, t_2) = \sigma^2 Q_0(|t_1 - t_2|) = \frac{\sigma^2}{\alpha} |t_1 - t_2|^{-\alpha+1} \quad (\text{G.19})$$

where we have used $\langle v^2(t) \rangle_c = \sigma^2$ for $r = 0$.

Appendix G.2.3 For $r = 1$

For $r = 1$, using $g_r(s) = (1 - f_r(s))/s$, $\tilde{\Psi}(s) = (1 - \tilde{\psi}(s))/s$, and $\tilde{\psi}(s) \simeq 1 - \alpha s/(\alpha - 1) + \mathcal{O}(s^\alpha)$ for $\alpha > 1$ in the limit $s \rightarrow 0$ we can simplify Eq. (G.14) and get

$$\tilde{Q}_1(s) = \frac{1}{s} - \frac{2\tilde{f}_r(s)}{s(1 + \tilde{\psi}(s))} \simeq \frac{1 - \tilde{f}_r(s)}{s} \simeq \tilde{g}_r(s). \quad (\text{G.20})$$

It implies Eq. (G.18) is also valid for $r = 1$ in the limit of large t , but the correlation function is modified because $\langle v^2(t) \rangle \simeq \sigma^2 t / \langle \tau \rangle_c$ in this case, instead of σ^2 . Hence we can get

$$C_{vv}(t_1, t_2) \simeq \langle v^2 \min\{t_1, t_2\} \rangle_c Q_1(|t_1 - t_2|) \simeq \frac{\sigma^2(\alpha - 1)}{\alpha^2} \min\{t_1, t_2\} |t_1 - t_2|^{-\alpha+1}. \quad (\text{G.21})$$

Appendix H Variance of the position of Lévy Walk

Let $P_{lw}(x, t)$ denote the position $x(t)$ made by a space-time coupled Lévy walker after time t . Also let $\mathcal{Q}_{lw}(x, t)$ denote the probability distribution that the walker lands at x exactly at time t . This probability distribution satisfies the following balance equation [26, 27]

$$\mathcal{Q}_{lw}(x, t) = \int_{-\infty}^{\infty} dx' \int_0^{\infty} dt' \mathcal{Q}_{lw}(x', t') \psi_{lw}(x - x', t - t') + \delta(x)\delta(t). \quad (\text{H.1})$$

Here, $\mathcal{Q}_{lw}(x', t')$ denotes the distribution of the position $x'(t')$ at the last completed step in time $t' < t$ with $\psi_{lw}(x, \tau)$ denoting the joint distribution of ‘jump’ length x and jump duration τ . The second term in Eq. (H.1) arises from the initial condition $P_{lw}(x = 0, t = 0) = \delta(x)\delta(t)$. The evolution equation for $P_{lw}(x, t)$ is related to the distribution $\mathcal{Q}_{lw}(x, t)$ by

$$P_{lw}(x, t) = \int dx' \int dt' \mathcal{Q}_{lw}(x', t') \Psi_{lw}(x - x', t - t') \quad (\text{H.2})$$

where $\Psi_{lw}(x, t)$ denotes the joint distribution of ‘jump’ length and time of the last incomplete step. Given the distribution $p(v)$ of velocity and the distribution $\rho(\tau)$ of the jump duration τ , $\psi_{lw}(x, t)$ can be written as $\psi_{lw}(x, \tau) = \rho(\tau) \int_{-\infty}^{\infty} dv p(v) \delta(x - v\tau)$ which simplifies to $\psi(x, \tau) = \frac{p(x/\tau)}{\tau} \rho(\tau)$. Similarly, $\Psi_{lw}(x, t)$ can be written as $\Psi_{lw}(x, \tau) = \frac{p(x/\tau)}{\tau} \int_{\tau}^{\infty} du \rho(u)$. Performing joint Fourier-Laplace transform on both sides of Eqs. (H.1) and (H.2) we get

$$\tilde{\mathcal{Q}}_{lw}(k, s) = \frac{1}{1 - \tilde{\psi}_{lw}(k, s)}, \quad \text{and}, \quad (\text{H.3})$$

$$\tilde{P}_{lw}(k, s) = \tilde{\Psi}_{lw}(k, s) \tilde{\mathcal{Q}}_{lw}(k, s) = \frac{\tilde{\Psi}_{lw}(k, s)}{1 - \tilde{\psi}_{lw}(k, s)}, \quad (\text{H.4})$$

where $\tilde{F}_{lw}(k, s) = \int_{-\infty}^{\infty} e^{ikx} e^{-s\tau} F_{lw}(x, \tau)$ is the Fourier-Laplace transform of the function $F_{lw}(x, \tau)$.

Note that $\tilde{\psi}_{lw}(k=0, s) = \tilde{\psi}(s) = \mathcal{L}[\rho(\tau)]$ and $\tilde{\Psi}_{lw}(0, s) = \tilde{\Psi}(s) = \mathcal{L}[\int_{\tau}^{\infty} du \rho(u)]$ as given in Eqs. (10) and (11). Taking second derivative of $\tilde{P}_{lw}(k, s)$ with respect to k at $k=0$ provides the Laplace transform of the variance of the position of the Lévy walker at time t

$$\begin{aligned} \tilde{\sigma}_x^2(s) &= -\frac{d^2}{dk^2} \left[\tilde{P}(k, s) \right]_{k=0} = -\frac{d^2}{dk^2} \left[\frac{\tilde{\Psi}_{lw}(k, s)}{1 - \tilde{\psi}_{lw}(k, s)} \right]_{k=0} \\ &= -\left(\frac{\tilde{\Psi}_{lw}(0, s) \tilde{\psi}_{lw}''(0, s)}{(1 - \tilde{\psi}_{lw}(0, s))^2} + \frac{\tilde{\Psi}_{lw}''(0, s)}{1 - \tilde{\psi}_{lw}(0, s)} \right) = \langle v^2 \rangle \frac{\tilde{\psi}''(s) + s \tilde{\Psi}''(s)}{s(1 - \tilde{\psi}(s))}. \end{aligned} \quad (\text{H.5})$$

where we have used the following relations $\tilde{\psi}'_{lw}(0, s) = -i\langle v \rangle \tilde{\psi}(s)$, $\tilde{\psi}''_{lw}(0, s) = -\langle v^2 \rangle \tilde{\psi}(s)$, $\tilde{\Psi}'_{lw}(0, s) = -i\langle v \rangle \tilde{\Psi}'(s)$ and $\tilde{\Psi}''_{lw}(0, s) = -\langle v^2 \rangle \tilde{\Psi}''(s)$ with $\langle v \rangle$ and $\langle v^2 \rangle_c$ being the mean and variance of $p(v)$. Remember that in this paper we have takes $p(v)$ to be Gaussian with $\langle v \rangle = 0$.

Appendix I Distribution of displacement made in a single step for $r = 0$ in case II

The distribution $P(x, t)$ of the position x after time t is given approximately by

$$P(x, t) \simeq \sum_{m=0}^{\infty} \mathcal{P}_x(x|m) \mathcal{P}(m, t), \quad (\text{I.1})$$

for large t where, remember, $\mathcal{P}(m, t)$ is the probability of taking m steps within time t and $\mathcal{P}_x(x|m)$ is probability distribution of finding the particle at position x after m jump steps. The approximately equal sign in the above expression is because we can neglect the contribution of the position of the last incomplete step for large t in the case of $\rho(\tau) = \beta e^{-\beta\tau}$. Note for $r = 0$ the position of the walker at m^{th} step is given by $x_m = \sum_{i=0}^{m-1} \xi_i$ where the distribution of the position $\xi = \tau\eta$ in a single step can be calculated as follows

$$\begin{aligned} \varrho(\xi) &= \int_0^{\infty} d\tau \rho(\tau) \int_{-\infty}^{\infty} d\eta p(\eta) \delta(\xi - \eta\tau) \\ &= \frac{\beta}{\sqrt{2\pi\sigma^2}} \int_0^{\infty} d\tau e^{-\beta\tau} \int_{-\infty}^{\infty} d\eta e^{-\eta^2/2\sigma^2} \delta(\xi - \eta\tau). \end{aligned} \quad (\text{I.2})$$

Using $\delta(\xi - \eta\tau) = \delta(\xi/\tau - \eta)/|\tau|$ we get

$$\varrho(\xi) = \frac{\beta}{\sqrt{2\pi\sigma^2}} \int_0^{\infty} \frac{d\tau}{\tau} \exp \left[-\beta\tau - \frac{\xi^2}{2\sigma^2\tau^2} \right] \underset{\xi \rightarrow \infty}{\simeq} \frac{2\sqrt{2}\sigma^{1/3}}{\beta^{1/3}} \frac{1}{\xi^{1/3}} \exp \left(-\frac{3\beta^{2/3}}{2\sigma^{2/3}} \xi^{2/3} \right), \quad (\text{I.3})$$

which shows $\varrho(\xi)$ decays faster than a power law at large ξ . The characteristic function of $\varrho(\xi)$ is given by

$$\lambda(k) = \int_{-\infty}^{\infty} d\xi e^{ik\xi} \varrho(\xi) = \sqrt{\frac{\pi\beta^2}{2k^2\sigma^2}} \exp \left[\frac{\beta^2}{2k^2\sigma^2} \right] \text{Erfc} \left[\sqrt{\frac{\beta^2}{2k^2\sigma^2}} \right] \quad (\text{I.4})$$

where $\text{Erfc}[z] = (2/\sqrt{\pi}) \int_z^\infty du e^{-u^2}$ is complimentary error function. Using this $\lambda(k)$ we write the distribution of the position $x_m = \sum_{i=0}^{m-1} \xi_i$ after m jumps or steps as

$$\mathcal{P}_x(x|m) = \frac{1}{2\pi} \int_{-\infty}^{\infty} dk e^{-ikx} \lambda^m(k). \quad (\text{I.5})$$

On the other hand, to compute $\mathcal{P}(m, t)$ in this case we note that the time interval between all successive events are taken from exponential distribution. Hence, the probability of making m steps within time t is given by $p(m, t) = e^{-\beta t} (\beta t)^m / m!$. Using this result and Eq. (I.5) in Eq. (I.1) we get

$$P(x, t) \simeq \frac{1}{2\pi} \int_{-\infty}^{\infty} dk e^{-ikx} \sum_{m=0}^{\infty} \frac{e^{-\beta t}}{m!} (\beta t \lambda(k))^m \simeq \frac{1}{2\pi} \int_{-\infty}^{\infty} dk e^{-ikx + \beta t (\lambda(k) - 1)}. \quad (\text{I.6})$$

For large t one can perform a saddle point calculation keeping the ratio x/t fixed and get a large deviation form of the distribution $P(x, t)$. From this calculation it is easy to show that, this distribution behaves as a Gaussian around the mean with a variance $2\sigma^2 t / \beta$.

Appendix J Calculation of $\mathcal{P}(\tau_{\max}|t)$ for $\alpha = 1$:

To obtain the behaviour of $\mathcal{P}(\tau_{\max}|t)$, we start with Laplace transform $\tilde{\mathcal{H}}_{\max}(\tau, s)$ of the cumulative distribution function $\mathcal{H}_{\max}(\tau, t) = \text{Prob}(\tau_{\max}(t) \leq \tau)$ of $\mathcal{P}(\tau_{\max}|t)$. Since for large t we expect τ_{\max} would also be large. Hence we focus in the small s behaviour the function $\tilde{\mathcal{H}}_{\max}(\tau, s)$. This function is given in Ref. [36], from which we write

$$\frac{1}{s} - \tilde{\mathcal{H}}_{\max}(\tau, s) \simeq \frac{\mathcal{G}_{\max}(\tau s)}{s} \quad \text{where} \quad (\text{J.1})$$

$$\mathcal{G}_{\max}(\tau s) \simeq \left(1 + \tau s e^{\tau s} \int_s^{\tau s} du u^{-1} e^{-u} \right)^{-1} \simeq (1 + \tau s \ln(\tau) + \mathcal{O}(s^2))^{-1}. \quad (\text{J.2})$$

Performing inverse Laplace transform, we get

$$\mathcal{H}_{\max}(\tau, t) \simeq \text{Exp} \left[-\frac{t}{\tau \ln(\tau)} \right]. \quad (\text{J.3})$$

Now, using the relation $\mathcal{P}(\tau_{\max}|t) = \left[\frac{d}{d\tau} \mathcal{H}_{\max}(\tau, t) \right]_{\tau=\tau_{\max}}$ we get

$$\mathcal{P}(\tau_{\max} = \tau|t) \simeq \frac{t(\ln(\tau) + 1)}{\tau^2 (\ln \tau)^2} \text{Exp} \left[-\frac{t}{\tau \ln \tau} \right]. \quad (\text{J.4})$$

Appendix K Calculation of fourth moment of the position for $r = \mp 1$ in case II

In this section we calculate the fourth moment of position exactly after m ‘jump’ steps. Note from Eq. (7) that $x_m = \sum_{i=1}^{m-1} v_i \tau_i$. Using $v_i = \sum_{j=0}^i \eta_i (-r)^{i-j}$ from Eq. (4) we can write

$$x_m = \sum_{i=1}^{m-1} \tau_i \sum_{j=0}^i \eta_i (-r)^{i-j}. \quad (\text{K.1})$$

Starting from this expression, the fourth moment of x_m is written as

$$\langle x_m^4 \rangle = \sum_{i=0}^{m-1} \sum_{j=0}^{m-1} \sum_{k=0}^{m-1} \sum_{l=0}^{m-1} \langle \tau_i \tau_j \tau_k \tau_l \rangle \sum_{p=0}^i \sum_{q=0}^j \sum_{w=0}^k \sum_{s=0}^l \langle \eta_p \eta_q \eta_w \eta_s \rangle (-r)^{i+j+k+l-p-q-w-s}. \quad (\text{K.2})$$

To compute the averages of the noises, we use the Wick's theorem $\langle \eta_p \eta_q \eta_w \eta_s \rangle = \delta_{p,q} \delta_{w,s} + \delta_{p,w} \delta_{q,s} + \delta_{p,s} \delta_{q,w}$ and calculate different parts of the fourth moment one by one. First we consider the case $i = j = k = l$ in Eq. (K.2) for which we get

$$\begin{aligned} \langle x_m^4 \rangle_{i=j=k=l} &= \sum_{i=0}^{m-1} \langle \tau_i^4 \rangle (-r)^{4i} \sum_{p=0}^i \sum_{q=0}^i \sum_{w=0}^i \sum_{s=0}^i \langle \eta_p \eta_q \eta_w \eta_s \rangle (-r)^{-p-q-w-s} \\ &= \langle \tau^4 \rangle \langle \eta^2 \rangle^2 \sum_{i=0}^{m-1} \sum_{p=0}^i \sum_{q=0}^i \sum_{w=0}^i \sum_{s=0}^i [\delta_{p,q} \delta_{w,s} + \delta_{p,w} \delta_{q,s} + \delta_{p,s} \delta_{q,w}] \\ &= 3 \langle \tau^4 \rangle \langle \eta^2 \rangle^2 \sum_{i=0}^{m-1} \sum_{p=0}^i \sum_{w=0}^i 1 \simeq 4! \frac{\sigma^4 m^3}{\beta^4} + \mathcal{O}(m^2) \quad \text{for } r = \mp 1. \end{aligned} \quad (\text{K.3})$$

Note that we have used $r = \mp 1$ in the second line in Eq. (K.3). We now follow the same method to compute the contribution to $\langle x_m^4 \rangle$ if $i = j = k \neq l$,

$$\begin{aligned} \langle x_m^4 \rangle_{i=j=k \neq l} &= \left(\sum_{i=0}^{m-2} \sum_{l=i+1}^{m-1} + \sum_{l=0}^{m-2} \sum_{i=l+1}^{m-1} \right) \langle \tau_i^3 \rangle \langle \tau_l \rangle (-r)^{3i+l} \sum_{p=0}^i \sum_{q=0}^i \sum_{w=0}^i \sum_{s=0}^l \langle \eta_p \eta_q \eta_w \eta_s \rangle \\ &\quad \times (-r)^{-p-q-w-s} = \langle \tau \rangle \langle \tau^3 \rangle \langle \eta^2 \rangle^2 \left(\sum_{i=0}^{m-2} \sum_{l=i+1}^{m-1} + \sum_{l=0}^{m-2} \sum_{i=l+1}^{m-1} \right) (-1)^{3i+l} \\ &\quad \times \sum_{p=0}^i \sum_{q=0}^i \sum_{w=0}^i \sum_{s=0}^l [\delta_{p,q} \delta_{w,s} + \delta_{p,w} \delta_{q,s} + \delta_{p,s} \delta_{q,w}] = 3 \langle \tau \rangle \langle \tau^3 \rangle \langle \eta^2 \rangle^2 \left(\sum_{i=0}^{m-2} \sum_{l=i+1}^{m-1} (i+1)^2 \right. \\ &\quad \left. \times (\pm 1)^{3i+l} + \sum_{l=0}^{m-2} \sum_{i=l+1}^{m-1} (i+1)(l+1)(\pm 1)^{3i+l} \right) \simeq \begin{cases} \frac{5}{4} \frac{\sigma^4 m^4}{\beta^4} + \mathcal{O}(m^3) & \text{for } r = -1 \\ -3! \frac{\sigma^4 m^3}{\beta^4} + \mathcal{O}(m^2) & \text{for } r = 1. \end{cases} \end{aligned} \quad (\text{K.4})$$

In the second line in Eq. (K.4) we have used $r = \mp 1$ and employed Wick's theorem. Same method can be followed to compute the contribution from the remaining two cases $i = j \neq k = l$, $i = j \neq k \neq l$, and $i \neq j \neq k \neq l$ to $\langle x_m^4 \rangle$ as following:

$$\begin{aligned} \langle x_m^4 \rangle_{i=j \neq k=l} &= 3 \times 2 \sum_{i=0}^{m-2} \sum_{k=i+1}^{m-1} \langle \tau_i^2 \rangle \langle \tau_k^2 \rangle (-r)^{2i+2k} \sum_{p=0}^i \sum_{q=0}^i \sum_{w=0}^k \sum_{s=0}^k \langle \eta_p \eta_q \eta_w \eta_s \rangle (-r)^{-p-q-w-s} \\ &= 6 \langle \tau^2 \rangle^2 \langle \eta^2 \rangle^2 \sum_{i=0}^{m-2} \sum_{k=i+1}^{m-1} \sum_{p=0}^i \sum_{q=0}^i \sum_{w=0}^k \sum_{s=0}^k [\delta_{p,q} \delta_{w,s} + \delta_{p,w} \delta_{q,s} + \delta_{p,s} \delta_{q,w}] \\ &= 6 \langle \tau^2 \rangle^2 \langle \eta^2 \rangle^2 \sum_{i=0}^{m-2} \sum_{k=i+1}^{m-1} [(i+1)(k+1) + 2(i+1)^2] \\ &\simeq 7 \left(\frac{\sigma m}{\beta} \right)^4 + \mathcal{O}(m^3) \quad \text{for } r = \mp 1. \end{aligned} \quad (\text{K.5})$$

$$\begin{aligned}
\langle x_m^4 \rangle_{i \neq j \neq k \neq l} &= 6 \times 2 \left(\sum_{i=0}^{m-3} \sum_{k=i+1}^{m-2} \sum_{l=k+1}^{m-1} + \sum_{k=0}^{m-3} \sum_{i=k+1}^{m-2} \sum_{l=k+1}^{m-1} + \sum_{k=0}^{m-3} \sum_{l=k+1}^{m-2} \sum_{i=l+1}^{m-1} \right) \\
&\times \langle \tau_i^2 \rangle \langle \tau_k \rangle \langle \tau_l \rangle (-r)^{2i+k+l} \times \sum_{p=0}^i \sum_{q=0}^i \sum_{w=0}^k \sum_{s=0}^l \langle \eta_p \eta_q \eta_r \eta_s \rangle (-r)^{-p-q-r-s} \\
&= 12 \langle \tau^2 \rangle \langle \tau \rangle^2 \langle \eta^2 \rangle^2 \left(\sum_{i=0}^{m-3} \sum_{k=i+1}^{m-2} \sum_{l=k+1}^{m-1} + \sum_{k=0}^{m-3} \sum_{i=k+1}^{m-2} \sum_{l=k+1}^{m-1} + \sum_{k=0}^{m-3} \sum_{l=k+1}^{m-2} \sum_{i=l+1}^{m-1} \right) \\
&\times (-r)^{2i+k+l} \sum_{p=0}^i \sum_{q=0}^i \sum_{w=0}^k \sum_{s=0}^l [\delta_{p,q} \delta_{w,s} + \delta_{p,w} \delta_{q,s} + \delta_{p,s} \delta_{q,w}] \\
&= 12 \langle \tau^2 \rangle \langle \tau \rangle^2 \langle \eta^2 \rangle^2 \left(\sum_{i=0}^{m-3} \sum_{k=i+1}^{m-2} \sum_{l=k+1}^{m-1} + \sum_{k=0}^{m-3} \sum_{i=k+1}^{m-2} \sum_{l=k+1}^{m-1} + \sum_{k=0}^{m-3} \sum_{l=k+1}^{m-2} \sum_{i=l+1}^{m-1} \right) (-r)^{2i+k+l} \\
&\times [(i+1)(\min(k, l) + 1) + 2(\min(i, k) + 1)(\min(i, l) + 1)] \\
&\simeq \begin{cases} \frac{36}{5} \left(\frac{\sigma^4 m^5}{\beta^4} \right) + \mathcal{O}(m^4) & \text{for } r = -1 \\ -7 \left(\frac{\sigma m}{\beta} \right)^4 + \mathcal{O}(m^3) & \text{for } r = 1 \end{cases} . \tag{K.6}
\end{aligned}$$

$$\begin{aligned}
\langle x_m^4 \rangle_{i \neq j \neq k \neq l} &= 4! \sum_{i=0}^{m-4} \sum_{j=i+1}^{m-3} \sum_{k=j+1}^{m-2} \sum_{l=k+1}^{m-1} \langle \tau_i \tau_j \tau_k \tau_l \rangle \\
&\times \sum_{p=0}^i \sum_{q=0}^j \sum_{w=0}^k \sum_{s=0}^l \langle \eta_p \eta_q \eta_w \eta_s \rangle (-r)^{i+j+k+l-p-q-w-s} \\
&= 4! \langle \tau \rangle^4 \langle \eta^2 \rangle^2 \sum_{i=0}^{m-4} \sum_{j=i+1}^{m-3} \sum_{k=j+1}^{m-2} \sum_{l=k+1}^{m-1} (-r)^{i+j+k+l} \\
&\times \sum_{p=0}^i \sum_{q=0}^j \sum_{w=0}^k \sum_{s=0}^l [\delta_{p,q} \delta_{w,s} + \delta_{p,w} \delta_{q,s} + \delta_{p,s} \delta_{q,w}] \\
&= 4! \langle \tau \rangle^4 \langle \eta^2 \rangle^2 \sum_{i=0}^{m-4} \sum_{j=i+1}^{m-3} \sum_{k=j+1}^{m-2} \sum_{l=k+1}^{m-1} (-r)^{i+j+k+l} [(1+i)(1+k) + 2(1+i)(1+j)] \\
&\simeq \begin{cases} \frac{1}{3} \left(\frac{\sigma^4 m^6}{\beta^4} \right) + \mathcal{O}(m^5) & \text{for } r = -1 \\ \frac{7}{4} \left(\frac{\sigma m}{\beta} \right)^4 + \mathcal{O}(m^3) & \text{for } r = 1 \end{cases} . \tag{K.7}
\end{aligned}$$

Now, adding Eqs. (K.3), (K.4), (K.5), (K.6), and (K.7) and keeping only leading order contributions, we get

$$\langle x_m^4 \rangle \simeq \begin{cases} \frac{1}{3} \left(\frac{\sigma^4 m^6}{\beta^4} \right) + \mathcal{O}(m^5) & \text{for } r = -1 \\ \frac{7}{4} \left(\frac{\sigma m}{\beta} \right)^4 + \mathcal{O}(m^3) & \text{for } r = 1. \end{cases} \tag{K.8}$$

From the above calculation it is quite clear that the dominant contribution of $\langle x_m^4 \rangle$ for $r = -1$ is coming from off-diagonal elements of the matrix Σ_m which are different

from each others, whereas for $r = 1$ dominant contributions are coming from the both diagonal and off-diagonal terms.

Appendix L Determination of higher order moments of position $x(t)$ for $r = 1$ and $0 < \alpha \leq 2$ in case III

Moments of any order can be computed from the generating function $\tilde{P}_x(k, s)$ in Eq. (27). by taking derivatives with respect to k . The Laplace transform of the $2n^{\text{th}}$ order moment is given by

$$\langle \widetilde{x^{2n}} \rangle(s) = (-1)^n \frac{d^{2n}}{dk^{2n}} \tilde{P}_x(k, s) = \sum_{m=0}^{\infty} \sigma^{2n} \frac{1}{n!} \frac{(2n)!}{2^n} \langle (\bar{\tau}_m^T \Sigma_m \bar{\tau}_m)^n e^{-s(\tau_0 + \tau_1 + \dots + \tau_{m-1} + \tau_m^*)} \rangle. \quad (\text{L.1})$$

Using the explicit form of the matrix Σ_m in Eq. (28) one can write

$$\begin{aligned} \bar{\tau}_m^T \Sigma_m \bar{\tau}_m &= \left(\mathbb{I}(m \geq 1) \sum_{l=0}^{m-1} \tau_l^2 \sum_{j=0}^l r^{2j} + \tau_m^{*2} \sum_{l=0}^m r^{2l} + 2 \mathbb{I}(m \geq 2) \sum_{l=0}^{m-1} \tau_l \right. \\ &\quad \left. \times \sum_{j=l+1}^{m-1} \tau_j (-r)^{j-l} \sum_{p=0}^l r^{2p} + 2 \mathbb{I}(m \geq 1) \tau_m^* \sum_{l=0}^{m-1} \tau_l (-r)^{m-l} \sum_{p=0}^l r^{2p} \right) \quad (\text{L.2}) \end{aligned}$$

which for $r = 1$ becomes

$$\begin{aligned} \bar{\tau}_m^T \Sigma_m \bar{\tau}_m &= \left(\mathbb{I}(m \geq 1) \sum_{l=0}^{m-1} \tau_l^2 (l+1) + \tau_m^{*2} (m+1) + 2 \mathbb{I}(m \geq 2) \sum_{l=0}^{m-1} \tau_l \right. \\ &\quad \left. \times \sum_{j=l+1}^{m-1} \tau_j (-1)^{j-l} (l+1) + 2 \mathbb{I}(m \geq 1) \tau_m^* \sum_{l=0}^{m-1} \tau_l (-1)^{m-l} (l+1) \right). \quad (\text{L.3}) \end{aligned}$$

Now we would like approximate this expression by using the fact that for $r = 1$, as can be observed in fig. 13(2nd row), fig. 15(b) and fig. 17, the position $x(t)$ for large t gets dominant contribution from the jump of longest duration *i.e.* $x(t) \simeq \Delta_{\max}(t)$. Using this fact we identify the contribution from this jump only and disregard contribution from other steps or correlations with other steps. Hence retaining contributions from longest jumps only we get

$$(\bar{\tau}_m^T \Sigma_m \bar{\tau}_m)^n \simeq \left(\mathbb{I}(m \geq 1) \sum_{l=0}^{m-1} \tau_l^{2n} (l+1)^n + \tau_m^{*2n} (m+1)^n \right). \quad (\text{L.4})$$

The first term represents the contribution from the event in which the longest jump occurs at l th step [$l = 0, 1, \dots, (m-1)$] and the second term represents the event in which the longest jump occurs in the last incomplete step in a trajectory of duration t having m steps. Using this approximate expression of $(\bar{\tau}_m^T \Sigma_m \bar{\tau}_m)^n$ in Eq. (L.1) and

simplifying we get

$$\begin{aligned}
\langle \widetilde{x^{2n}} \rangle(s) &\simeq \sum_{m=0}^{\infty} \sigma^{2n} \frac{1}{n!} \frac{(2n)!}{2^n} \\
&\times \left\langle \left(\mathbb{I}(m \geq 1) \sum_{l=0}^{m-1} \tau_l^{2n} (l+1)^n + \tau_m^{*2n} (m+1)^n \right) e^{-s(\tau_0 + \tau_1 + \dots + \tau_{m-1} + \tau_m^*)} \right\rangle \\
&\simeq \sigma^{2n} \frac{(2n)!}{2^n n!} \sum_{m=0}^{\infty} \left(\mathbb{I}(m \geq 1) \tilde{\Psi}(s) \tilde{\psi}^{(2n)}(s) H_{m,-n} \tilde{\psi}(s)^{m-1} + (m+1)^n \Psi^{(2n)}(s) \tilde{\psi}(s)^m \right) \\
&\simeq \sigma^{2n} \frac{(2n)!}{2^n n!} \left(\tilde{\Psi}(s) \tilde{\psi}^{(2n)}(s) \frac{Li_{-n}(\tilde{\psi}(s))}{(1-\tilde{\psi}(s))\tilde{\psi}(s)} + \Psi^{(2n)}(s) \frac{Li_{-n}(\tilde{\psi}(s))}{\tilde{\psi}(s)} \right) \\
&\simeq \sigma^{2n} \frac{(2n)!}{2^n} \frac{Li_{-n}(\tilde{\psi}(s))(1-\tilde{\psi}(s))^{n+1}}{\tilde{\psi}(s)n!} \left(\frac{\tilde{\psi}^{(2n)}(s) + s \Psi^{(2n)}(s)}{s(1-\tilde{\psi}(s))^{n+1}} \right), \tag{L.5}
\end{aligned}$$

where $H_{m,-n}$ is Harmonic number and $Li_{-n}(z)$ is PolyLog function. In going from the 3rd line to the 4th line, we have used $\tilde{\Psi}(s) = \frac{1-\tilde{\psi}(s)}{s}$. Using the following $s \rightarrow 0$ limit $\frac{Li_{-n}(\tilde{\psi}(s))(1-\tilde{\psi}(s))^{n+1}}{\tilde{\psi}(s)n!} \rightarrow 1$, we get

$$\langle \widetilde{x^{2n}} \rangle(s) \simeq \sigma^{2n} \frac{(2n)!}{2^n} \left(\frac{\tilde{\psi}^{(2n)}(s) + s \Psi^{(2n)}(s)}{s(1-\tilde{\psi}(s))^{n+1}} \right). \tag{L.6}$$

We now use the small s behaviour of $\tilde{\psi}(s)$ and $\tilde{\Psi}(s)$ in different ranges of α to compute the small s behaviour of $\langle \widetilde{x^{2n}} \rangle(s)$.

In this regime $\tilde{\psi}(s) \simeq 1 - \Gamma(1-\alpha)s^\alpha + O(s)$ for small s as can be seen from Eq. (16). Hence $\tilde{\Psi}(s) \simeq \Gamma(1-\alpha)s^{\alpha-1}$. Using these approximation in Eq. (L.6) one gets $\langle \widetilde{x^{2n}} \rangle(s) \propto s^{-(2+\alpha)n-1}$ for small s which via Tauberian theorem provides us

$$\langle x^{2n}(t) \rangle \sim t^{2n(1+\alpha/2)}, \quad \text{for } n = 1, 2, 3, \dots \text{ and } \alpha < 1. \tag{L.7}$$

In this regime of α , $\tilde{\psi}(s) \simeq 1 - \frac{\alpha s}{\alpha-1} - \Gamma(1-\alpha)s^\alpha + \mathcal{O}(s^2)$ implying $\langle \widetilde{x^{2n}} \rangle(s) \propto s^{-(3n+2-\alpha)}$ which through Tauberian theorem provides

$$\langle x^{2n}(t) \rangle \sim t^{(3n+1-\alpha)}, \quad \text{for } n = 1, 2, 3, \dots \text{ and } 1 < \alpha < 2. \tag{L.8}$$

Similarly using small s behaviour of $\tilde{\psi}(s)$ and $\tilde{\Psi}(s)$ in Eq. (L.6) for other different ranges of α , one can obtain the moments $\langle x^{2n}(t) \rangle$ at large t . Below we summarise the results

$$\langle x^{2n}(t) \rangle \sim \begin{cases} t^{2n(1+\alpha/2)}, & \text{for } \alpha < 1 \\ \frac{t^{3n}}{(\ln t)^{n+1}}, & \text{for } \alpha = 1 \\ t^{(3n+1-\alpha)}, & \text{for } 1 < \alpha < 2 \\ \frac{1}{4}t^2 \log(t) \delta_{n,1} + \mathbb{I}(n \geq 2) t^{(3n+1-\alpha)}, & \text{for } \alpha = 2. \end{cases} \tag{L.9}$$

Here $\delta_{n,m}$ is Kronecker delta function which yields 1 if $n = m$, otherwise it is 0. $\mathbb{I}(z)$ is the indicator function. Note that for $\alpha > 2$ contribution of total displacement arises from all the ‘jumps’ taken within a given time and hence the approximation $x(t) \simeq \Delta_{\max}(t)$ no longer remain valid.

- [1] N. G. Van Kampen, *Stochastic processes in physics and chemistry*, vol. 1. Elsevier, 1992.
- [2] L. M. Ricciardi, *Diffusion processes and related topics in biology*, vol. 14. Springer Science & Business Media, 2013.
- [3] S. Chandrasekhar, “Stochastic problems in physics and astronomy,” *Reviews of modern physics*, vol. 15, no. 1, p. 1, 1943.
- [4] G. I. Taylor, “Diffusion by continuous movements,” *Proceedings of the london mathematical society*, vol. 2, no. 1, pp. 196–212, 1922.
- [5] K. L. Chong, J.-Q. Shi, G.-Y. Ding, S.-S. Ding, H.-Y. Lu, J.-Q. Zhong, and K.-Q. Xia, “Vortices as brownian particles in turbulent flows,” *Science advances*, vol. 6, no. 34, p. eaaz1110, 2020.
- [6] H. M. Jaeger, S. R. Nagel, and R. P. Behringer, “Granular solids, liquids, and gases,” *Reviews of modern physics*, vol. 68, no. 4, p. 1259, 1996.
- [7] A. Barrat, E. Trizac, and M. H. Ernst, “Granular gases: dynamics and collective effects,” *Journal of Physics: Condensed Matter*, vol. 17, no. 24, p. S2429, 2005.
- [8] R. McWilliams and M. Okubo, “The transport of test ions in a quiet plasma,” *The Physics of fluids*, vol. 30, no. 9, pp. 2849–2854, 1987.
- [9] C. Bechinger, R. Di Leonardo, H. Löwen, C. Reichhardt, G. Volpe, and G. Volpe, “Active particles in complex and crowded environments,” *Reviews of Modern Physics*, vol. 88, no. 4, p. 045006, 2016.
- [10] J. W. Haus and K. W. Kehr, “Diffusion in regular and disordered lattices,” *Physics Reports*, vol. 150, no. 5-6, pp. 263–406, 1987.
- [11] J.-P. Bouchaud and A. Georges, “Anomalous diffusion in disordered media: statistical mechanisms, models and physical applications,” *Physics reports*, vol. 195, no. 4-5, pp. 127–293, 1990.
- [12] A. Dhar, K. Saito, and B. Derrida, “Exact solution of a lévy walk model for anomalous heat transport,” *Physical Review E*, vol. 87, no. 1, p. 010103, 2013.
- [13] H. Spohn, “Nonlinear fluctuating hydrodynamics for anharmonic chains,” *Journal of Statistical Physics*, vol. 154, no. 5, pp. 1191–1227, 2014.
- [14] V. Zaburdaev, S. Denisov, and P. Hänggi, “Perturbation spreading in many-particle systems: a random walk approach,” *Physical review letters*, vol. 106, no. 18, p. 180601, 2011.
- [15] A. Dhar, A. Kundu, and A. Kundu, “Anomalous heat transport in one dimensional systems: a description using non-local fractional-type diffusion equation,” *arXiv preprint arXiv:1911.04457*, 2019.
- [16] M. Shlesinger and J. Klafter, “Comment on” accelerated diffusion in josephson junctions and related chaotic systems,” *Physical review letters*, vol. 54, no. 23, p. 2551, 1985.
- [17] T. Geisel, J. Nierwetberg, and A. Zacherl, “Accelerated diffusion in josephson junctions and related chaotic systems,” *Physical Review Letters*, vol. 54, no. 7, p. 616, 1985.
- [18] A. Okubo, V. Andreasen, and J. Mitchell, “Chaos-induced turbulent diffusion,” *Physics Letters A*, vol. 105, no. 4-5, pp. 169–172, 1984.
- [19] C. Holm, J. Joanny, K. Kremer, R. Netz, P. Reineker, C. Seidel, T. A. Vilgis, and R. Winkler, “Polyelectrolyte theory,” *Polyelectrolytes with defined molecular architecture II*, pp. 67–111, 2004.
- [20] S. Marksteiner, K. Ellinger, and P. Zoller, “Anomalous diffusion and lévy walks in optical lattices,” *Physical Review A*, vol. 53, no. 5, p. 3409, 1996.
- [21] T. Solomon, E. R. Weeks, and H. L. Swinney, “Observation of anomalous diffusion and lévy flights in a two-dimensional rotating flow,” *Physical Review Letters*, vol. 71, no. 24, p. 3975, 1993.

- [22] G. M. Viswanathan, V. Afanasyev, S. Buldyrev, E. Murphy, P. Prince, and H. E. Stanley, “Lévy flight search patterns of wandering albatrosses,” *Nature*, vol. 381, no. 6581, pp. 413–415, 1996.
- [23] M. F. Shlesinger, “Random searching,” *Journal of Physics A: Mathematical and Theoretical*, vol. 42, no. 43, p. 434001, 2009.
- [24] M. Shlesinger, B. West, and J. Klafter, “Lévy dynamics of enhanced diffusion: Application to turbulence,” *Physical Review Letters*, vol. 58, no. 11, p. 1100, 1987.
- [25] J. Klafter and G. Zumofen, “Lévy statistics in a hamiltonian system,” *Physical Review E*, vol. 49, no. 6, p. 4873, 1994.
- [26] V. Zaburdaev, S. Denisov, and J. Klafter, “Lévy walks,” *Reviews of Modern Physics*, vol. 87, no. 2, p. 483, 2015.
- [27] J. Klafter and I. M. Sokolov, *First steps in random walks: from tools to applications*. Oxford University Press, 2011.
- [28] S. Denisov, V. Zaburdaev, and P. Hänggi, “Lévy walks with velocity fluctuations,” *Physical Review E*, vol. 85, no. 3, p. 031148, 2012.
- [29] D. Froemberg, M. Schmiedeberg, E. Barkai, and V. Zaburdaev, “Asymptotic densities of ballistic lévy walks,” *Physical Review E*, vol. 91, no. 2, p. 022131, 2015.
- [30] V. Zaburdaev, M. Schmiedeberg, and H. Stark, “Random walks with random velocities,” *Physical Review E*, vol. 78, no. 1, p. 011119, 2008.
- [31] I. Norros, “On the use of fractional brownian motion in the theory of connectionless networks,” *IEEE Journal on selected areas in communications*, vol. 13, no. 6, pp. 953–962, 1995.
- [32] L. Decreusefond *et al.*, “Stochastic analysis of the fractional brownian motion,” *Potential analysis*, vol. 10, no. 2, pp. 177–214, 1999.
- [33] V. Prasad, S. Sabhapandit, and A. Dhar, “High-energy tail of the velocity distribution of driven inelastic maxwell gases,” *EPL (Europhysics Letters)*, vol. 104, no. 5, p. 54003, 2014.
- [34] V. Prasad, S. Sabhapandit, and A. Dhar, “Driven inelastic maxwell gases,” *Physical Review E*, vol. 90, no. 6, p. 062130, 2014.
- [35] S. N. Majumdar and M. J. Kearney, “Inelastic collapse of a ball bouncing on a randomly vibrating platform,” *Physical Review E*, vol. 76, no. 3, p. 031130, 2007.
- [36] C. Godrèche, S. N. Majumdar, and G. Schehr, “Statistics of the longest interval in renewal processes,” *Journal of Statistical Mechanics: Theory and Experiment*, vol. 2015, no. 3, p. P03014, 2015.
- [37] F. Mainardi, R. Gorenflo, and A. Vivoli, “Beyond the poisson renewal process: A tutorial survey,” *Journal of Computational and Applied Mathematics*, vol. 205, no. 2, pp. 725–735, 2007.
- [38] M. Niemann, E. Barkai, and H. Kantz, “Renewal theory for a system with internal states,” *Mathematical Modelling of Natural Phenomena*, vol. 11, no. 3, pp. 191–239, 2016.
- [39] H. J. Haubold, A. M. Mathai, and R. K. Saxena, “Mittag-leffler functions and their applications,” *Journal of Applied Mathematics*, vol. 2011, 2011.
- [40] P. Dolai, A. Das, A. Kundu, C. Dasgupta, A. Dhar, and K. V. Kumar, “Universal scaling in active single-file dynamics,” *arXiv preprint arXiv:2004.01150*, 2020.
- [41] S. N. Majumdar, “Persistence in nonequilibrium systems,” *Current Science*, pp. 370–375, 1999.
- [42] T. W. Burkhardt, “The random acceleration process in bounded geometries,” *Journal of Statistical Mechanics: Theory and Experiment*, vol. 2007, no. 07, p. P07004, 2007.
- [43] H. Touchette, “The large deviation approach to statistical mechanics,” *Physics Reports*, vol. 478, no. 1-3, pp. 1–69, 2009.
- [44] E. W. Montroll and J. T. Bendler, “On lévy (or stable) distributions and the williams-watts model of dielectric relaxation,” *JSP*, vol. 34, no. 1-2, pp. 129–162, 1984.
- [45] M. R. Spiegel, “Laplace transforms. schaum’s outline series,” *McGraw-Hill, New York*, vol. 160, pp. 47–50, 1965.
- [46] W. Feller, *An introduction to probability theory and its applications*, vol. 2. John Wiley & Sons, 2008.
- [47] T. Burkhardt, “Semiflexible polymer in the half plane and statistics of the integral of a brownian

- curve,” *Journal of Physics A: Mathematical and General*, vol. 26, no. 22, p. L1157, 1993.
- [48] P. Singh, “Random acceleration process under stochastic resetting,” *Journal of Physics A: Mathematical and Theoretical*, vol. 53, no. 40, p. 405005, 2020.
- [49] O. Ibe, *Fundamentals of applied probability and random processes*. Academic Press, 2014.